A Framework for a Self-Sustained Traffic Operations System Using V2V Communications

by

Peiheng Li

A Dissertation Presented in Partial Fulfillment
of the Requirements for the Degree
Doctor of Philosophy

Approved November 2017 by the
Graduate Supervisory Committee:

Yingyan Lou, Chair
Xuesong Zhou
Pitu Mirchandani

ARIZONA STATE UNIVERSITY

December 2017

ABSTRACT

This study explores an innovative framework for a self-sustained traffic operations system using vehicle-to-vehicle (V2V) communications alone. The proposed framework is envisioned as the foundation to an alternative or supplemental traffic operation and management system, which could be particularly helpful under abnormal traffic conditions caused by unforeseen disasters and special events. Its two major components, a distributed traffic monitoring and platoon information aggregation system and a platoon-based automated intersection control system, are investigated in this study.

The distributed traffic monitoring and platoon information aggregation system serves as the foundation. Specifically, each equipped vehicle, through the distributed protocols developed, keeps track of the average traffic density and speed within a certain range, flags itself as micro-discontinuity in traffic if appropriate, and cross-checks its flag status with its immediate up- and down-stream vehicles. The micro-discontinuity flags define vehicle groups with similar traffic states, for initiating and terminating traffic information aggregation. The impact of market penetration rate (MPR) is also investigated with a new methodology for performance evaluation under multiple traffic scenarios.

In addition to MPR, the performance of the distributed traffic monitoring and platoon information aggregation system depends on the spatial distribution of equipped vehicles in the road network as well. The latter is affected by traffic dynamics. Traffic signal controls at intersections play a significant role in governing traffic dynamics and

will in turn impact the distributed monitoring system. The performance of the monitoring framework is investigated with different g/C ratios under multiple traffic scenarios.

With the distributed traffic monitoring and platoon information aggregation system, platoons can be dynamically identified on the network in real time. This enables a platoon-based automated intersection control system for connected and autonomous vehicles. An exploratory study on such a control system with two control stages are proposed. At Stage I, vehicles of each platoon will synchronize into a target speed through cooperative speed harmonization. Then, a platoon of vehicles with the same speed can be treated as a single vehicle for speed profile planning at Stage II. Its speed profile will be immediately determined given speed profiles of other platoons and the control goal.

DEDICATION

To

My Parents

Mr. Li, Xiande and Mrs. Wang, Caixia

and

My Brother

Mr. Li, Yiheng

ACKNOWLEDGMENTS

This work would not have been possible without the advice and support of many people. First and foremost, I would like to thank my advisor Dr. Yingyan Lou for providing me the great opportunity to pursue my master and Ph.D. in civil engineering in the U.S. She has been a great advisor and a good friend throughout my whole graduate studies in the past six years. I am very grateful to Dr. Xuesong Zhou for his great guidance in transportation network modeling and his kind support of my career path in the field of operations research. I would like to thank Dr. Pitu Mirchandani for being a mentor to guide me throughout the world of optimization and his valuable suggestions to this dissertation. Many thanks go to Dr. Jay Lindly for his great advice through my master study and his tremendous help improving my English. I would also like to thank Dr. Steven Jones for his guidance, which leads to my very first publication on a top journal. Special thanks to Dr. Xiangjun Cheng for being a great mentor since my undergraduate study in China. Great thanks go to Bob Sandel, Becky Sandel, Tommy Raburn, and Maggie Raburn for being my host families and their love. I am also very grateful to Drs. Chen and Yuan for their kind help during my initial setup in the U.S. Very special thanks to Peiyao Zhang for her great emotional support in the past three years and for helping me rehearse my dissertation presentation.

I would also like to thank all my friends and fellow students for making my graduate studies experience pleasant and enjoyable, especially Drs. Xiong Yuan, Changgeng Feng, Dr. Zhonghai Deng and his family, Dr. Yuguang Wei, Sravani Vadlamani, Jiangtao Liu, Tie Shi, Dr. Jinjin Tang, Jun Xiao, Dr. Jianrui Miao, Hossein Jalali, Dr. Jing Li, Monireh

Mahmoudi, Joshua Frisby, Dr. Pengfei Li, Frances Green, Golnoosh Miri, Drs. Kofi Adanu, Gaurav Mehta, Abhay Lidbe, Lu Tong, Venu Garikapati, Padmini Gudipudi, Yunchao Qu, Junhua Chen, Dae Hyun You, and Sumanta Das.

Finally, I would like to express my acknowledgements to everyone who helped me during my Ph.D. study and in my life.

TABLE OF CONTENTS

Page

LIST OF FIGURES

Figure Page

Figure Page

Figure Page

LIST OF TABLES

Table Page

CHAPTER 1

INTRODUCTION

Connected vehicle (CV) technologies employ dedicated short-range communications (DSRC) at 5.9GHz to enable safe, interoperable networked wireless communications among equipped vehicles, infrastructure, and passengers' personal communication devices (USDOT, 2015). The rapid advancements of CV technologies have enabled both safety and mobility applications that utilize vehicle-to-infrastructure (V2I) and vehicle-to-vehicle (V2V) communications.

With CV technologies on the horizon, we envision an alternative / supplemental traffic operations system for transportation networks, supported solely by V2V DSRC. The envisioned system is not meant to replace existing traffic operation practices based on current roadway and intelligent transportation system (ITS) infrastructures, or the slew of emerging ITS's exploiting V2I communications, but rather as an alternative or supplemental system that is particularly suitable under abnormal traffic scenarios caused by extreme and special events. These events, such as unforeseen disasters and emergency evacuation or major sport and culture occasions, can cause unusual traffic volume and irregular spatial distribution of vehicles in transportation networks. A major disaster often paralyzes cities for an extended period, not only because of physical damages to roadway infrastructures, but also the lack of coordinated traffic control as existing traffic operation infrastructures may suffer damages as well. V2I systems or even V2V systems that rely on infrastructure (such as cellular communication technologies) may not function well either due to the same reason. V2V DSRC systems, however, would withstand this

situation as long as vehicles are running in the network. On the other hand, the unusual traffic volume and patterns caused by special events may not be readily handled by existing traffic operation systems, and can add extreme stress to communication infrastructures (such as cellular base stations) due to demand surge. V2V DSRC systems, again, could prevail in this situation without causing excessive communication overhead. Therefore, we believe traffic operation and management systems based solely on V2V DSRC are a relevant concept worth investigating.

In this study, we propose a self-sustained traffic operations system which is solely based on V2V DSRC. First, a distributed traffic monitoring and platoon information aggregation framework, which consists of distributed traffic monitoring for platoon identification and cooperative platoon information aggregation, is presented in Chapter 3. The system performance on freeway is evaluated in terms of effectiveness and accuracy under different scenarios. With the presence of traffic controls, the performance of the monitoring system is different with that on freeway. Thus, Chapter 4 analyzes the impact of traffic signal controls on the performance of the traffic monitoring and platoon information aggregation system. This framework allows traffic monitoring and platoon information provision to be carried out in a localized, distributed, and cooperative manner and is capable of supporting cooperative traffic operations strategies. Therefore, a platoon-based automated intersection control is explored in Chapter 5. It followed by a conclusion and future research in Chapter 6.

CHAPTER 2

BACKGROUND

ITS has been involved in almost every aspect of our transportation systems since the first deployment of three-colored traffic signal in Ohio in 1914 (USDOT, 2016). Currently, high occupancy toll lanes, adaptive traffic signal controls (e.g. Split Cycle Offset Optimization Technique (SCOOT), Sydney Coordinated Adaptive Traffic System (SCATS), Real Time Hierarchical Optimized Distributed Effective System (RHODES), etc.) (Federal Highway Administration, 2017), dynamic message signs, route guidance/navigation systems are some of the major ITS applications.

Communication technologies are underlying the recent fast development of ITS. After the Federal Communications Commission allocated 75MHz of spectrum in the 5.9 GHz band to the transportation sector for ITS in 1999, the United States Department of Transportation (USDOT) Initiative "a 5.9 GHz-based vehicle-infrastructure-integration (VII) proof of concept" in 2005 initiated the era of CV (USDOT, 2016).

CV technologies leads to improved traffic safety through in-vehicle warning. Safety applications of CV includes forward collision warning (FCW), blind spot/lane change warning (BSW/LCW), reduced speed/work zone warning, red light violation warning and so on (USDOT, n.d.). As one of the three pilot sites in the CV Pilot Deployment Program, the Wyoming DOT pilot concentration on applying CV technologies to address blow-over incidents and weather-related incidents of commercial vehicles along I-80 to improve safety and truck movements. It has entered into the design/build/test phase starting from 2016 (USDOT, n.d.).

On the other hand, CVs can benefit traffic mobility as a mean of collecting and disseminating enhanced traffic information and alters, which are key inputs to existing traffic operations and management strategies (e.g., signal priority for freight and transit, emergency vehicle preemption, dynamic speed harmonization, queue warning, etc.) (USDOT, n.d.). One recent example is the Federal Highway Administration pooled fund study Multi-Modal Intelligent Traffic Signal Systems (MMITSS) (USDOT, n.d.). MMITSS are a set of traffic systems that seeks to provide a comprehensive traffic information framework to service all modes of transportation, including general vehicles, transit, emergency vehicles, freight fleets, and pedestrians and bicyclists in a CV environment (Head, 2013).

Some of the state-of-art of CV applications aim at addressing traffic safety and traffic mobility simultaneously. For example, the New York City DOT pilot exploits V2V and intersection communications to improve vehicle flow and pedestrian safety in high-priority corridors, while the Tampa pilot focuses on congestion and collisions mitigation, and wrong way entry prevention through deploying CV technology on and in proximity to reversible freeway lanes (USDOT, 2015, n.d.).

Vehicles with autonomous driving features and CV communication capacity are also the trend of ITS (e.g. 2018 Cadillac CT6 (Trop, 2017)). These capabilities enable some cooperative maneuvers among equipped vehicles, such as cooperative adaptive cruise control (CACC) (USDOT, n.d.). Furthermore, automated intersection control without traditional signal controllers/lights is made possible with such vehicles (Dresner and Stone, 2008, 2004).

The framework explored in this study concentrates on improving traffic mobility using V2V communications only through dynamically identifying platoons, cooperatively synchronizing vehicular speeds within platoons, collaboratively manipulating the speed profiles of platoons to enable a platoon-based automated intersection control.

CHAPTER 3

A DISTRIBUTED TRAFFIC MONITORING AND PLATOON INFORMAITON AGGREGATION FRAMEWORK

As a mobility application of CV, traffic monitoring and platoon information provision are two essential functional requirements of such a system. Constantly monitoring the traffic condition in a transportation network will enable traffic-responsive transportation operation methods that are generally more effective. With the exception of individual intersection control at a very fine detailed level, aggregate vehicular traffic pattern is often a more common and ready-to-use input to transportation operations. For example, prevailing vehicular flow rate and speed at certain locations and the evolution of vehicle queue formation in a road network is often more important than individual vehicle trajectories for arterial management and operations. On the other hand, due to communication limitations such as communication bandwidth and reliability, as well as the storage and processing capacity of (mobile and some undamaged fixed) relay and control infrastructure, not all vehicles will be able to, nor shall they do, communicate with the infrastructure individually. (This precludes machine learning or statistical classification as potential platoon identification methods as they are centralized in nature and require large amount of training data.) Therefore, the essential traffic monitoring and platoon information provision to the envisioned system must be carried out in a localized, distributed, and cooperative manner.

3.1 Related Work

The focus of the literature review in this chapter is on emerging traffic monitoring and information processing methods exploiting connected vehicle technologies. Existing research can be categorized into two groups based on whether infrastructure (both transportation and communications) is involved or not.

When supporting infrastructure is considered, V2I and other communication networks (e.g. GPS-enabled mobile phones) are the predominant underlying technologies. In this case, centralized approaches are adopted by many, if not all, previous studies. Centralized approaches rely on roadside equipment (RSE) or a server to communicate with each equipped vehicle to gather and process traffic information. For example, different methodologies have been proposed to estimate queue length at signalized intersections using probe vehicle data including travel times (Ban et al., 2011), vehicle positions (Comert and Cetin, 2011, 2009) and trajectories (Hao and Ban, 2013). Positions from probe vehicles have also been combined with signal timing plans (event-based data) to detect possible queue spillback (Christofa et al., 2013; Li et al., 2013). In He et al. (2012), a queue at an intersection is considered as a stopped platoon, and a pseudo-platoon recognition algorithm was developed based on critical headway. The estimated queue and platoon information can be used to adjust signal timings (Christofa et al., 2013; Feng et al., 2015; He et al., 2012). Goodall et al. (2013) proposed to tie individual vehicle information collected through V2I communications within an intersection into a real-time simulation-in-the-loop traffic signal timing optimization program. It can be seen from the aforementioned studies that, due to the requirement of RSE or the limited bandwidth of

other communication networks (e.g., cellular network), mobility applications of the centralized approaches are limited to intersections, or otherwise relatively small areas.

Vehicular ad hoc network, on the other hand, does not require RSE or other communication infrastructures. It is intensively based on V2V communications and distributed computing. One of its major applications is traffic condition monitoring and information dissemination (e.g. Fukumoto et al, 2007). However, each individual vehicle periodically transmitting its local vehicular traffic information in addition to broadcasting general beacons may result in additional communication load. To relief the potential communication overload, a "need to say" principle is usually adopted (Dornbush and Joshi, 2007). Therefore, information aggregation and dissemination is restricted to extreme conditions such as traffic congestion or incidents (Bauza et al., 2010; Lakas and Cheqfah, 2009; Lin and Osafune, 2011; Terroso-sáenz et al., 2012; Vaqar and Basir, 2009). These works often adopt data aggregation as an additional approach to reducing communication load. Generally, each vehicle would periodically estimate its local congestion level from received beacons. The congestion level is usually measured by density (Fukumoto et al., 2007; Terroso-sáenz et al., 2012), speed (Lin and Osafune, 2011), or travel time (Lakas and Cheqfah, 2009), etc. Bauza et al. (2010) adopted a fuzzy logic to determine local congestion level using both density and speed. Each vehicle then compares its local congestion level with a predefined threshold to determine whether to trigger information aggregation or not. Once triggered, a cooperative protocol will assemble and pass on aggregate information about the congestion encountered, including its position, size and congestion level, instead of the local traffic condition from each individual vehicle (e.g. Bauza et al., 2010). One limit of the "need to say" principle is that

no information is available for uncongested sections of the road. However, both uncongested (especially near capacity) and congested traffic states are valuable to mobility applications for large and complex transportation networks. Huang et al. (2010) also proposed a distributed congestion detection and prediction algorithm. Unlike other studies, it employs the concept of shockwave and is only applicable to merging bottlenecks. Furthermore, all of the above studies assumed 100% market penetration rate (MPR). At the early stage of CV implementations, a relatively low MPR is expected and it is important that any proposed distributed algorithms would work relatively well under such a condition.

The new framework proposed in this chapter has many benefits from previous research without suffering from some of the drawbacks. A platoon identification approach takes advantage of traffic flow theory. Aggregated traffic information under both uncongested and congested conditions is monitored and reported for the entire road network. A contention-based forwarding protocol reduces the communication overhead. The proposed framework also performs relatively well even under low MPRs.

3.2 Methodologies

The proposed framework will consist of two major components: 1) distributed traffic monitoring for platoon identification and 2) cooperative platoon information aggregation. The former involves two processes: micro-discontinuity detection and self-correction; and the latter three: initiation, re-transmission, and termination.

3.2.1 Distributed Platoon Identification

A platoon is a group of vehicles with similar states. This simple statement is in fact ambiguous: the terms “similar” and “state” are both subject to interpretation. To identify a platoon, the metric(s) to determine “state” and the threshold(s) to define “similar” must be specified.

Space and time headway measures such as critical and cumulative headways are often adopted as metrics for platoon recognition both in the literature (Chaudhary et al., 2003; He et al., 2012; Jiang et al., 2006) and in practice. Most of such approaches require infrastructure, and are not able to effectively pinpoint vehicular traffic state variation. As Huang et al. (2010) pointed out, individual headways may fluctuate substantially even among a group of vehicles with the same speed. In this case, using headway as the metric would likely result in significantly more platoons being reported than necessary. Therefore, except for intersection signal timing, headways are not suitable as the metric for platoon identification.

Alternatively, if we consider a platoon as a group of vehicles with similar states, then two adjacent platoons should display different traffic states, in terms of both platoon density and speed. The boundary vehicles of the two platoons should be able to detect such difference, which we term micro-discontinuity to differentiate it from the concept of shockwave (Lighthill and Whitham, 1955; Richards, 1956; Stephanopoulos et al., 1979) in macroscopic traffic flow theory. Thus, platoon identification becomes micro-discontinuity identification, and the problem now lends itself very well to distributed computing based on V2V DSRC.

Micro-Discontinuity Detection

In first-order continuum traffic flow models (Jin and Yang, 2013; Lighthill and Whitham, 1955; Richards, 1956), the vehicular traffic state at location x and time point t, denoted by $s(x,t)$, is defined by two field functions: density $k(x,t)$ and speed $v(x,t)$. The models are macroscopic in nature, and describe traffic dynamics with a partial differential equation. Shockwaves represent abrupt changes in the traffic state over continuous space and time, and are in fact mathematical discontinuities in these macroscopic models.

Due to limited communication range, the proposed distributed traffic state monitoring is conducted at a microscopic level. Therefore, direct application of the concept of shockwave from continuum traffic flow models is inappropriate, and a new methodology is needed to quantitatively define micro-discontinuity.

For an equipped vehicle i, denote its down- and up-stream traffic states at the n^{th} time interval as $s(x_i^d, n\Delta t)$ and $s(x_i^u, n\Delta t)$, where x_i^d and x_i^u represent the lengths of road fragments in consideration down- and up-stream. The choice of x_i^d and x_i^u will be discussed later, but they must be within the communication range of vehicle i.

$$s\left(x_i^d, n\Delta t\right) \coloneqq \begin{cases} k\left(x_i^d, n\Delta t\right) = \dfrac{|N_i^d(n\Delta t)|}{x_i^d} \\ v\left(x_i^d, n\Delta t\right) = \dfrac{1}{\left|N_i^d(n\Delta t)\right|} \displaystyle\sum_{j \in N_i^d(n\Delta t)} v_j\,(n\Delta t) \end{cases} \tag{3.1}$$

where $N_i^d(n\Delta t)$ is the subset of vehicles which are in x_i^d at time $n\Delta t$, and $|\cdot|$ denotes cardinality. $v\left(x_i^d, n\Delta t\right)$ is in fact the space-mean speed. Note that $s(x_i^u, n\Delta t)$ is defined

similarly, and vehicle i itself is not included in $s(x_i^d, n\Delta t)$ or $s(x_i^u, n\Delta t)$. We further define the following variables:

$$\Delta_v(i, n\Delta t) := v(x_i^u, n\Delta t) - v\left(x_i^d, n\Delta t\right) \tag{3.2}$$

$$\Delta_k(i, n\Delta t) := k(x_i^u, n\Delta t) - k\left(x_i^d, n\Delta t\right) \tag{3.3}$$

The metric for micro-discontinuity detection is subsequently defined as $\Delta_s(i, n\Delta t) := |\Delta_v(i, n\Delta t)| + |\Delta_k(i, n\Delta t)|$, which is the 1-norm of vector $\left(\Delta_v(i, n\Delta t), \Delta_k(i, n\Delta t)\right)$. Vehicle i is said to have detected a micro-discontinuity if $\Delta_s(i, n\Delta t)$ is greater than a predefined threshold value Δ (to be discussed later). It will then set a flag $f(i, n\Delta t)$ in its own memory for future computation. Common cases of micro-discontinuity can be observed when a queue is being formed or discharged, in a moving bottleneck, and a group of loosely spaced vehicles traveling at similar speeds etc.

Since a platoon is uniquely defined by a lead and an anchor vehicle, we further differentiate a lead micro-discontinuity flag from an anchor flag, and an isolated vehicle is considered a special micro-discontinuity. The following pseudocode describes the identification process.

process *micro-discontinuity identification* // each vehicle i performs this process at time $n\Delta t$

begin

set $f(i, n\Delta t) = 0$;

calculate $\Delta_s(i, t)$;

if $(\Delta_s(i, t) \geq \Delta \; and \; \Delta_k(i, t) > 0) \; or \; (\left|N_i^d(t)\right| = 0 \; and \; |N_i^u(t)| > 0)$ **then**

$f(i, t) = 1$; // lead vehicle

if $(\Delta_s(i,t) \geq \Delta \; and \; \Delta_k(i,t) < 0) \; or \; (|N_i^u(t)| = 0 \; and \; |N_i^d(t)| > 0)$ **then**

$f(i,t) = -1$; // anchor vehicle

if $|N_i^d(t)| = |N_i^u(t)| = 0$ **then**

$f(i,t) = 2$; // isolated vehicle

end;

In the above pseudocode, the values of x_i^d, x_i^u and Δ need additional specification. The determination of Δ is further related to consecutive and missing micro-discontinuity flags of the same type.

Computation Radius

Although x_i^d and x_i^u can take any value, it is essential to a distributed algorithm that these values stay constant across individual vehicles. Denote $r_c = x_i^d = x_i^u$ as the computation radius for traffic state determination. Obviously, the communication range of CV's, r (usually from 200 to 300 meters for DSRC), is the upper bound of r_c. Existing research on congestion detection based on vehicular ad hoc networks does not differentiate r_c from r, and usually set $r_c = r$ (Bauza et al., 2010; Fukumoto et al., 2007). However, the communication range is often too large for the distributed algorithm to detect sizable headways within the range. For example, suppose all vehicles are traveling at constant speed v, and there is a sizeable headway between vehicles j and k. From a traffic operations perspective (for example, traffic signal timing), it is possible that these vehicles should be treated as two platoons. But with $r_c = r$, vehicles k and j may not detect any difference between their downstream and upstream traffic conditions, and would consider themselves as part of a single platoon. To avoid this problem, r_c is set to 50 meters in this study. This is not to say that the minimum space headway the algorithm

is able to detect is 50 meters. We will further demonstrate this in Section 3.3 Simulation Results.

Consecutive and Missing Micro-Discontinuity Flags

It is possible that multiple consecutive vehicles within close vicinity will flag the same type of micro-discontinuity. An example of a queue being formed is shown in Figure 3-1 where the first three stopped vehicles all flag lead micro-discontinuity. With $r_c = 50\text{m}$ and no vehicle further downstream, vehicles 1 – 3 could all detect a much more congested traffic state upstream, and flag themselves as the lead.

On the other hand, it is also possible that vehicles at the boundaries of potential platoons may not flag themselves as micro-discontinuities. As shown in Figure 3-1, vehicle k is supposed to be the lead of the vehicle platoon consisting of vehicles k to l, but it did not flag itself as a discontinuity since its downstream and upstream traffic states are very similar.

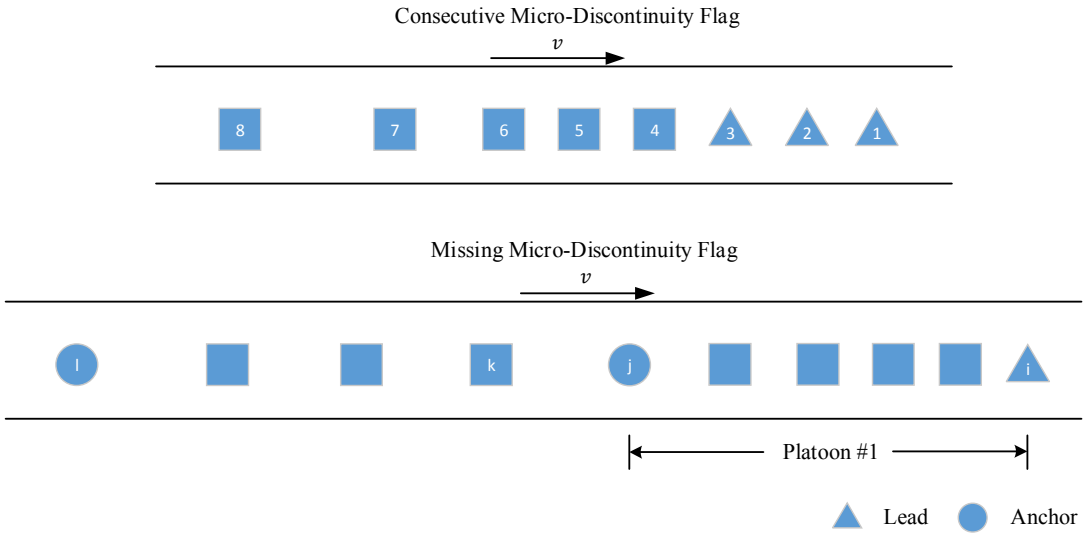

Figure 3-1 Consecutive and Missing Micro-Discontinuity Flags

Such consecutive and missing discontinuity flags cause problems in the determination of vehicle groups, and should be resolved and avoided if possible. To reduce the number of consecutive flags generated, the value of the threshold Δ should be chosen carefully. Furthermore, to clean up consecutive and correct missing flags when they do occur, a self-correcting mechanism is proposed.

Threshold Δ

A good threshold should allow us to correctly identify potential micro-discontinuities while minimizing the number of consecutive discontinuities. The value of Δ is related to the computation radius r_c. We performed a series of tests using microscopic traffic simulation to find a good threshold value with $r_c = 50$m. A straight single-lane road segment was built in VISSIM 6 for this purpose. Different free-flow speeds (FFS's) from 40 km/h to 120 km/h were tested. Figure 3-2 shows the cumulative density function (CDF) of Δ_s computed by all simulated vehicles over a 200-second simulation. It can be seen that regardless of the FFS, the increase of the CDFs becomes gradual and smooth when $\Delta_s \geq 75$, which is approximately the 70th-percentile value. In other words, if $\Delta = 75$, about 30% of vehicles will flag themselves as micro-discontinuities. A manual check confirmed that when $\Delta = 75$, the issue of consecutive micro-discontinuity flags of the same type is not pronounced. It is also possible to adopt any value higher than 75 as a potential threshold. However, a rather high threshold value may lead to a very low identification rate of potential micro-discontinuities (and thus platoons). In this sense, Δ=

75 is a reasonable threshold. Note that we do not intend to find an "optimal" Δ in this study, as there is arguably a well-defined optimality condition.

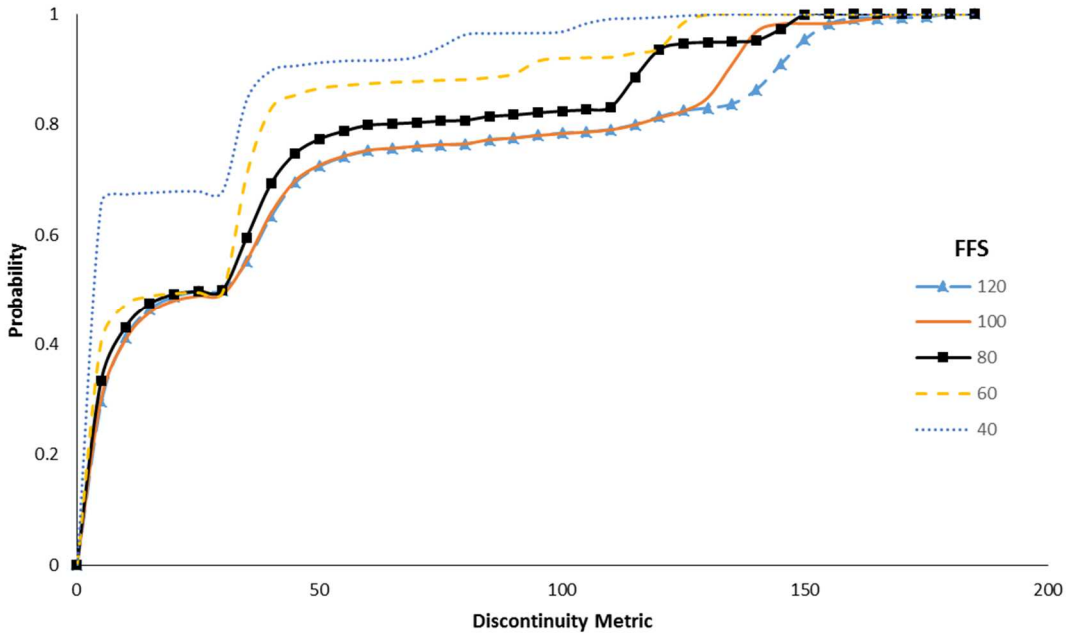

Figure 3-2 CDFs of Calculated Discontinuity Metric

Self-Correcting Mechanism

Even with a carefully-chosen threshold value, consecutive and missing micro-discontinuity flags may still occur due to intrinsic randomness in traffic. To resolve these problems, a self-correcting mechanism is proposed.

The micro-discontinuity identification process is performed every time interval. In this study, the interval Δt is set to one second. A small time lag ε, $\varepsilon \ll \Delta t$, after the process is finished, each vehicle will launch the self-correcting mechanism to check the status of its immediate downstream (if itself is a lead) or upstream (if itself is an anchor) vehicle, if

there is any vehicle within its computation range. If the other vehicle has 1) no flag, the vehicle will send a message to the other vehicle to correct the missing flag; 2) same type of flag, the vehicle simply removes its own flag; 3) a different type of flag, the vehicle does nothing. This is equivalent to setting the first (last) vehicle with a lead (an anchor) flag the actual lead (anchor) of the platoon. The following pseudo code details the self-correcting mechanism. For convenience, assume vehicles are numbered ascendingly from downstream to upstream.

process *self-correcting mechanism* //every vehicle i performs this process at time $n\Delta t + \varepsilon$

begin

if $f(i, n\Delta t) \neq 0$ **then**

if $f(i, n\Delta t) = 1$ and $\left|N_i^d(n\Delta t)\right| > 0$ **then**

//check the flag status of its immediate downstream vehicle $f(i-1, n\Delta t)$

if $f(i-1, n\Delta t) = 0$ **then** // no anchor

send message $Anchor(i-1, n\Delta t)$ to vehicle $i-1$ and set $f(i-1, n\Delta t) = -1$;

if $f(i-1, n\Delta t) = 1$ **then** // consecutive leads

set $f(i, n\Delta t) = 0$;

if $f(i, n\Delta t) = -1$ and $|N_i^u(n\Delta t)| > 0$ **then**

//check the flag status of its immediate upstream vehicle $f(i+1, n\Delta t)$

if $f(i+1, n\Delta t) = 0$ **then** // no lead

send message $Lead(i+1, n\Delta t)$ to vehicle $i+1$ and set $f(i+1, n\Delta t) = 1$;

if $f(i+1, n\Delta t) = -1$ **then** // consecutive anchors

set $f(i, n\Delta t) = 0$;

end;

3.2.2 Traffic Information Aggregation

Once platoons are identified, a contention-based cooperative multi-hop protocol is developed to make sure that platoon information is aggregated in the most effective and accurate manner with minimum communication overhead. The identified lead vehicles will start a cooperative traffic information aggregation protocol, a process of forwarding and aggregating local traffic information through multi-hop V2V DSRC. This process could be initiated at time $n\Delta t + 2\varepsilon$. Figure 3-3 provides an illustration of the concept.

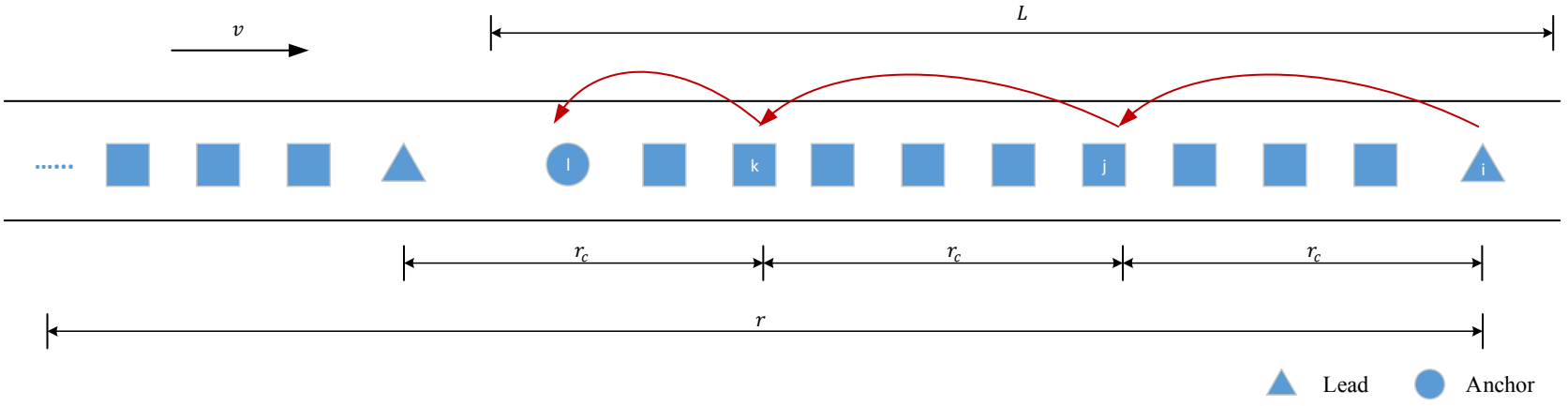

Figure 3-3 Information Aggregation

The local information forwarding during an aggregation process will follow "the most forwarded within-range" manner (Jin and Recker, 2006). As shown in Figure 3-3, the local information computed by the lead vehicle i will be forwarded to the furthest upstream vehicle j within its computation range r_c, processed by vehicle j to incorporate the local information computed by vehicle j, forwarded again in a similar manner, and finally terminated at the anchor vehicle l of the group.

In order to achieve this, a modified contention-based forwarding protocol is proposed based on methods described in Füßler et al. (2003) and Bauza et al. (2010). A lead vehicle i will first broadcast the initial aggregation request $aggInfo(i, i, n\Delta t)$ with its local traffic information. In this notation, the first argument denotes that the message is sent by vehicle i; later this argument will be updated according to the relaying vehicle j of this message. The second and third arguments indicate that the aggregation request is originally initiated by lead vehicle i for traffic information at time $t = n\Delta t$. A pseudocode is provided below detailing the content of $aggInfo(j, i, n\Delta t)$.

message $aggInfo(j, i, n\Delta t)$

begin

> ***version*:** version number to document updates in the aggregation process, equals to 1 when first broadcasted by a lead vehicle i;
>
> ***time stamp*:** time of last update of $aggInfo(i, n\Delta t)$, equals to $n\Delta t$ when first broadcasted by a lead vehicle i;
>
> ***lead vehicle info*:** lead vehicle ID (i) and position;

***sending vehicle info*:** sending vehicle ID (j) and position;

***local traffic info*:** length, aggregated density and speed of the vehicle platoon led by vehicle i;

end;

In fact, when a lead vehicle i sends $aggInfo(i, i, n\Delta t)$, every vehicle within its communication range r (both down- and up-stream) will receive the message. Downstream vehicles, as well as upstream vehicles beyond r_c should simply discard the cooperative aggregation request. The latter is because the local traffic information from vehicle i is valid only for the computation range r_c. Among the upstream vehicles, only vehicle j, the furthest within vehicle i's computation range needs to process and relay the information. It is possible for vehicle j to receive multiple aggregation requests simultaneously from downstream, and these requests will be stored in a re-transmission queue. If this is the case, only the request from the closest lead / relaying vehicle is considered to be active and all other requests will be discarded. If the anchor vehicle l of the platoon led by i is within r_c from vehicle i but not the furthest in this range, the anchor vehicle should broadcast a termination message $terminate(l, i, n\Delta t)$ right away with a reasonably small time lag. Once other vehicles receive this termination message, they will discard $aggInfo(i, i, n\Delta t)$ before it is time for any of them to relay the information. To achieve this, each upstream vehicle j within r_c of vehicle i will set a distance-based timer for re-transmitting $aggInfo(i, i, n\Delta t)$ or terminating the process:

$$timer(i,j,n\Delta t) = \begin{cases} \dfrac{1}{distance(i,j,n\Delta t)} & if\ f(j,t) = 0 \\ \dfrac{1}{distance(i,j,n\Delta t) + r_c} & if\ f(j,t) = -1 \end{cases} \quad (3.4)$$

The pseudocodes below describe the initiation, re-transmission, and termination processes of the cooperative information aggregation protocol respectively. The re-transmission process also involves a sub-process that updates the aggregated traffic information. Details of this sub-process is further discussed at the end of this section.

process *initiate aggregation* // each lead vehicle i performs this process at time $n\Delta t + 2\varepsilon$

begin

if $f(i,n\Delta t) = 1$ **then**

generate message $aggInfo(i,i,n\Delta t)$;

broadcast cooperative aggregation request $aggInfo(i,i,n\Delta t)$;

end;

process *re-transmit* // each vehicle k performs this process upon receiving $aggInfo(j,i,n\Delta t)$ at time t

begin

if $t \in (n\Delta t + 2\varepsilon, n\Delta t + \Delta t)$ and $k \in N_j^u(n\Delta t)$ **then**

set Boolean $isupdate(j, i, n\Delta t) =$ false;

if the re-transmission queue of vehicle j is empty **then**

$isupdate(j, i, n\Delta t) =$ true;

else

// if multiple *aggInfo* messages from different downstream lead vehicles are received by vehicle k

if vehicle i is closer to k than any other lead vehicle p with $aggInfo(q, p, n\Delta t)$ in the re-transmission queue of vehicle k **then**

$isupdate(j, i, n\Delta t) =$ true;

discard $aggInfo(q, p, n\Delta t), \forall p$ further downstream of i;

// if multiple *aggInfo* messages from the same downstream lead vehicle but different downstream relay vehicles are received by vehicle k

if vehicle j is closer to k than any other relay vehicle q with $aggInfo(q, i, n\Delta t)$ in the re-transmission queue of vehicle k **then**

$isupdate(j, i, n\Delta t) =$ true;

discard $aggInfo(q, i, n\Delta t), \forall q$ further downstream of j;

// vehicle k is the next relay vehicle and the message $aggInfo(j, i, n \triangle t)$ will be updated up to vehicle k

if $isupdate(j, i, n\Delta t) ==$ true **then**

call **process** *aggInfoUpdate* to revise **message** $aggInfo(j, i, n\Delta t)$ to **message** $aggInfo(k, i, n\Delta t)$;

if $f(k, n\Delta t) = 0$ **then**

set $timer(j, k, n\Delta t) = \frac{1}{distance(j,k,n\Delta t)}$;

store **message** $aggInfo(k, i, n\Delta t)$ in the re-transmission queue of vehicle k for broadcasting at $t + timer(j, k, n\Delta t)$;

if $f(k, n\Delta t) = -1$ **then**

set $timer(j, k, n\Delta t) = \frac{1}{distance(j,k,n\Delta t)+r_c}$;

store **message** $termInfo(k, i, n\Delta t)$ in the re-transmission queue of vehicle k for broadcasting at $t + timer(j, k, n\Delta t)$;

else discard $aggInfo(j, i, n\Delta t)$;

else discard $aggInfo(j, i, n\Delta t)$;

end;

process *terminate* // each vehicle k performs this process upon receiving $termInfo(l, i, n\Delta t)$ at time t

begin

if $t \in (n\Delta t + 2\varepsilon, n\Delta t + \Delta t)$ **then**

discard $aggInfo(j, i, n\Delta t), \forall j$ in the re-transmission queue of vehicle k;

else discard $termInfo(l, i, n\Delta t)$;

end;

When updating the message $aggInfo(j, i, n\Delta t)$ to $aggInfo(k, i, n\Delta t)$, vehicle k would first check the version number of $aggInfo(j, i, n\Delta t)$. Denote this version number as m, which is in fact the number of hops performed so far. Denote the length of the vehicle platoon up to the m^{th} ($m \geq 1$) update as L_m. For the $(m+1)^{th}$ update being performed by vehicle k,

$$L_{m+1} = L_m + distance(j, k, n\Delta t) \tag{3.5}$$

where j is the previous, and k the current, sending vehicle of the message. Note L_1 (i.e., $m = 1$) is the distance between the lead vehicle and the front virtual boundary of the platoon (see Figure 3-4). If vehicle k is the anchor vehicle of the platoon led by vehicle i, then the $(m+1)^{th}$ update is also the last update, and

$$L_{m+1} = L_m + distance(j, k, n\Delta t) + L_{-1} \tag{3.6}$$

where L_{-1} is the distance between the anchor vehicle and its rear virtual boundary. The determination of L_1 and L_{-1} is not trivial. In the case as shown in Figure 3-4, if the distance between an anchor vehicle j and a lead vehicle k is less than $2r_c$, the virtual

boundary (the actual separation) of the two adjacent platoons is defined as the middle point between the two boundary vehicles. In this case, L_1 for the second platoon is the same as L_{-1} of the first platoon, equal to half the distance between vehicle k and vehicle j. The final lengths of the two platoons are L and L' as seen in Figure 3-4.

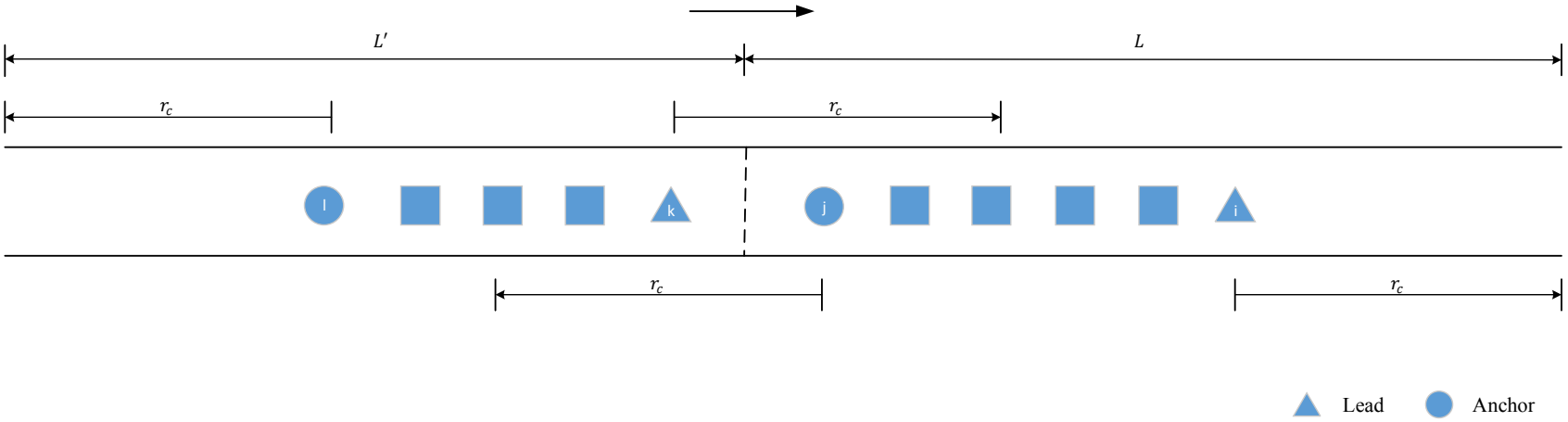

Figure 3-4 Illustration of Calculating Vehicle Platoon Lengths

The total number of vehicles in the group is updated as

$$Num_{m+1} = Num_m + Num(j, k, n\Delta t) \tag{3.7}$$

where $Num(j, k, n\Delta t)$ is the number of vehicles between vehicles j (excluding j) and k (including k) at time $n\Delta t$, and $Num_1 = 1$.

The group density after the $(m+1)^{th}$ hop is calculated as

$$GD_{m+1} = \frac{Num_{m+1}}{L_{m+1}} \tag{3.8}$$

For an isolated vehicle, there is only itself in the group and the group density is defined as

$$GD_1 = \frac{1}{L_{-1} + L_1} \tag{3.9}$$

Similarly, the average speed of the platoon is updated as follows:

$$GS_{m+1} = \frac{Num_m \cdot GS_m + \sum_{p=j+1}^{k} v_p(n\Delta t)}{Num_{m+1}} \tag{3.10}$$

The initial average speed is essentially the speed of the lead/isolated vehicle i at time $t = n\Delta t$, i.e., $GS_1 = v_i(n\Delta t)$.

The following pseudocode shows the process of updating aggregation information, which is a sub-routine of the information forwarding process (process *re-transmit*).

process *aggInfoUpdate*// performed by relaying and / or terminating vehicles k as a sub-process of **process** *re-transmit*

begin

$m = m + 1$;

If $f(j, n\Delta t) = 0$ **then**

$L_m = L_{m-1} + distance(j, k, n\Delta t)$;

If $f(j, n\Delta t) = -1$ **then**

$L_m = L_{m-1} + distance(j, k, n\Delta t) + L_{-1}$;

$Num_m = Num_{m-1} + Num(j, k, n\Delta t)$;

$GD_m = \frac{Num_m}{L_m}$;

$GS_m = \frac{Num_{m-1} \cdot GS_{m-1} + \sum_{p=j+1}^{k} v_p(n\Delta t)}{Num_m}$;

end;

Upon termination of the information aggregation protocol, the group density, average speed, number of vehicles, and length will be available immediately. The aggregated information can be disseminated to all vehicles on the network and signal controllers through multi-hop V2V communications. Such information dissemination is beyond the scope of this study and will be explored in our future research.

3.3 Simulation Results

The proposed framework is implemented in Visual Basic with a microscopic traffic simulation package VISSIM and its built-in component object model (COM). Two types of traffic conditions, stable traffic and queueing, are simulated and analyzed in this study. A one-lane segment is used for our experiments. We further analyzed the impacts of

MPR on the performance of our proposed framework under both stable and queueing traffic.

3.3.1 Platoon Detection

For stable traffic, the single-lane road segment is simulated as a freeway section without any merges or diverges. The proposed distributed framework is able to identify vehicle platoons in a reasonable manner. Stable traffic in Figure 3-5 shows snapshots of the road segment in 5 consecutive seconds. Blue rectangles represent vehicles that did not flag traffic discontinuity. Green and red rectangles are vehicles self-identified as leads and anchors, respectively. In this stable-traffic experiment, no consecutive flags of the same type are reported. As shown in the top subfigure in Figure 3-5, there are two vehicle platoons at $t = 0, 1, 4$ second. At $t = 2$ and 3 second, the fourth vehicle from downstream reported itself as an isolated vehicle (shown in black) since there was no vehicle within its computation range both up- and down-stream. Note that at $t = 4$ second, this vehicle became the anchor of the first vehicle platoon as it got closer to the first three vehicles. One noteworthy observation is that in stable traffic, the speeds of different vehicles are similar, and vehicle positions/headways (and thus densities) largely affect identified platoons.

Queueing scenarios present more complicated traffic conditions where multiple consecutive flags of the same type may occur. The proposed framework is able to resolve this issue with the self-correcting mechanism and identify reasonable vehicle platoons. The bottom two subfigures in Figure 3-5 are results from an experiment with a traffic signal at the immediate downstream of the simulated segment. They are snapshots of 11

consecutive seconds during which the signal was red and a queue was being formed. For the first two seconds ($t = 65, 66$), only one vehicle group is reported with a single lead and a single anchor. Starting from $t = 67$ second, multiple consecutive discontinuity flags of the same type were reported (see Before Self-Correction in Figure 3-5). As the first several vehicles pulled into full stop, they all identified themselves as leads. This is because the average upstream density within their computation range is higher comparing to the downstream traffic, and so is speed as there was no vehicle further downstream of the signal. At $t = 71$ second, vehicle 6 flagged itself as an anchor. In the next 5 seconds, multiple consecutive anchor flags were reported by vehicles 6 – 9 as they joined the queue. Two problems were raised in this particular scenario: 1) multiple consecutive discontinuity flags of the same type, and 2) no vehicle flagged itself as an anchor (lead) immediately downstream (upstream) of the group of multiple lead (anchor) flags. These problems, however, are successfully addressed by the self-correction mechanism as part of the proposed framework (see After Self-Correction of Figure 3-5).

Figure 3-5 Platoons Detected

As described in Section 3.2.1, the self-correcting mechanism simply identifies the first (furthest downstream) lead vehicle as the actual start of a vehicle platoon (vehicle 1 in this example, see After Self-Correction in Figure 3-5), and the last (furthest upstream) anchor vehicle as the actual end of a vehicle platoon (vehicle 7 at $t = 72$, vehicle 8 at $t = 73, 74$, and vehicle 9 at $t = 75$). According to the mechanism, these vehicles would also send a request to their immediate downstream (upstream) neighbors to flag the opposite type of discontinuity. In this example, vehicle 7 at $t = 71$, vehicle 8 at $t = 72$, vehicle 9 at $t = 73, 74$, and vehicle 10 at $t = 75$ were marked as lead per request from the vehicle they were following.

3.3.2 Impact of Market Penetration Rate

Since our proposed framework for traffic condition monitoring is distributed and relies on equipped vehicles, a low MPR may affect its effectiveness and accuracy. Note that vehicle platoons essentially divide a road segment into a set of fragments in a dynamic manner. With 100% MPR, traffic information is available for every fragment. Even when there is radio silence between two platoons, it is straightforward to conclude that there is no vehicle present in the fragment defined by the gap between these two platoons. In this sense, the proposed framework is able to achieve 100% coverage of a road segment with 100% MPR. On the other hand, a lower MPR will not only lead to a lower coverage ratio, the aggregated information may also be inaccurate due to the presence of non-equipped vehicles in a platoon.

To quantitatively analyze the impact of MPR, we consider the aggregated traffic condition under 100% MPR as the ground truth, and compare results from lower MPR

scenarios to the ground truth in terms of both coverage ratio and relative errors of aggregated density and speed. The former evaluates the effectiveness, and the latter the accuracy, of the proposed distributed traffic monitoring framework.

Our results indicate that the average coverage ratio increases with MPR. A decreasing relationship is also observed between the average relative error in density/speed and MPR. Free flow speed and traffic demand level both affect the performance of the proposed framework.

Evaluation Methodology

For convenience, denote 100% MPR as case g and a p% MPR as case p, where $0 < p < 100$. To compare cases p and g on a fair ground, we first combine their fragmentation (platooning) as illustrated in Figure 3-6. Note that the figure only shows the fragmentation at a specific time interval, and the fragmentation will evolve with time as the traffic dynamics evolve.

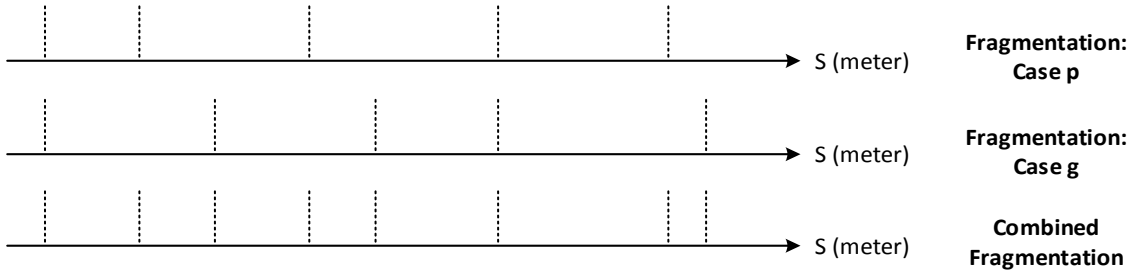

Figure 3-6 Illustration of Dynamic Road Fragmentation

This allows us to compare the differences in traffic states for each fragment between cases p and g. The sum of the relative differences of each fragment, weighted by

fragment length, over the entire road segment is considered another overall performance measure.

Denote the traffic state of fragment x at time t under case g as $s_g(x,t) = (k_g(x,t), v_g(x,t))$ and that under case p as $s_p(x,t) = (k_p(x,t), v_p(x,t))$. If fragment x is not covered by equipped vehicles under case p, then $s_p(x,t) = \Phi$ (no information available), and this fragment is excluded from the accuracy evaluation. Let L_g and L_p represent the total lengths of the covered segments under cases g and p. Note that $0 < L_p(t) \leq L_g(t) = L$. The coverage ratio can then be mathematically defined as

$$cr_p(t) = \frac{L_p(t)}{L_g(t)} \tag{3.11}$$

When $s_p(x,t) \neq \Phi$, define the relative error in density of segment x at time t as

$$re_{density}(x,t) = \frac{\left|k_p(x,t) - k_g(x,t)\right|}{k_g(x,t)} \tag{3.12}$$

Similarly, the relative error in speed is defined as

$$re_{speed}(x,t) = \begin{cases} \frac{|v_p(x,t) - v_g(x,t)|}{v_g(x,t)} & if\ v_g(x,t) > 0 \\ 0 & if\ v_g(x,t) = 0 \end{cases} \tag{3.13}$$

Note that $k_g(x,t)$ is always greater than zero when $s_p(x,t) \neq \Phi$. However, $v_g(x,t)$ could be zero due to traffic signals (e.g. queuing traffic as shown in Section 3.3.1) or stop-and-go traffic condition. In this case, $v_p(x,t)$ is also zero and there is no relative error in speed for fragment x at time t, i.e., $re_{speed}(x,t) = 0$.

The overall relative differences at time t can now be expressed as:

$$re_{density}(t) = \sum_{x:s_p(x,t)\neq\Phi} \frac{l_x(t)}{L_p(t)} \cdot re_{density}(x,t) \tag{3.14}$$

$$re_{speed}(t) = \sum_{x:s_p(x,t)\neq\Phi} \frac{l_x(t)}{L_p(t)} \cdot re_{speed}(x,t) \tag{3.15}$$

where $l_x(t)$ is the length of fragment x at time t.

For a simulation of duration T, define the average of the above performance measures over time as

$$cr_p = \frac{\sum_t cr_p(t)}{T} \tag{3.16}$$

$$re_{density} = \frac{\sum_t re_{density}(t)}{T} \tag{3.17}$$

$$re_{speed} = \frac{\sum_t re_{speed}(t)}{T} \tag{3.18}$$

Evaluation Scenarios

In order to analyze the impacts of MPR under different traffic conditions, four scenarios are created. They are low speed low demand (LSLD), low speed high demand (LSHD), high speed low demand (HSLD), and high speed high demand (HSHD). Free flow speeds are 50 km/h and 120 km/h for low- and high-speed settings respectively. The low-demand scenario has a vehicle input of 1,000 vph. This value is increased to 2,000 for the high demand level.

For each traffic scenario, five MPR's, 20%, 50%, 70%, 90% and 100%, are examined. Equipped vehicles are discharged randomly into the simulated traffic flow. More specifically, when a vehicle is generated from the source onto the network, a uniform random number is further generated based on the MPR to determine whether this vehicle is equipped or not.

For a given traffic condition scenario and a given MPR, multiple simulation replicates are performed with a range of random seeds of VISSIM traffic simulation. The simulation duration is 180 seconds for each run, with an additional 180-second traffic warm-up period.

Analysis is performed for both stable and queueing traffic. For the former, a single-lane freeway basic segment of 2365 meters is simulated. For the latter, we used the same freeway segment with the last 1000 meters set as a reduced speed zone in VISSIM. The speed limit for the reduced speed zone is set as 15 km/h for all traffic scenarios.

Results Analysis

Step-by-Step Comparison (Stable Traffic)

Figure 3-7 shows the step-by-step outputs of the three performance measures from one representative simulation run with LSHD and 50% MPR. Two phases are observed for the coverage ratio: before and after $t = 76$. The coverage ratio is related to the number of equipped vehicles and their spatial distribution. Under this particular scenario, some equipped vehicles have already traversed the road segment at $t = 76$. But no new equipped vehicles would enter the roadway as a result of the random number generation.

Therefore the coverage ratio is relative high over the first phase, with a sizable decrease after $t = 76$. The coverage ratio is always above 88% and the maximum fluctuation is no more than 10% over the entire simulation. $re_{density}(t)$ is approximately between 40% and 51%. Furthermore, it can be seen from Figure 3-7 that the relative error in density estimation has increased after $t = 76$, suggesting a potential correlation between coverage ratio and $re_{density}(t)$. $re_{speed}(t)$ is rather stable with a maximum of 4.82% and a minimum of 1.40%. No clear trend is observed over time.

Under the same LSHD scenario with the same VISSIM traffic random seed, it can be seen that the coverage ratio towards the end of the simulation is higher and more stable when MPR is increased to 90% (see Figure 3-8). As expected, the average relative errors of density and speed over time are lower as compared to the 50% MPR scenario.

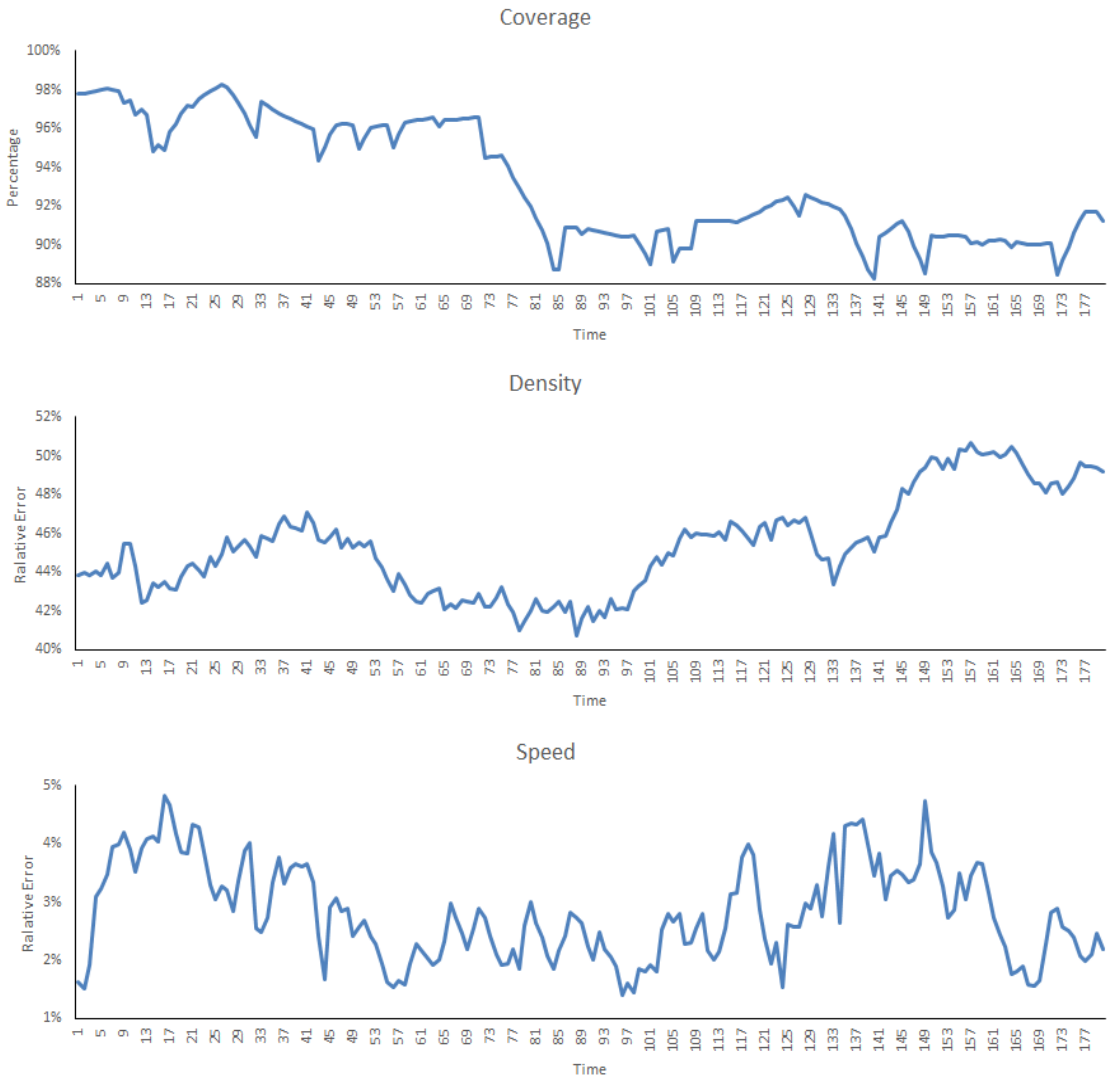

Figure 3-7 Step-By-Step Outputs under LSHD Stable Traffic with 50% MPR

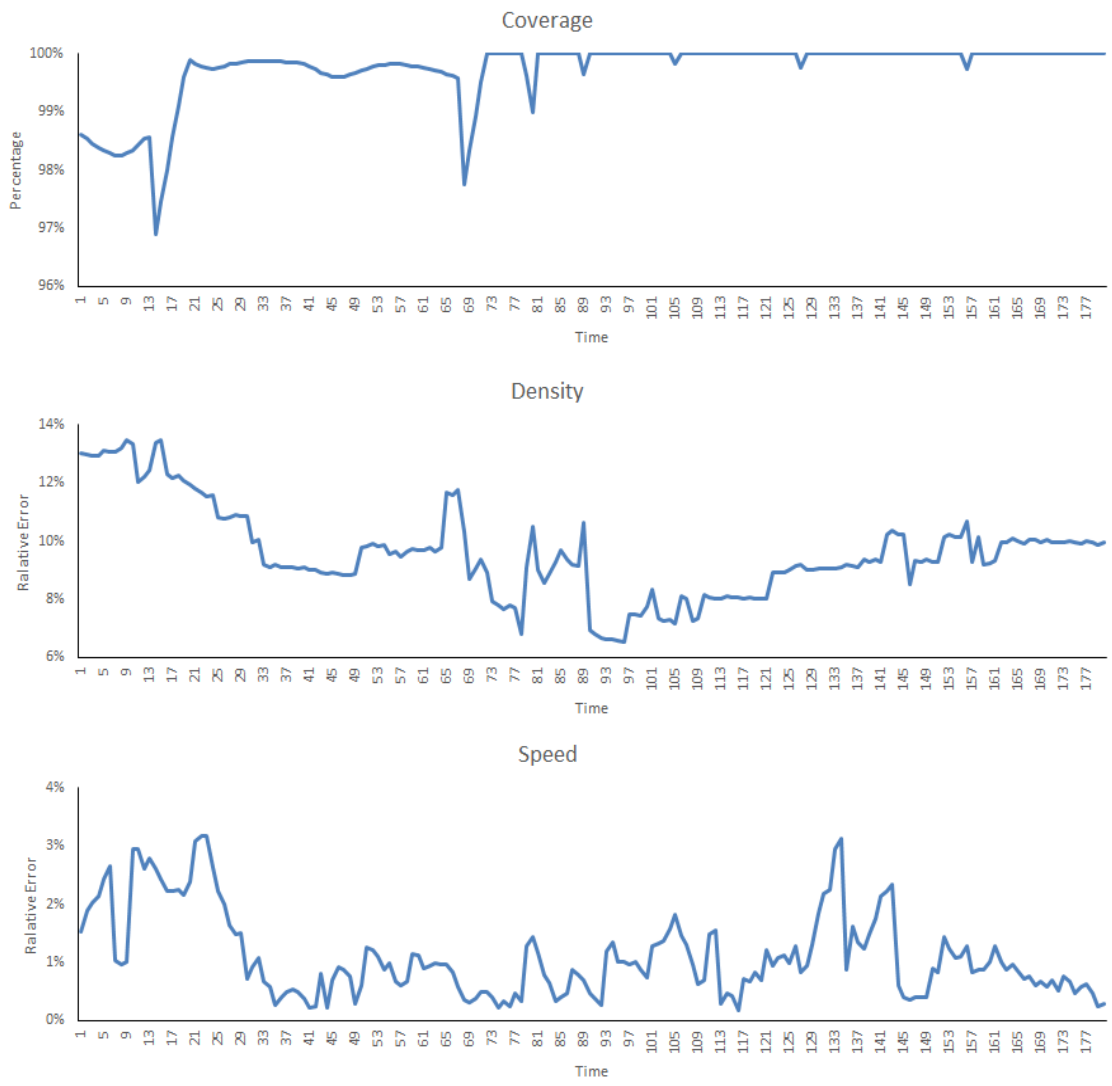

Figure 3-8 Step-By-Step Outputs under LSHD Stable Traffic with 90% MPR

Abrupt changes in relative error of speed are observed at several time steps from Figure 3-8 (e.g., $t = 10, 133$). To further explain this curious phenomenon, the detailed fragmentation at $t = 133$ is shown in Figure 3-9. The pair of numbers above each fragment represents the number of equipped vehicles and the space-mean speed of this fragment. The number below each dashed line indicates the location of a fragment boundary in meters.

Speed differences occur at fragments 716 m – 1,698 m, 1,698 m – 2,022 m, 2,022 m – 2,046 m, and 2,046 m – 2,336 m. The first two fragments are the main cause of the relatively high overall speed relative error of 3.13%. Take the second fragment for example, for the 90% MPR simulation, the space-mean speed is 46 km/h; but it is 41 km/h with 100% MPR, which contributed 1.67% to the overall relative error of 3.13%.

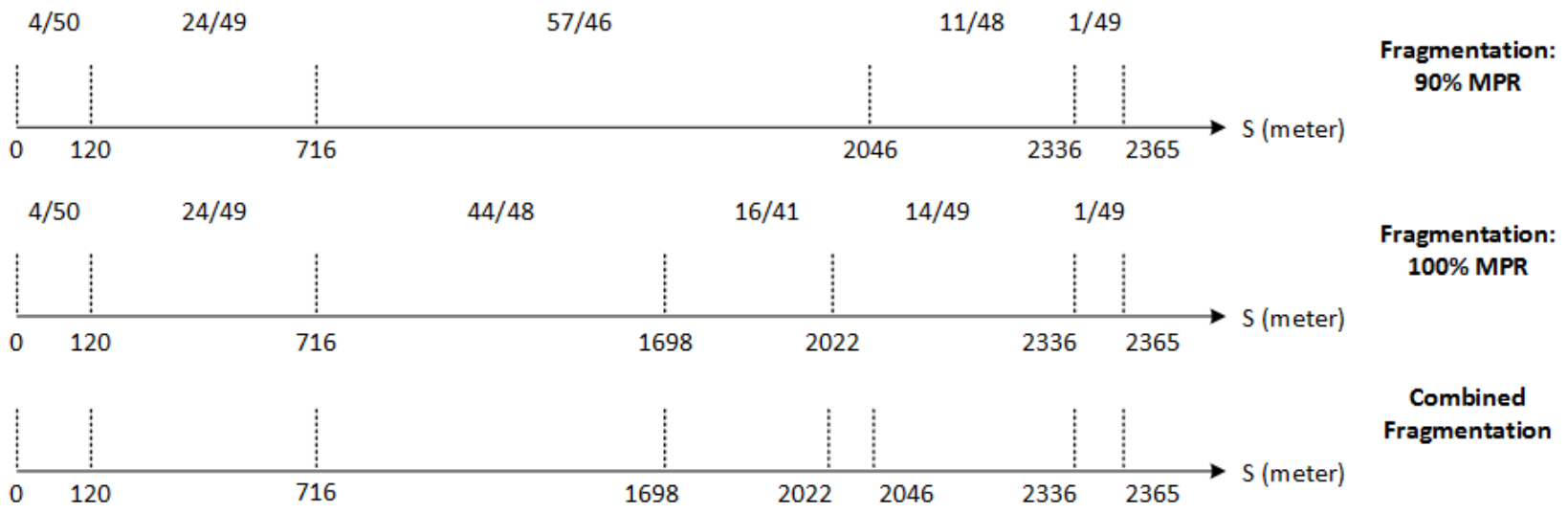

Figure 3-9 Detailed Fragmentations at t=133

Step-by-Step Comparison (Queueing Traffic)

Figure 3-10 shows the step-by-step performance of the proposed framework under the LSHD scenario with 90% MPR. As expected, coverage ratio increases with time as vehicles reach the downstream end of the road and more vehicles are on the road. With the introduction of reduced speed zone, it takes longer for vehicles to traverse the road segment compared to the case of stable traffic. In other words, traffic is less evenly distributed on the road at any given time step under queueing traffic comparing to stable traffic. This is why it takes longer for the coverage ratio to reach 90%.

For the other two measures, there is more variation for the relative error in speed compared to that in density. This is directly related to speed fluctuations caused by queueing traffic. As shown in Figure 3-10, large errors are observed from approximately 77s to 81s for both relative errors. This is because the framework is more sensitive to where equipped vehicles are under queueing traffic as compared to stable traffic, due to the fact that traffic state (speed and density) intrinsically fluctuates more under queueing traffic. Moreover, the platoons detected under queueing traffic tend to be larger than those in stable traffic because of higher congestion. The spatial distribution of unequipped vehicles in this particular simulation run with 90% MPR lead to significantly different fragmentations than those from 100% MPR. For example, at t =77s, two major vehicle platoons are identified in case g, whose locations are 3m – 548m and 595m – 1963m respectively. Under 90% MPR, however, only one major platoon from 3m – 1963m is identified. This is the cause of large errors in both density and speed during 77s to 81s.

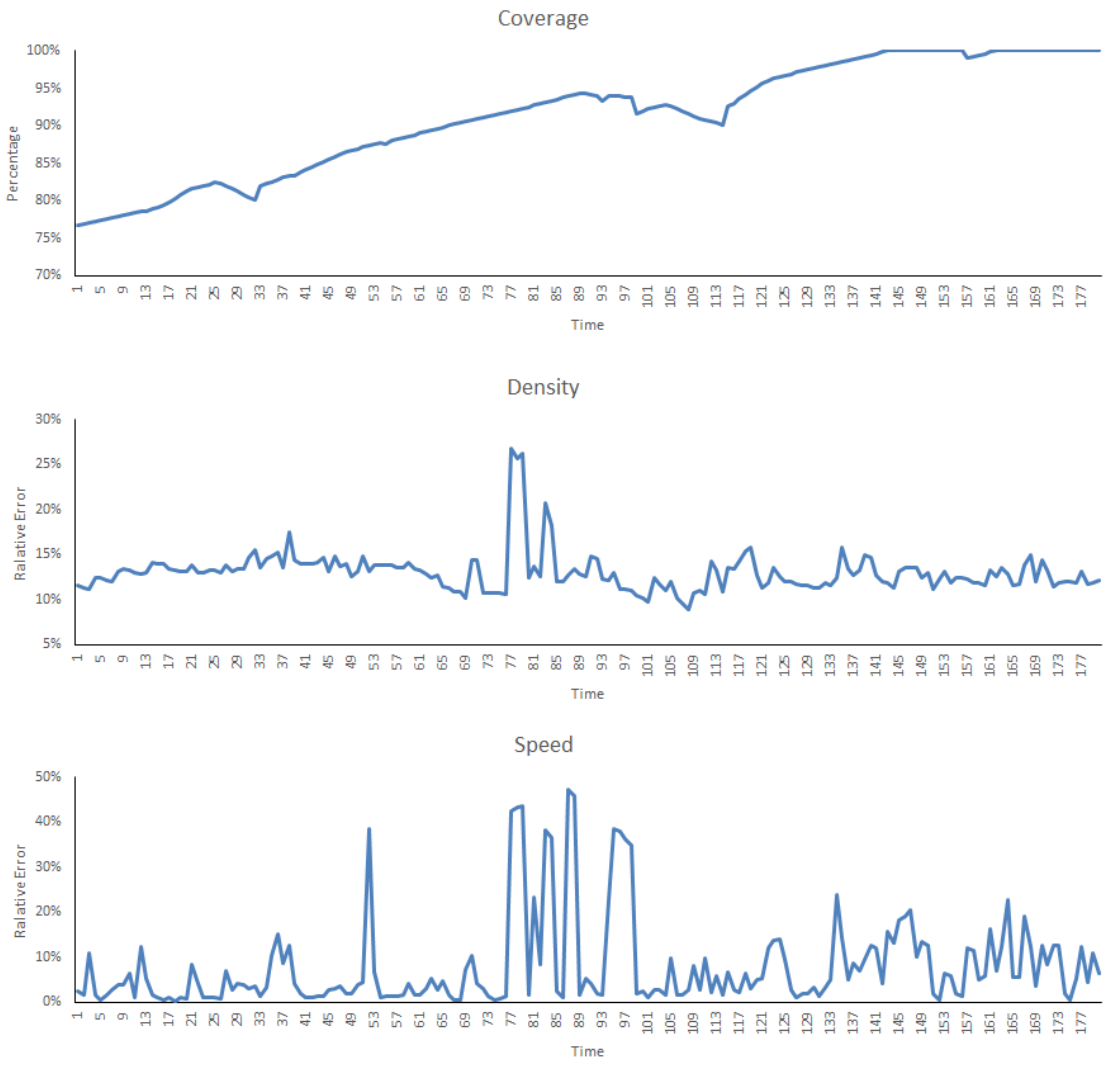

Figure 3-10 Step-By-Step Outputs under LSHD Queueing Traffic with 90% MPR

Overall Comparison (Stable Traffic)

Figure 3-11 shows the three overall performance measures from multiple simulation runs for each traffic scenario and MPR. Nine initial simulation runs are performed for each scenario and each MPR with three traffic random seeds. The mean and standard deviation for each of the three performance measures are then calculated to determine the confidence interval and whether additional runs are needed or not. For five scenarios

(HSHD with 50%, 70%, and 90% MPR; LSHD with 20% MPR; LSLD with 20% MPR), it is determined that 20 simulation runs are needed. For the rest of the scenarios, results from the nine initial simulation runs are sufficient to guarantee a 90% confidence interval of ± 0.05 or tighter. Among those five scenarios requiring additional runs, all but one are able to produce 90% confidence intervals of ± 0.05 or tighter with 20 simulation runs. Results from the 20 simulation runs for LSHD with 20% MPR have a 90% confidence interval of ± 0.06.

It can be observed that the coverage ratio increases with MPR for all four traffic scenarios. When the demand level is fixed, the coverage ratio under low-speed traffic scenarios is always higher than that under high-speed scenarios. This is due to the lower percentage of isolated vehicles under low-speed scenarios. If we fix the speed level, the high-demand scenario results in a higher coverage ratio due to fewer isolated vehicles. In other words, the proposed framework lends itself better to more congested traffic condition for any given MPR, as far as its effectiveness is concerned. Moreover, when MPR$\geq$50%, the coverage ratio has reached a minimum of 37.76% even under light traffic. This indicates that proposed framework could be useful with an MPR as low as 50%. Even with an MRP of 20%, the coverage ratio, under relatively congested traffic, can still reach around 55.65%.

The average overall relative error in density under each traffic scenario decreases roughly linearly with the increase of MPR. For any MPR (except 90%), LSHD always lead to highest relative error due to the sparsity of vehicles on the road.

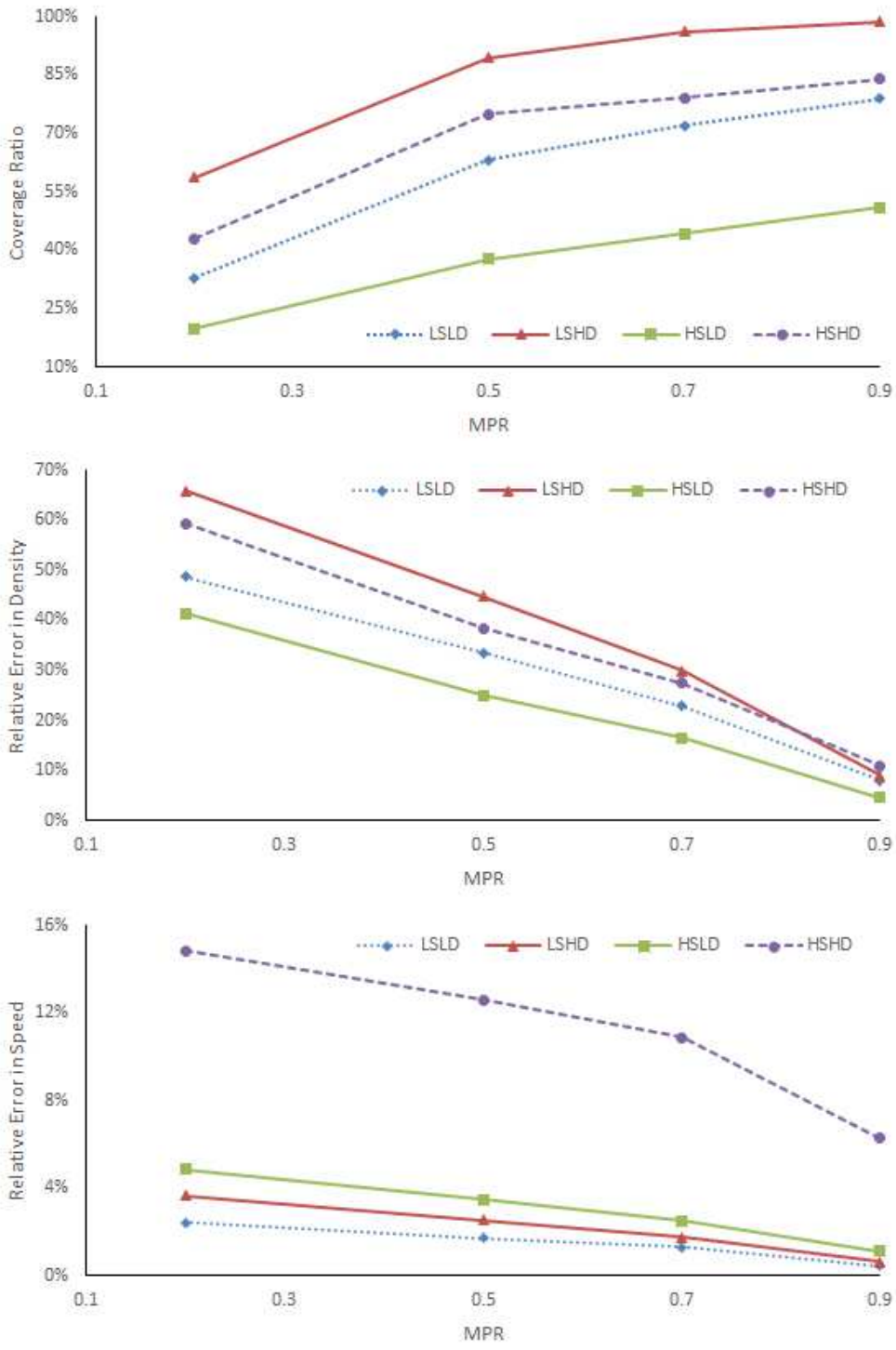

Figure 3-11 Overall Performance Measures under Stable Traffic

Similarly, the average overall relative error in speed also decreases as MPR increases. It seems that the low-demand scenarios will result in similar relative low errors in speed for any given MPR. For the high-demand scenarios, however, a big difference can be observed between LSHD and HSHD. In fact, it can be seen that the differences among LSLD, and LSHD, HSLD are small, especially with higher MPRs. But HSHD scenario leads to a much higher relative error in speed. This is because unequipped vehicles do not affect speed estimation very much under relatively stable traffic (in LSLD, LSHD, HSLD scenarios). However, in HSHD scenario, there is a much bigger range of individual vehicle speed distribution, and the impact of MPR is therefore much more pronounced. This also explains that for a given demand level, the scenario with higher speed would observe higher relative error in speed estimation, as seen in Figure 3-11.

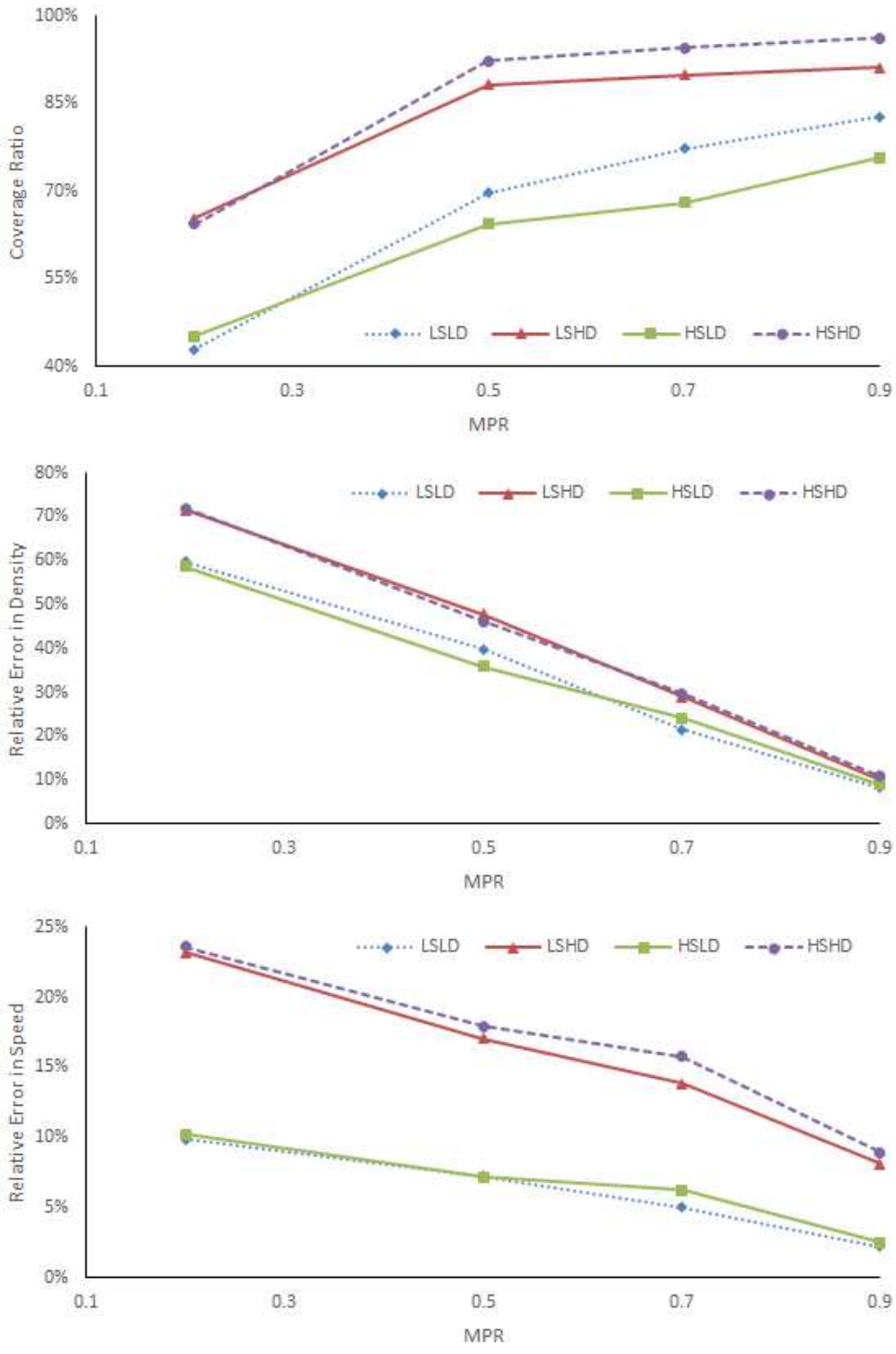

Figure 3-12 Overall Performance Measures under Queueing Traffic

Overall Comparison (Queueing Traffic)

Figure 3-12 shows that the three performance measures under queueing traffic follow similar trends as stable traffic: coverage ratio increases with MPR, and relative errors in density and speed decrease with MPR. These results are from 9 simulation runs for each scenario and MPR, except HSLD with 20% MPR, which requires 20 simulation runs. With the respective minimum number of simulation runs, all results have achieve 90% confidence intervals of ± 0.05 or tighter.

Note that the coverage ratio under every traffic scenario with 20% MPR is higher than the corresponding value under stable traffic. This is due to more vehicles on the network caused by queueing. Queueing traffic also leads to more speed fluctuations, which causes the relative error in speed to be more pronounced at low MPRs. These results are as expected.

3.4 Summary

In this chapter, we have investigated a distributed framework for network-wide traffic monitoring and platoon information aggregation using V2V DSRC alone. Through distributed protocols, each vehicle will monitor its local traffic condition, flag itself as either the lead or the anchor of a vehicle platoon as appropriate, and validate and self-correct its flag by communicating with its immediate up- and down-stream vehicles. A contention-based cooperative multi-hop information forwarding protocol is developed to make sure that platoon information is aggregated in the most effective and accurate manner with minimum communication overhead. The framework is tested using VISSIM and its built-in COM. A simple freeway and a freeway with a reduced speed zone are

created to test the framework under stable traffic and unstable traffic (namely, a queue being formed). The framework is proved to be valid. A new evaluation methodology is proposed to investigate the impact of MPR on the proposed framework. The results suggest that the average coverage ratio increases with MPR. With 50% MPR, the framework is able to provide information coverage for at least 37.76% of the simulated roadway facility. This indicates that the proposed framework could be useful with an MPR as low as 50%. Even with an MRP of 20%, the coverage ratio, under relatively congested traffic, can still reach around 55.65%. The framework is able to provide accurate speed estimation at high spatial resolution for the simulated roadway facility. The maximum relative error is under 10% for relatively congested traffic even with MPR as low as 20%. When there is a wider range of speed distribution (less congested traffic), the worst-case maximum relative error is still under 15% when MPR $= 20\%$. The density estimation is more sensitive to MPR, and is more accurate under low demand and high MPR scenarios. As expected, the accuracy of both speed and density estimation increases with MPR for any given traffic scenario. For the simulated roadway facility, we conclude that the proposed framework works better under low-speed high-demand scenarios, and can produce reasonable results with MPR as low as 50%. On the other hand, this Chapter concentrate on dynamically identifying platoons through micro-discontinuities detection using V2V communications. Evolution of platoons or equivalently micro-discontinuities could be of interest for the monitoring framework to be incorporated with existing platoon-based intersection controls. Discussion on predicting evolution of micro-discontinuities can be found in APPENDIX B.

CHAPTER 4

IMPACT OF TRAFFIC SIGNAL CONTROLS ON THE PERFORMANCE OF A DISTRIBUTED TRAFFIC MONITORING SYSTEM USING V2V COMMUNICATIONS

4.1 Introduction

We have developed a distributed framework for network-wide traffic monitoring and platoon information aggregation using V2V communications alone in Chapter 3 to support cooperative traffic operations / management strategies. A set of distributed protocols, which are performed by each equipped vehicle, are developed to identify platoons and compute aggregated traffic information (density and speed) of identified platoons. This framework allows traffic monitoring and platoon information provision to be carried out in a localized, distributed, and cooperative manner. The framework is capable of monitoring and reporting vehicular traffic condition for the entire road network, instead of only at specific locations where RSUs are installed. This framework could serve as an alternative or supplemental system that is particularly suitable under abnormal traffic scenarios caused by extreme and special events. The system is validated using VISSIM and its built-in component object model under multiple traffic scenarios and MPR. The simulation demonstrated the distributed traffic monitoring system can produce reasonable results with MPR as low as 20%. In addition to MPR, the performance of the distributed monitoring framework also depends on the spatial distribution of equipped vehicles in the road network, which is affected by traffic dynamics. Intersection control plays a significant role in governing traffic dynamics and

will in turn have impacts on the distributed traffic monitoring and information aggregation framework. The objective of this study is to investigate such impacts.

Although the relationship between vehicular traffic dynamics and V2V communication has been extensively studied in both transportation and wireless communication communities, no prior work has explicitly looked into the relationship between intersection control and the performance of V2V communications or any traffic monitoring or information dissemination system based on V2V communications.

Relevant works can be divided into two categories. The first category examines information propagation through V2V communications. The performances of interest include connectivity, propagation delay, propagation distance, message delivery ratio and packet reception rate, etc. MPR, traffic conditions, and transmission range are factors that would affect theses performance measures. Many studies have developed either analytical or simulation methodologies to quantify such relationship (Chen et al., 2010; Du and Ukkusuri, 2007; Jin and Recker, 2006, 2007; Jin and Wang, 2008; Schonhof et al., 2006; Wang et al., 2011; Wang, 2007; Wu et al., 2005; Yang and Recker, 2005; Yin et al., 2013; Zhuang et al., 2010). The other stream of studies focuses on the performance of traffic monitoring (e.g. congestion detection and traffic pattern classification) through V2V. Accuracy is the main concern of such monitoring systems and is often assessed using simulations with similar influencing factors as adopted by studies in the first category (Bauza et al., 2010; Dornbush and Joshi, 2007; Fukumoto et al., 2007; Lakas and Cheqfah, 2009; Lee et al., 2006; Miller, 2008; Terroso-sáenz et al., 2012; Vaqar and Basir, 2009; Wischhof et al., 2005; Younes and Boukerche, 2013). This Chapter takes

one step further to explore how intersection control affects the distributed traffic monitoring system based on V2V communications in Chapter 3.

Since accurate traffic monitoring sets the foundation for advanced traffic control strategies, we argue it is important to consider the resulting performance of traffic monitoring, together with other mobility measures (such as throughput, delay, vehicle progression, etc.), when designing intersection control mechanisms. By examining how intersection control affects the distributed traffic monitoring framework in Chapter 3, this work will bridge this gap and provide insights on this issue.

4.2 Methodology

This work will focus on signalized intersections, one of the most common intersection control mechanisms. With the presence of traffic signal controls, signal timing plans as event data should be considered for evaluating the performance of the distributed traffic monitoring and platoon information aggregation system. Among various signal control factors, such as the operation mode of a traffic controller and signal timing parameters, this paper will investigate the impacts of g/C ratio as one of the possible key factors. To quantify the relationship, the performance evaluation methodology developed in Chapter 3 is adopted and new evaluation scenarios that incorporate traffic signal controls are designed.

4.2.1 Measuring Performance of the Distributed Traffic Monitoring Framework

To quantitatively analyze the impact of MPR, Chapter 3 proposed a methodology on the basis of dynamic fragmentation as illustrated in Figure 4-1. Consider the aggregated traffic condition under 100% MPR (denoted as case g) as the ground truth, and denote

results from a $p\%$ MPR (denoted as case p) scenario (where $0 < p < 100$) as case g. Each fragment in the top two rows in Figure 4-1 is a platoon identified by the distributed traffic monitoring framework at any given time point t, for case p and case g respectively. In the bottom row of Figure 4-1, the road segment is further divided into smaller fragments by combining the fragmentation of both cases. We can now compare the differences in traffic states between cases p and g for each fragment as shown in the bottom row of Figure 4-1. Three performance measures are considered: coverage ratio, relative errors of aggregated density, and relative errors of aggregated speed. The sum of the relative differences of each fragment, weighted by fragment length, over the entire road segment is considered an overall performance measure at time t. This measure for a single simulation time step can be further averaged over the total simulation duration T. We will use the average performance over time as the metric for the analysis in this paper. For more details regarding their definitions and calculations, please refer to Chapter 3.

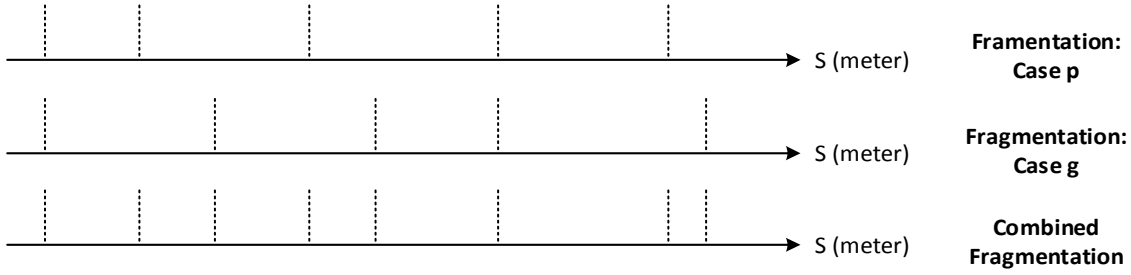

Figure 4-1 Illustration of Dynamic Road Fragmentation

The analysis of how traffic signal controls affect the performance of the distributed monitoring system utilizes the same comparison methodology. In this paper, the analysis

will concentrate on how the performances vary with respect to different traffic signal timing plans while fixing the traffic scenario and the MPR.

Traffic signals could operate in different modes, such as pre-timed, actuated and adaptive. Regardless of the operation mode, some basic timing parameters are universal. They include cycle length, phase sequence, phase times and so on, which will affect the performance of the distributed traffic monitoring system. For each approach, phase time directly governs the throughput and the spatial-temporal distribution of vehicles. This study will focus on the impacts of phase times. For a pre-timed signal timing plan with fixed cycle length, different phase times can be achieved by varying g/C ratios. Therefore, pre-timed signal timing plans with the same cycle length but different g/C ratios will be investigated with the evaluation framework, and the performances of the monitoring system with respect to different g/C ratios will be further analyzed and compared.

With the presence of a traffic signal controller, spatial and temporal separations are introduced to the traffic flow. Consider a simple traffic network with a single lane, a signal controller placed in the middle of network will divide the network into downstream and upstream segments. Meanwhile, the time domain will be separated into effective green and effective red for each movement. The performance of the monitoring system could be calculated for only the upstream segment, only the downstream segment, or both up- and down-stream segments. Similarly, we could calculate the performance of the monitoring system during the whole cycle, only during effective green, or only during effective red. This leads to $3 \times 3 = 9$ combinations of time-space windows for our

analysis. To gain detailed insights, this study will focus on the four elementary space-time windows, namely the downstream/effective green (DG), downstream/effective red (DR), upstream/effective green (UG), and upstream/effective red (UR).

Simulation results show very larger relative errors in speed exist for g/C<1 compared to g/C=1. Besides the speed fluctuations caused by traffic signals, this is also attributed to the fact that our algorithms in the distributed monitoring system would not split a platoon if it happens to cross the stop bar. It will reduce the accuracy of density estimation as well. The issue is easy to fix with an extended process of micro-discontinuity identification where event-data will be utilized.

4.2.2 Evaluation Scenarios with the Presence of Intersection Control

In this study, the same network as in Chapter 3 is adopted. A pre-timed traffic signal is placed at 1,000 m downstream from the vehicle input. Four different signal timing plans are created with the same cycle length of 120s, and g/C ratios of 1 (which is equivalent to a freeway segment without traffic signals), 2/3, 1/2, and 1/3. Four traffic scenarios are examined. They are low-speed low-demand (LSLD), low-speed high-demand (LSHD), high-speed low-demand (HSLD), and high-speed high-demand (HSHD). The settings of speed and demand for the four traffic scenarios will remain the same as in (Lou et al., 2016). Five different MPR values, namely 20%, 50%, 70%, 90% and 100%, are adopted. Multiple simulation replicates are performed with a range of random seeds using VISSIM traffic simulation for a given traffic scenario and a given MPR. The simulation has a 180-second traffic warm-up period followed by 180 seconds for the actual simulation. For a

given space-time window, the performances of the monitoring system under the same traffic scenario and MPR, but with different g/C ratios, are compared.

4.3 Results

Radar charts are presented to show the performances of the distributed monitoring system (Figure 4-2 to Figure 4-7). Each axis in any of the charts corresponds to a combination of a space-time window and a particular value of MPR. Take the first quadrant in Figure 4-2 (a) for example, the axes are DG_20%, DG_50%, DG_70%, and DG_90%. For a chart, there are several circles representing different values of the corresponding performance. The circles in Figure 4-2 correspond to 80%, 60%, 40% and 20% from outer to inner ones. The center represents 0% relative error. The performances with respect to g/C ratios of 1, 2/3, 1/2, and 1/3 are represented using blue, red, grey, and green lines respectively. That g/C ratio equals 1 represents the scenario without traffic signals at the intersection, so there are no blue lines for the DR and UR quadrants.

4.3.1 Relative Error in Density

Two main reasons would lead to high relative error in density estimation. The first reason is traffic being sparse traffic (i.e., traffic is low in density). One possible explanation is that a higher proportion of equipped vehicles are likely to identify themselves as isolated vehicles (see Chapter 3 for more details) with sparser traffic, which may not be the case and will result in higher estimation error. The other reason is the uneven spatial distribution of traffic. This means traffic density varies substantially over the roadway segment. With a non-100% MPR, the high variation in density itself may not be well

captured by the distributed monitoring system, and is likely to lead to high relative error in estimation.

Figure 4-2 shows that there is no significant difference in system performance for g/C ratios of 2/3, 1/2, and 1/3 under HSHD and HSLD. For DG under HSHD (first quadrant in Figure 4-2 (a)), removing the signal (g/C = 1) always leads to a higher relative error in density for any MPR. With the presence of a signal controller, the downstream traffic will be dominated by the discharged vehicles. With HSHD, vehicles will be discharged at a higher rate during green interval compared to the flow rate when g/C=1.On the contrast, a g/C ratio of 1 always leads to the lowest relative errors in density for UG. The reason is related to the spatial distribution of equipped vehicles. Newly generated vehicles from the upstream source will first speed up in the network and then decelerate when they approach the intersection. This is because that vehicles are generated with initial speeds below their desired speeds (speed limit) in VISSIM and that congestion exists near the intersection under HSHD scenario even during green intervals. As a result, traffic is not uniformly distributed over the upstream segment, which is denser near the intersection and less dense near the upstream source compared to g/C=1. A significant difference between free flow (g/C = 1) and interrupted flow (g/C < 1) is only observed for DG. This indicates that the introduction of traffic signals, under traffic scenario HSHD, has a positive effect on the performance in terms of accuracy in density for DG.

For HSLD, when a signal is present (g/C < 1), a lower g/C ratio usually leads to a higher relative error in density (shown in Figure 4-2 (b)). For downstream, sparser traffic is expected during either green or red phases with a lower g/C ratio. For upstream, more

stopped traffic is held near the intersection with a lower g/C ratio, and the overall spatial distribution of traffic in the upstream segment would have higher spatial variance during both phases. For DG, removing the signal altogether does not lead to much difference in relative error in density. The performance under g/C=1 for UG does not differentiate itself with those under g/C ratios of 2/3 and 1/2. Significant difference is only observed when comparing to g/C=1/3.

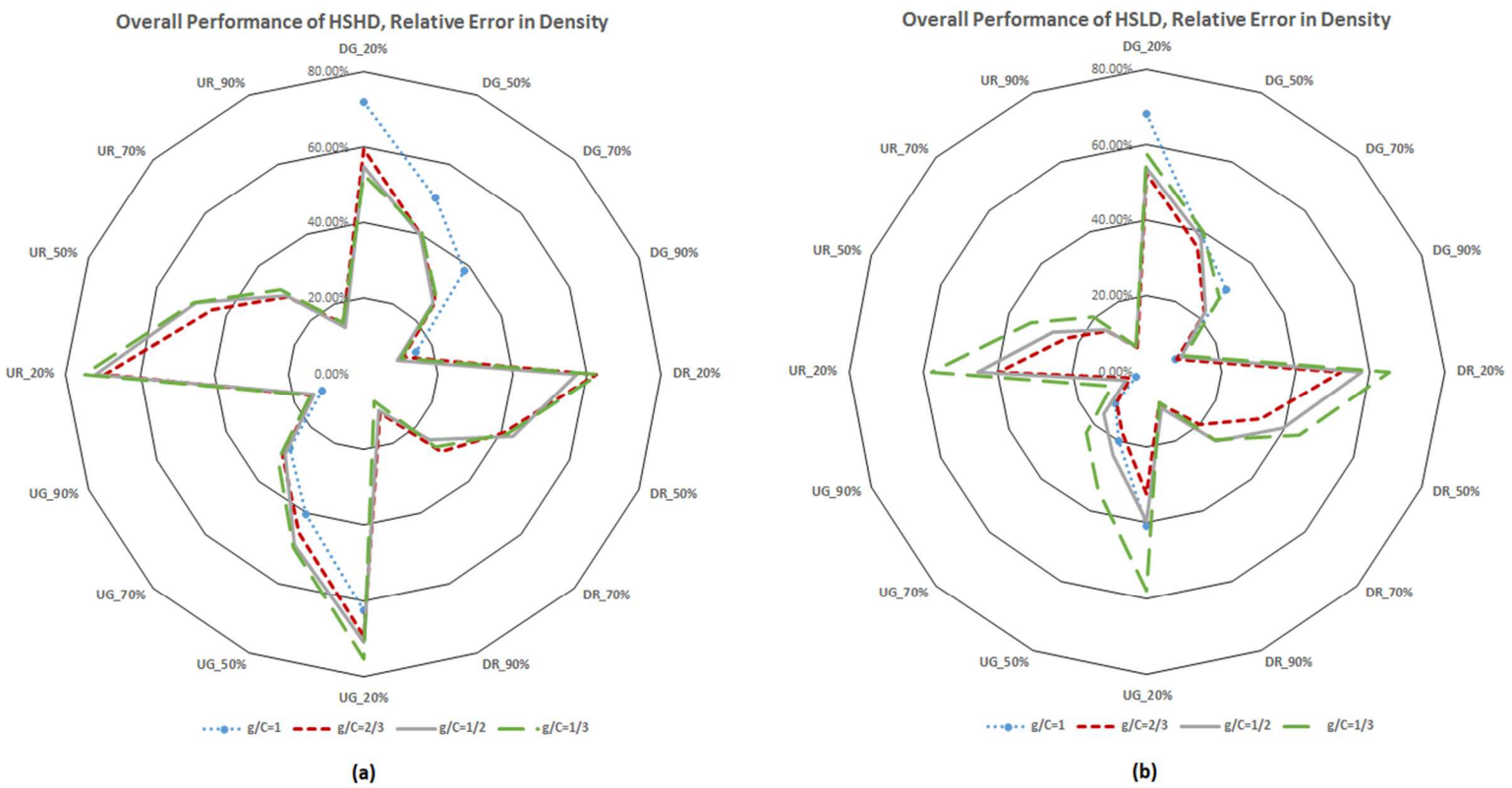

Figure 4-2 Relative Error in Density under HSHD and HSLD

The impact of traffic signals on relative error in density is minimal for LSHD. The system performances under the four g/C ratios are basically the same as illustrated in Figure 4-3 (a). The low speed and high demand setting may make traffic more uniformly distributed over both downstream and upstream segments during both green and red phases.

The g/C ratio does not seem to affect density estimation for DG and DR under LSLD either. For UG and UR, the relative errors corresponding to g/C ratios of 1/3 and 1/2 are greater than those with g/C ratios of 1 and 2/3 (see the second and third quadrants the Figure 4-3 (b)), but the differences can be ignored when MPR=70% and 90%. This is because that the traffic is less uniformly distributed with lower g/C ratios.

These analyses have revealed that there is no clear pattern of the impact of g/C ratio on the accuracy of density estimation, which seems to depend on the traffic scenario. Generally speaking, denser traffic and more uniformly distributed traffic usually lead to higher accuracy of density estimation.

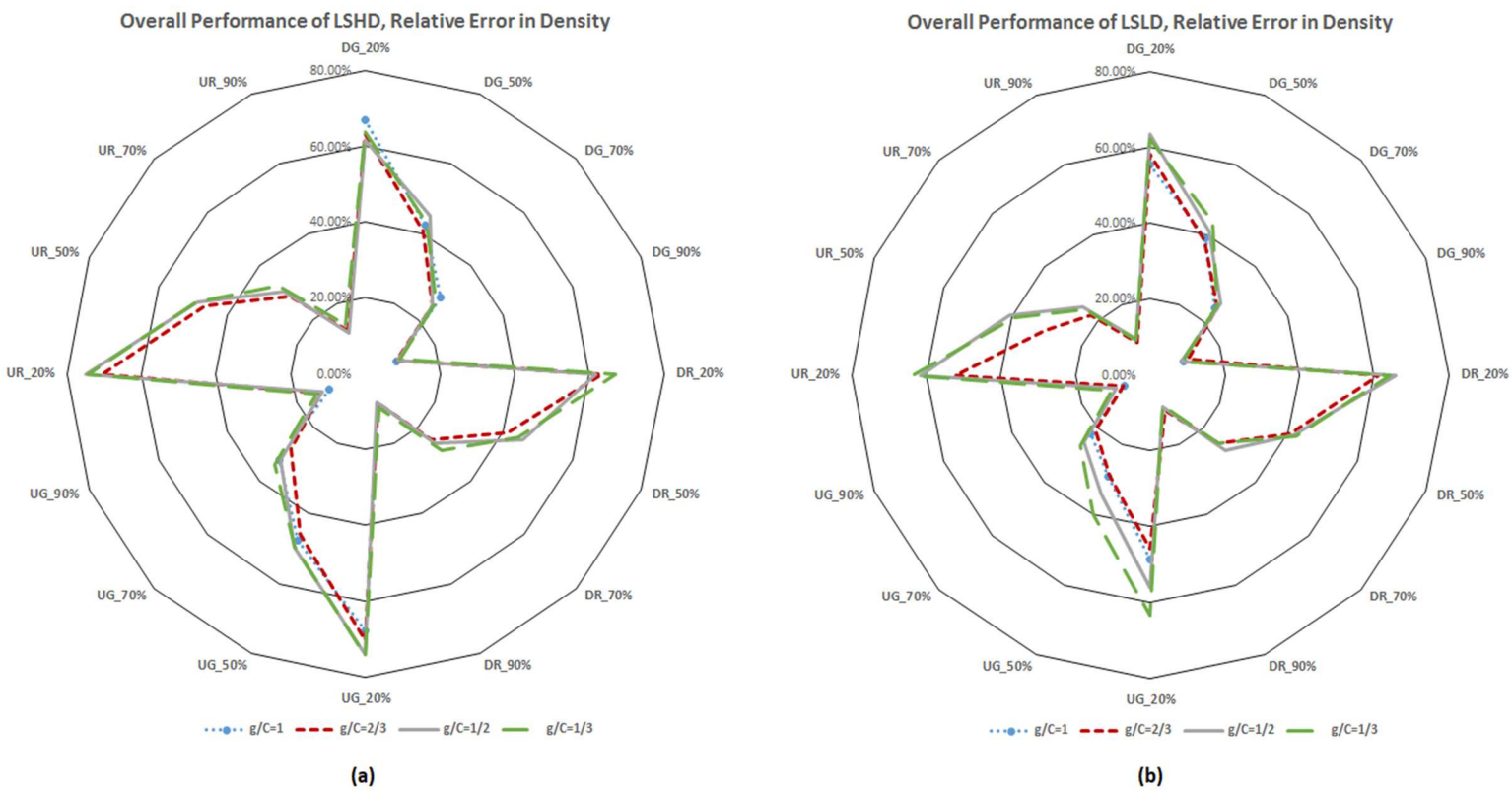

Figure 4-3 Relative Error in Density under LSHD and LSLD

4.3.2 Relative Error in Speed

Compared to relative error in density, relative error in speed shows a clear pattern with respect to g/C ratios (see and Figure 4-4 and Figure 4-5). As we can see from Figure 4-4, the presence of traffic signal significantly reduces the accuracy of the speed estimation for HSHD traffic scenario. Moreover, the smaller the g/C ratio, the higher the relative error in speed for any given space-time window and MPR. The reason is that with a smaller g/C ratio, a longer red interval within the cycle will lead to a greater amount of stop-and-go traffic. Speed fluctuation in stop-and-go traffic is general higher, and would result in a bigger relative error in speed. These observations hold for all four traffic scenarios.

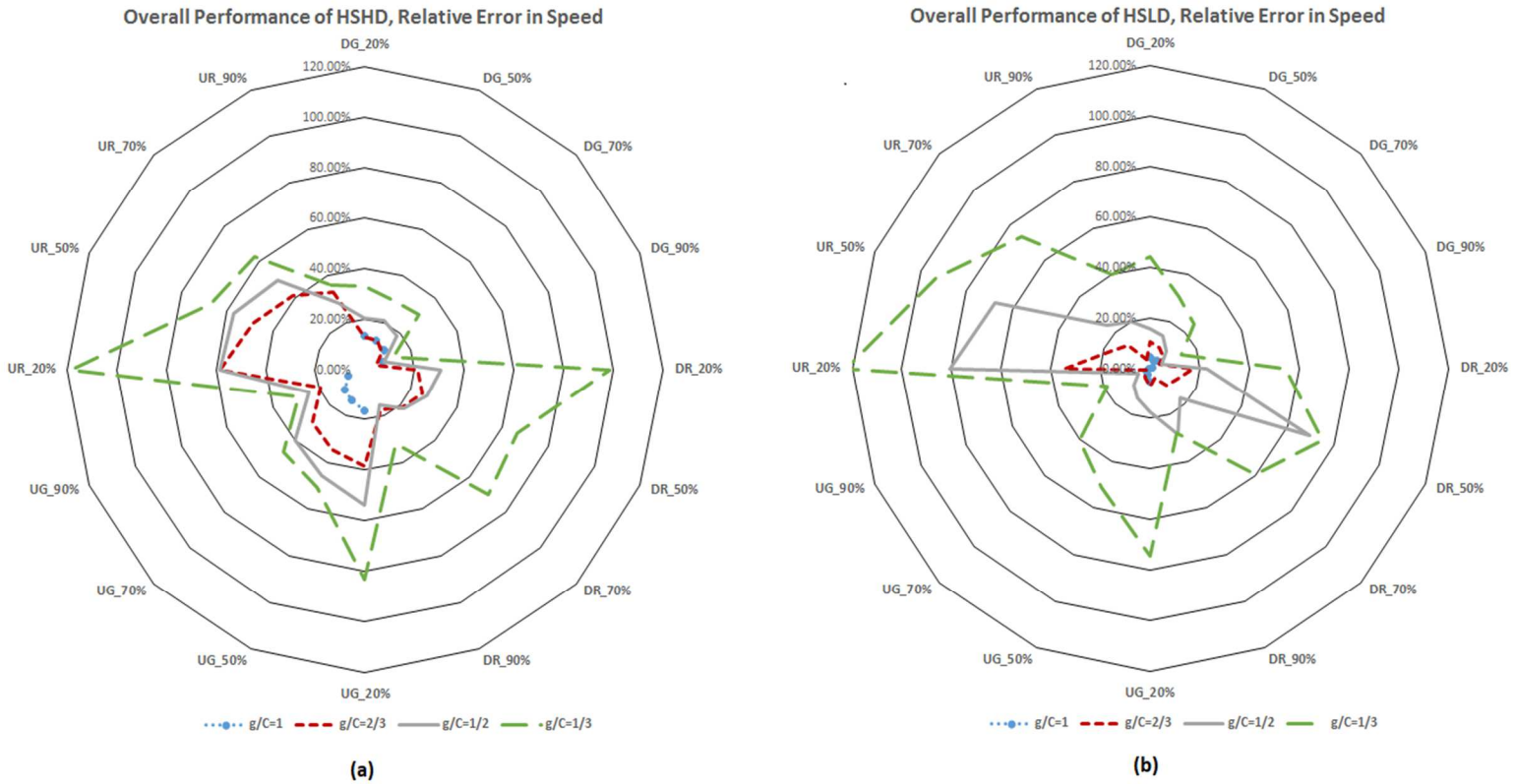

Figure 4-4 Relative Error in Speed under HSHD and HSLD

Compared to HSHD and HSLD, Figure 4-5 shows that the two low speed scenarios (i.e., LSHD and LSLD) have much lower relative error in speed for downstream segment during both phases. This is because that the low speed limit and less speed fluctuation (compared to upstream) reduce the variation in speed for downstream traffic.

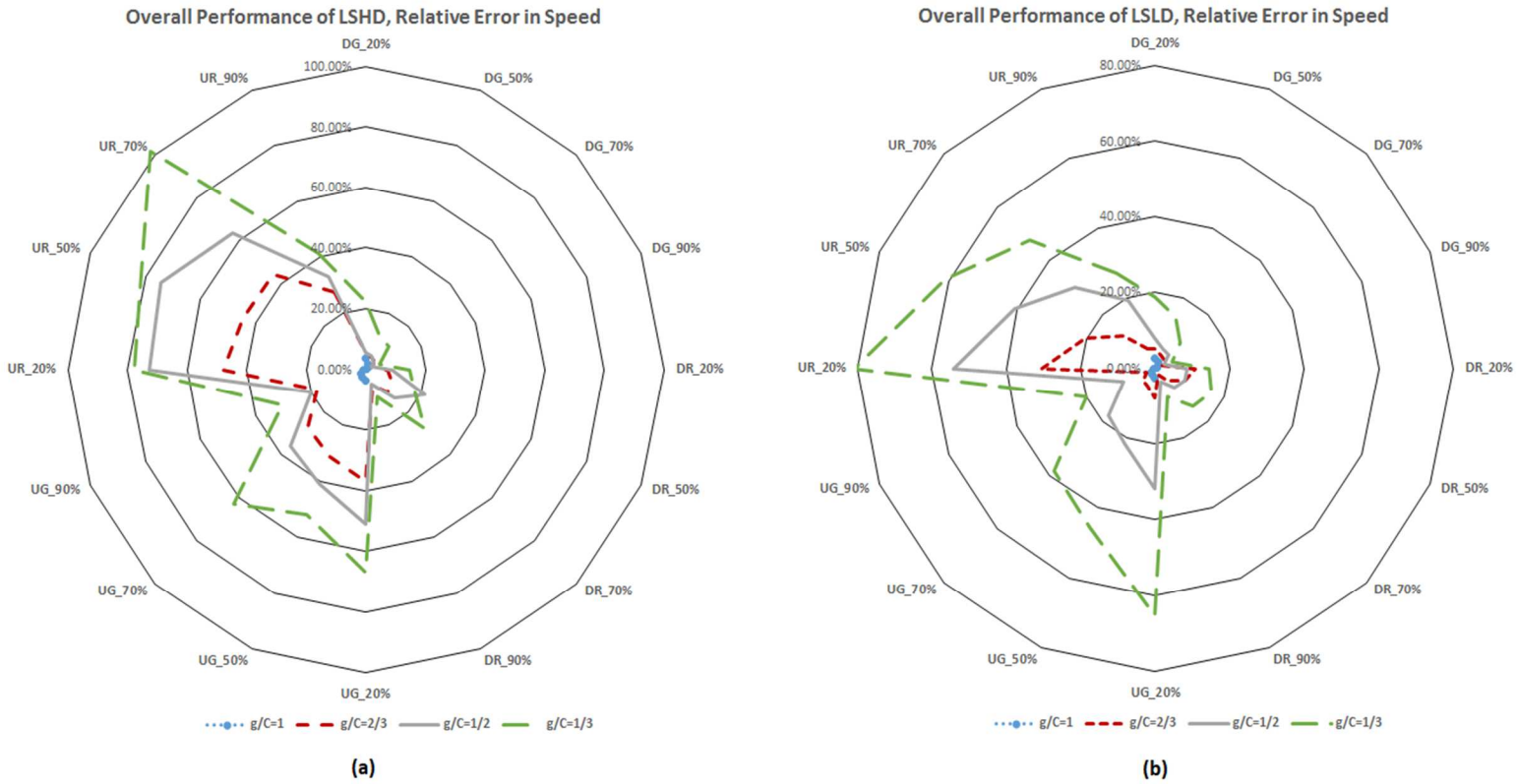

Figure 4-5 Relative Error in Speed under LSHD and LSLD

4.3.3 Coverage Ratio

Higher traffic demand or denser traffic leads to fewer isolated vehicles and thus tends to have higher coverage ratio on a roadway segment for a given MPR. This is the main reason behind the difference in coverage ratios with different g/C ratios.

Figure 4-6 shows the coverage ratios of the traffic monitoring system under HSHD and HSLD. From Figure 4-6 (a), it can be seen that the system performs similarly in space-time windows UG and UR (second and third quadrants) when a signal controller is present (g/C < 1), where no significant difference among different g/C ratios is observed. Comparing to free flow (g/C = 1), the presence of traffic signal will lead to higher coverage ratio for UG. This due to the fact that more traffic is held upstream as the result of traffic signals. But with the network being relatively congested, the amount of upstream traffic does not vary much with the g/C ratio, as long as it is less than 1. For DG, lower coverage ratios are reported for g/C ratios of 1/2 and 1/3 compared to g/C=1. However, the highest coverage is observed when g/C = 2/3. The discharge rate with g/C = 2/3 may be higher than the flow rate with g/C = 1. The observation also indicates an optimal g/C ratio with respect to coverage ratio for downstream traffic during green intervals may exist, and is left to be identified with more experiments. For both DG and DR, the coverage ratio increases with the g/C ratio (g/C<1).

For HSLD, a higher coverage ratio is associated with a lower g/C ratio for UR since longer red intervals lead to more traffic being held upstream when the network is not very congested. It applies to UG as well (except when MPR=70% where the lower g/C ratio, the smaller coverage ratio). The opposite is observed for DR (except MPR=50% where

the coverage with g/C = 2/3 is slightly lower than that with g/C = 1/2). The is straightforward since a lower g/C ratio will lead to less traffic discharged to downstream. Similar to DG under HSHD, the presence of traffic signals results in a higher coverage ratio for DG except for g/C = 1/3, comparing to g/C = 1. This is because for this traffic scenario, g/C = 2/3 and g/C = 1/2 both lead to higher total throughput during the same amount of time (green interval) comparing to g/C = 1 due to a higher discharge rate, but not g/C = 1/3.

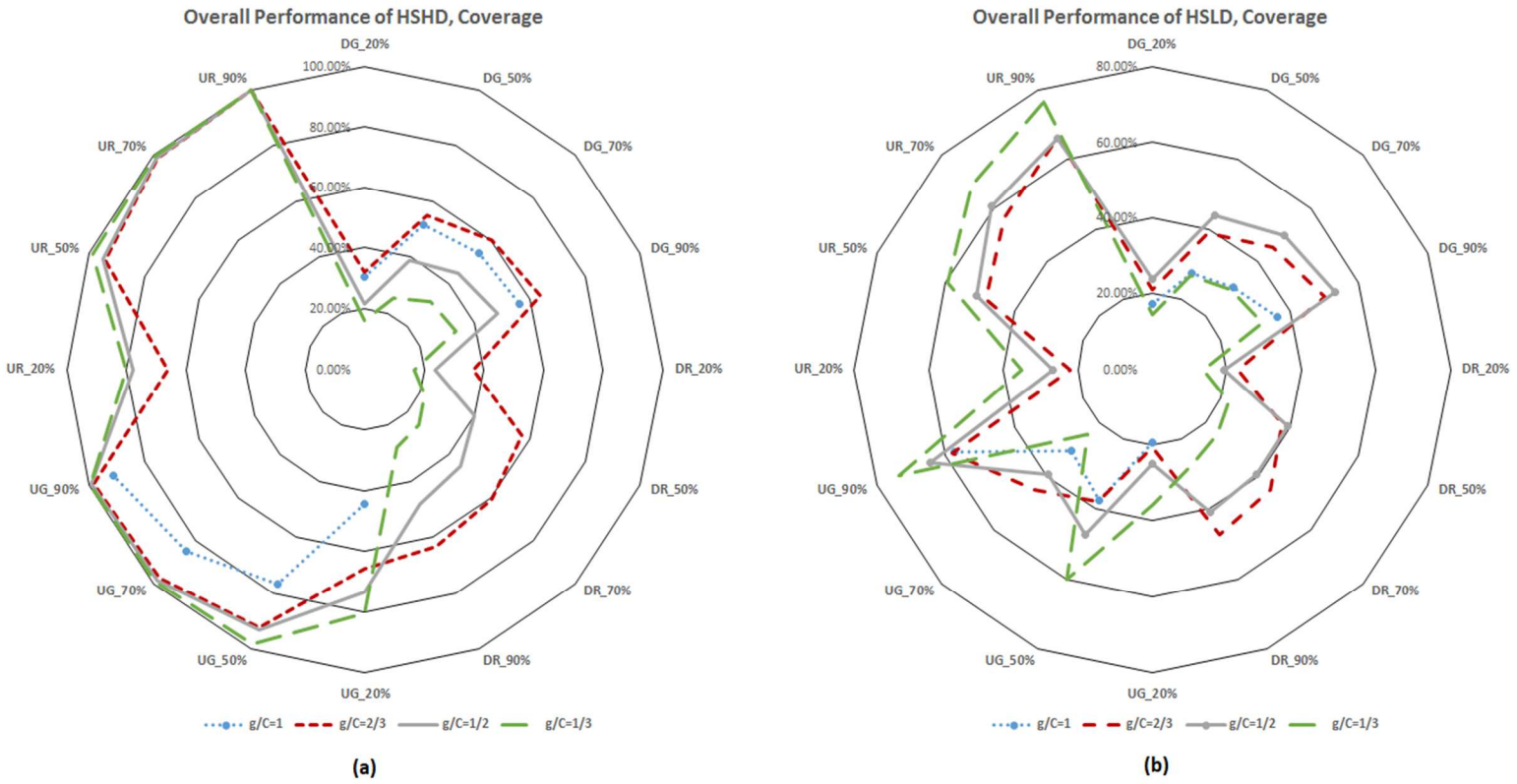

Figure 4-6 Coverage Ratio under HSHD and HSLD

Figure 4-7 (a) shows the performances under LSHD. The coverage ratios are comparable with each other under g/C ratios of 2/3 and 1 for DG. Similar to HSHD, lower coverage ratios are observed for the other two g/C ratios, and g/C = 1/3 results in the lowest coverage ratio for both DG and DR. The presence of traffic signal leads to a lower coverage ratio for UG, and the lower the g/C the lower the coverage ratio. For UR, the system performances are almost the same with traffic signal.

The patterns under LSLD are much clearer due to the fact that traffic is light. For DG and DR, a monotonically increasing relationship exists between coverage ratio and g/C ratio when a signal is present. For UG and UR, a decreasing relationship is observed. However, the differences in coverage ratio among the signals are smaller in comparison to those under DG and DR.

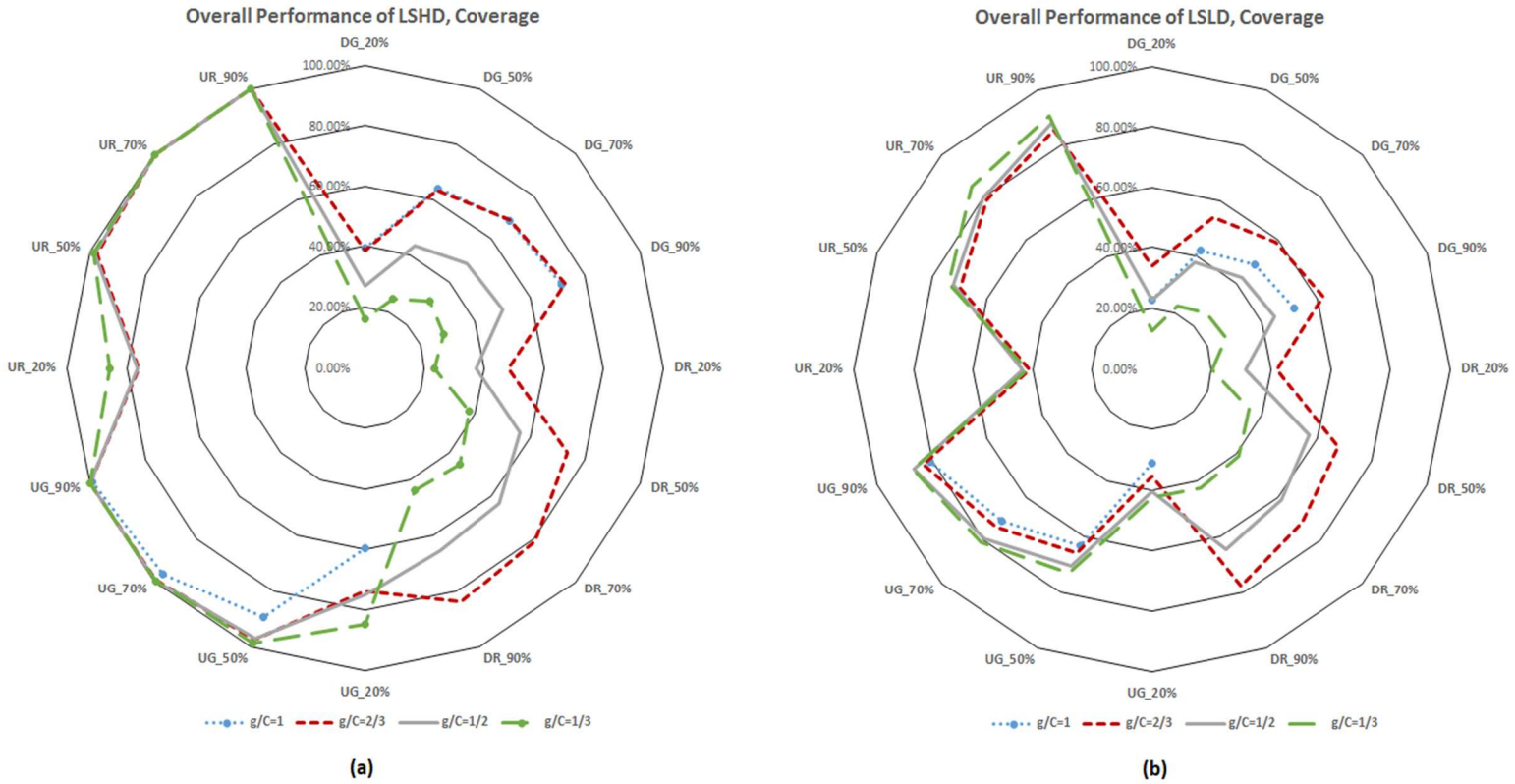

Figure 4-7 Coverage Ratio under LSHD and LSLD

4.4 Summary

This chapter investigates the relationship between the performance of a distributed traffic monitoring system proposed in Chapter 3 and the traffic signal controls. Only g/C ratios of pre-timed signal timing plans are examined as one of the possible key factors in this study. More specifically, the performances of the monitoring framework are investigated using VISSIM and its built-in COM on a simply network under three pre-timed signal timing plans with same cycle length but different g/C ratios. It is found that g/C ratio does have effects on the system performance. The simulation results show that a negative correlation exists between the relative error in speed and g/C ratio. Except for the high speed low demand traffic scenario, a positive correlation is found between the coverage ratio and the g/C ratio for the downstream segment only; the g/C ratio does not seem to affect the upstream coverage ratio significantly. The system performances vary in terms of the downstream coverage ratio and the accuracy of density estimation under different traffic scenarios and space-time windows.

CHAPTER 5

AN EXPLORATION OF PLATOON-BASED INTERSECTION CONTROL: SPEED PROFILE PLANNING FOR CONNECTED AND AUTONOMOUS VEHICLES

5.1 Introduction

CV technologies open the new possibilities of improving efficiency of transportation systems. Existing traffic operations and management highly rely on fixed-point detectors (e.g. loop detectors, cameras, etc.) as inputs of traffic information. With DSRC and other communication technologies, equipped vehicles can serve as additional data source to provide aggregated vehicular traffic pattern in a more accurate way with a reasonable MPR and support the development of better operations and management strategies (e.g. signal timing plans). Furthermore, the two-way communication enabled by DSRC makes the integration of equipped vehicles and fixed infrastructure possible and leads to new mobility applications.

Cooperative traffic operations / management strategies, as one category of CV mobility applications, have been gaining increasing attention in the past decade. Examples include cooperative intersection controls (Dresner and Stone, 2008, 2004), dynamic speed harmonization (variable speed limit) (Ubiergo and Jin, 2016), etc. Most of these applications rely on V2I DSRC and other communication networks (e.g., GPS-enabled mobile phones) and require RSUs or a server to communicate with each equipped vehicle to gather and process traffic information (see Chen and Englund, 2016; Ma et al., 2016 for comprehensive literature reviews).

In Chapter 3, we have developed a distributed framework for network-wide traffic monitoring and platoon information aggregation framework using V2V DSRC communications alone. The framework is capable of dynamically identifying vehicle groups with similar traffic states over space and time. Platoon-based cooperative traffic operations/management strategies can then be developed on the basis of the framework. Letting the infrastructure communicate with platoons of vehicles rather than individual equipped vehicles helps reduce potential communication and computation overhead. Therefore, we explore a two-stage platoon-based cooperative intersection control in this chapter, assuming that 100% vehicles are equipped. In Stage I, vehicles approaching intersections in each identified platoon will cooperatively adjust their speeds to achieve exactly the same speed before they reach the intersection. We further assume that CVs have certain autonomous driving features, and each platoon can be treated as a single vehicle whose maneuver will be taken over by a (mobile) controller at the intersection in Stage II. The speed profile of each individual platoon will be planned according to a specific control goal until it has passed through the intersection.

5.2 Related Work

Existing platoon-based intersection controls aim to update signal timing plans at intersections by utilizing information on identified platoons (or queues) and their predicted movement (or queue propagation and dispersion), rather than manipulating their trajectories/speed profiles (Gaur and Mirchandani, 2001; Jiang et al., 2006; Mirchandani and Head, 2001). The performance of such approaches highly relies on platoon identification and prediction. Better detection through CV technologies

(especially V2I communications) is possible and has resulted in new methodologies on identifying platoons (see related work in Chapter 3 and Lou et al. (2016) for a comprehensive review). New intersection control mechanisms, including platoon-based controls, have been developed to take advantage of V2I communications and fully utilize better detection of approaching traffic (Datesh et al., 2011; Feng et al., 2015; Goodall et al., 2013; He et al., 2012; Head, 2013; Priemer and Friedrich, 2009).

Furthermore, automated intersection controls are emerging with connected and autonomous vehicles. One key difference between automated and existing intersection controls is that the movement (or equivalently, the speed profile) of individual equipped vehicle approaching the intersection can be planned and manipulated accordingly by an automated intersection manager (AIM) at an automated intersection. The AIM could be either a RSU or a mobile controller (e.g. police cars, emergency vehicles, etc.). According to the interface between vehicles and AIM, there are two major types of automated intersection controls (Andert, 2017). The first type is query-based AIM (QB-AIM) or reservation-based AIM. The most representative work in this type is the First Come First Serve (FCFS) reservation-based protocol for an automated intersection control by Dresner and Stone (2008, 2004). Later on, it was extended to a mixed reality autonomous intersection, prioritizing schemes for batch processing of reservations, multi-intersection application, and auction-based scheme reflecting variation in travelers' value of time, and so on (Au et al., 2011; Carlino et al., 2013; Hausknecht et al., 2011; Quinlan et al., 2010). The major drawback of a QB-AIM is that the AIM only confirms or denies the query sent from an approaching vehicle following the First Come First Serve (FCFS) rule, and it does not directly compute and plan the vehicle's movement. In other words,

the vehicle itself needs to plan its trajectory / speed profile based on the feedback from the AIM and there is no explicit optimization of traffic flows.

This problem can be resolved through a velocity transaction AIM (VT-AIM), where speed (acceleration and deceleration) commands will be provided to approaching vehicles. For example, Lee and Park (2012) proposed a cooperative vehicle intersection control (CVIC) system where the maneuvers of each individual vehicle will be planned to eliminate the potential overlaps from conflicting approaches at the intersection. VT-AIM has attracted more attentions in comparison to QB-AIM. There are a great amount of related studies (Andert, 2017; Zhang et al., 2015; Zohdy et al., 2012). Similar methodology has also been reported for merging control to ensure safe maneuvering in the waving areas (Raravi and Shingde, 2007) and traffic controls for other transportation modes, such as railroad and aviation (Alonso-Ayuso et al., 2011; L. Zhou et al., 2017).

All the exiting automated intersection controls are for individual equipped vehicles. The speed variation of vehicles within each platoon and the corresponding potential string stability issue (amplified fluctuation of upstream vehicle speeds as a result of downstream speed perturbation (Zhou and Peng, 2015)) prevent the emerging of a platoon-based automated intersection control. String stability is the main consideration of designing spacing policy / strategy in both adaptive cruise control (ACC) and cooperative ACC (CACC) for forming a platoon (Dey et al., 2016). Common spacing policies include constant time headway and quadratic (with respect to vehicle speed) spacing policy, etc. Generally, a quadratic spacing policy outperforms the other policies (Bayar et al., 2016; Zhou and Peng, 2015). However, a target spacing, rather than speed, is in the control goal

of ACC and CACC, which imposes difficulty for a platoon of vehicles to achieve the same speed through ACC and CACC. On the other hand, advisory speed limit (ASL) application calculates and sets an advisory speed for each equipped vehicle to avoid stops and smooth vehicles' speed profiles at signalized intersections (Ubiergo and Jin, 2016). Similar to the speed limit posed through dynamic speed harmonization on freeway traffic management, those advisory speeds are not mandatory. Furthermore, the speed synchronization is handed over back to drivers (car-following models) and treated as a black box (Ma et al., 2016; Ubiergo and Jin, 2016). There is no guarantee that the pre-defined target speed is achievable or not. To address this issue, Wei et al. (2017) proposed a dynamic programing-based multi-vehicle longitudinal trajectory optimization for connected and autonomous vehicles, where both vehicle speed and system level platoon reaction time will be adjusted to enhance service rate at a signalized intersection.

All the exiting automated intersection controls are for individual vehicles. In other words, an AIM has to communicate with each approaching vehicle and calculate its speed profile. It will impose potential communication overhead and computational overload with heavy traffic approaching an AIM. However, a platoon-based intersection control, which could mitigate the issues, has not been reported in literature. By only communicating with the lead vehicle of a platoon and computing the platoon speed profile, a platoon-based automated intersection control, which can achieve communication and computational efficiency. This study investigates the two main components in such a system, which are cooperative speed harmonization to synchronize speeds within a platoon and speed profile planning given a specific control goal.

5.3 Stage I: Cooperative Speed Harmonization

After a platoon of vehicles is identified by the traffic monitoring and platoon information aggregation framework, it is likely that vehicles within the same platoon still vary from each other in speed, except the case of a platoon with a single isolated vehicle. The difference in speed will prevent platoon-based maneuvers. The goal of Stage I is for all vehicles in the same platoon to achieve the same target speed. Similar studies exist in the field of ACC and CACC using control theories (Dey et al., 2016) and leader-follower vehicle problem in car-following models (F. Zhou et al., 2017). Both of them are at the vehicle operations level and the target speed is adjusted dynamically over time. There is no guarantee that the pre-defined target speed is achievable or not especially for the second approach, where the whole process is handed over to car-following models and treated as a black box.

This chapter explores a cooperative approach, where the speed profiles of vehicles within a platoon will be planned ahead by each vehicle in collaboration with other vehicles through V2V communications, in order to achieve the target speed. We term this process as cooperative speed harmonization. The following subsections will start the discussion with two-vehicle case and three-vehicle cases, and then generalize into multi-vehicle case.

5.3.1 Target Speed

Target speed plays an important role in the process of cooperative speed harmonization. A proper target speed should be within the speed range of all vehicles that can be easily achieved by all vehicles in a timely manner. Potential target speed includes the leading

vehicle's speed (that is inexplicitly adopted in ACC and CACC), the average or the mean speed of the vehicles in a platoon.

In this study, we define the target speed as below.

$$\min \sum_{i \in I} |v_i(t) - v_T| \tag{5.1}$$

subject to constraints of vehicle dynamics and speed limits. (5.2)

where, I is set of vehicles in a platoon,

$v_i(t)$ is the speed of vehicle i at time t,

v_T is the target speed,

$i \in Z$ and $i \geq 1$.

It is a least absolute deviation problem over a set of real numbers. Its optimal solution, $\arg\min \sum_{i \in I} |v_i(t) - v_T|$, actually is the median of all vehicles' speeds.

$$v_T = median(V) \tag{5.3}$$

where, $V = \{v_i(t) | i \in I\}$.

Without loss of generality, assume all the vehicles are different in speed in a platoon. If $|I|$ ($|\cdot|$ denotes cardinality) is an odd number, the median speed is simply the middle value (v_m, where $m \in I$) over the all speeds.

$$v_T = v_m \tag{5.4}$$

If $|I|$ is an even number, the median speed could be any value between the two middle speeds (say, v_m and v_n and assume $v_m < v_n$, where, $m, n \in I$, $m \neq n$). A common way is to set the median as the average of the two middle values,

$$v_T = \frac{v_m + v_n}{2} \tag{5.5}$$

In this study, we define the target speed as the value as $v_T = v_m + \bar{a}t' = v_n + \underline{a}t'$, the speed value they reach at the same time t' if they accelerate at $\overline{a}$ and decelerate with $\underline{a}$ from their current speeds respectively. Assume the deceleration rate is always higher the acceleration rate in absolute values, i.e., $-\underline{a} > \underline{a}$. Then v_T is calculated as below if $|I|$ is an even number.

$$v_T = \frac{\underline{a}v_m - \overline{a}v_n}{\underline{a} - \overline{a}} \tag{5.6}$$

This is illustrated in Figure 5-1.

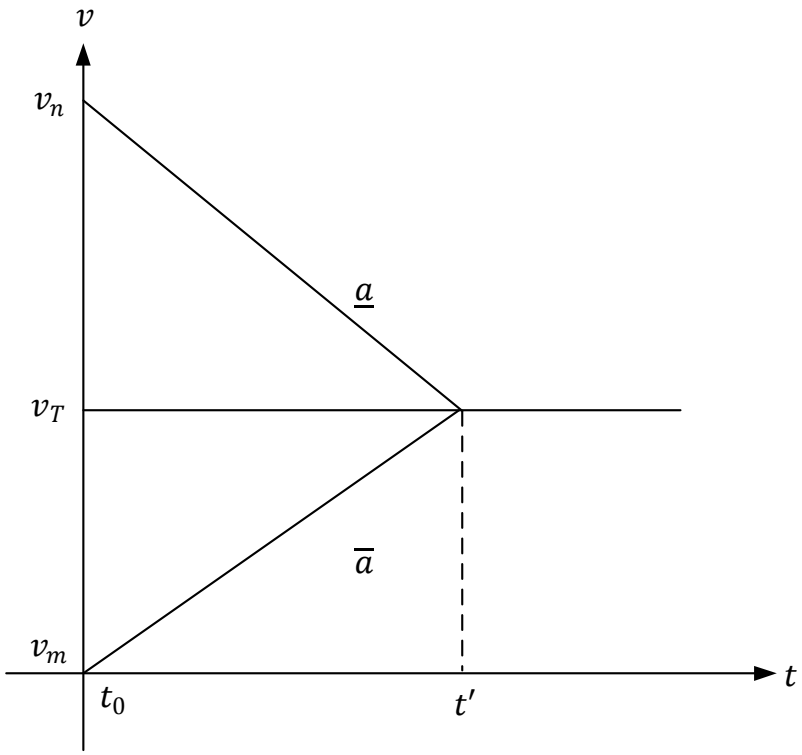

Figure 5-1 Illustration of Median Speed Definition if $|I|$ is Even

Definition in (5.6) may help eliminate the possibility of multiple maneuvers compared to (5.5). Figure 5-2 illustrates the speed profiles of vehicles m and n following the definition of (5.5). Assume the two vehicles are adjacent to each other. With assumption that $|\bar{a}| < |\underline{a}|$, we have $t_1 < t' < t_2$. There are two possible speed profiles for vehicle n to reach v_T.

1. vehicle n decreases to time t_1 and maintain v_T until t_2.
2. vehicle n decreases to time t' (reaches the same speed as vehicle m) and accelerates to t_2.

Nonetheless, t_2 is the earliest possible time for both vehicles m and n to reach v_T for the two speed profiles of vehicle n. It is greater than t', when the two vehicles first reach v_T by taking the unique speed profiles under (5.6) (see Figure 5-1).

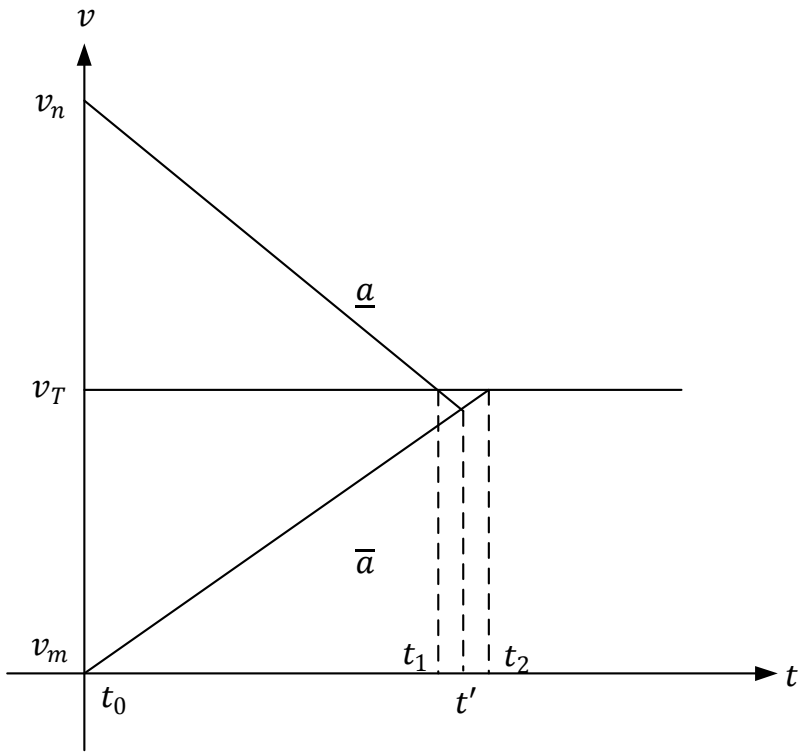

Figure 5-2 Possible Speed Profiles under Definition by (5.5)

Generally, the median speed can lead to better or the same result in terms of both speed synchronization time (unless a smaller maximum absolute deviation exists with the two optional target speeds) and fuel consumption for platoon speed synchronization compared to the first vehicle's speed and the average speed. Furthermore, the median speed could lead to less maneuvers with one less vehicle (the vehicle that is already traveling at the median speed) to synchronize, which simplifies the process of cooperative speed

harmonization. Analyses of three-vehicle cases will demonstrate such an advantage in details.

A vehicle within a platoon shall be selected to compute v_T and the preferred speed profiles once potential conflicts are identified with the default speed profiles calculated by all vehicles themselves. It could be the leading vehicle of a platoon. Information exchange between the leading vehicle and all other vehicles is made through V2V.

5.3.2 Two-Vehicle Cases

We will first start with two-vehicle cases. To concentrate on the cooperative maneuvers between vehicles within a platoon and further simplify the analysis, we assume that there are no surrounding vehicles on the network.

Introduce the following parameters for analysis.

$\delta(t)$: the relative distance between two consecutive vehicles at time t,

t_0: the start time of cooperative speed harmonization,

Δ: the minimum safety distance (i.e., space headway),

$\bar{a}$: acceleration rate,

$\underline{a}$: deceleration rate.

Define a conflict as violation of the minimum safety distance Δ between two consecutive vehicles. A conflict exists if $\delta(t) < \Delta$. Assume $\delta(t_0) > \Delta$ for all cases in this chapter. In addition, $\bar{a}$ are assumed to be the same among all vehicles, as well as $\underline{a}$. The homogenous

assumption on vehicle's characteristics will lead to conservative vehicle's dynamics and simplification for the process of speed synchronization.

Denote the speeds of the leading vehicle L and the following vehicle F as v_L and v_F respectively at time t_0. If $v_L = v_F$, then there is no need for the process of cooperative speed harmonization.

If $v_L > v_F$, vehicle L needs to decelerate at $\underline{a}$ while vehicle F accelerates at $\bar{a}$ as shown in Figure 5-3 (a). Following the speed profiles shown in Figure 5-3 (a), the relative distance between vehicles L and F (i.e., $\delta(t)$) keeps increasing until they reach the same speed at t'. With $\delta(t_0) > \Delta$, then $\delta(t) > \Delta$ at any time between t_0 and t'. In other words, there is no conflict for the case shown in Figure 5-3 (a). The two vehicles can follow the illustrated speed profiles to achieve v_T and complete speed harmonization.

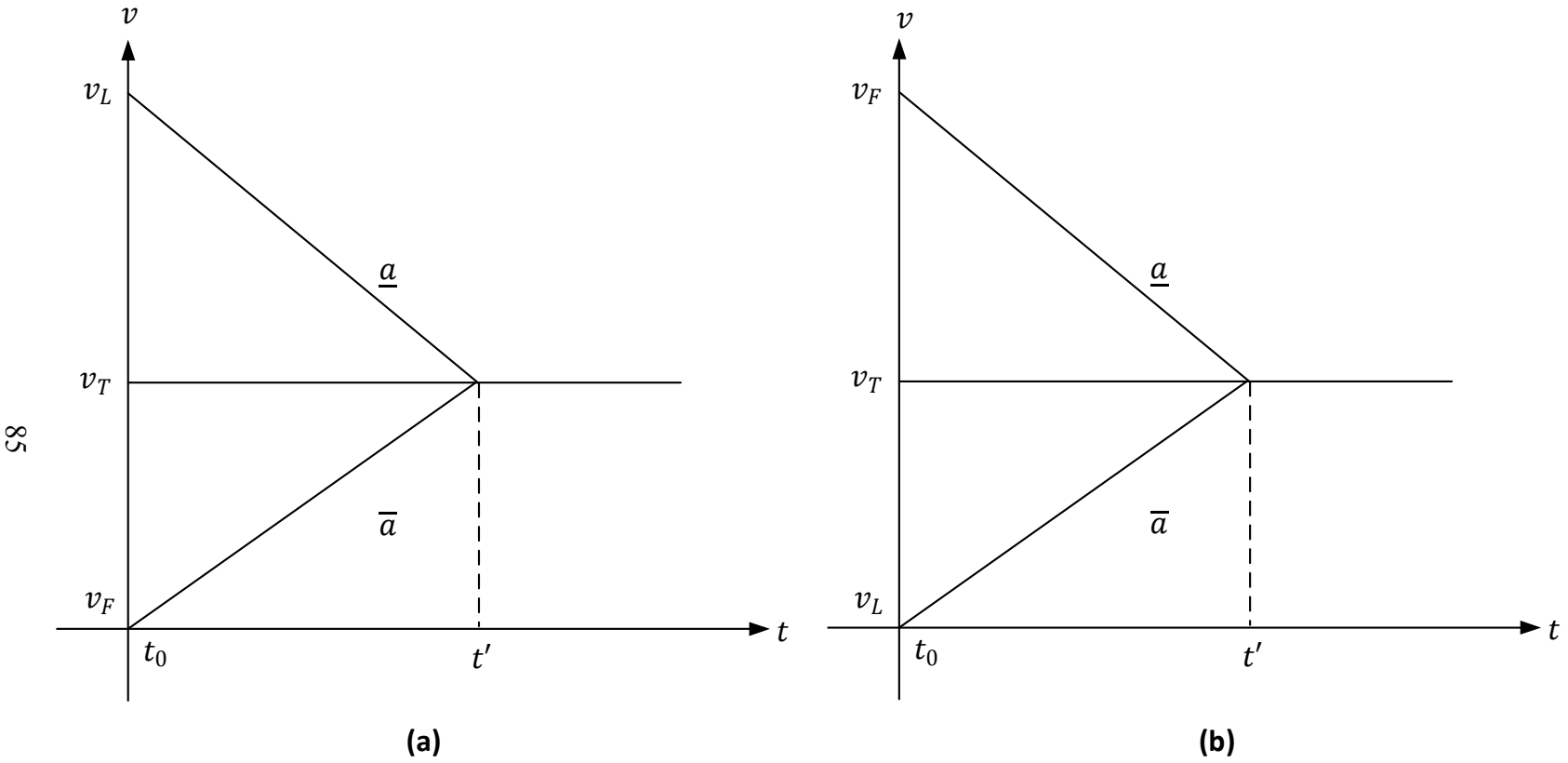

Figure 5-3 Two-Vehicle Case

If $v_F > v_L$, $\delta(t)$ will keep decreasing starting from t_0 until t'(see Figure 5-3 (b)). A conflict or even a collision may occur before v_T is achieved. Both vehicles are doing their best to avoid any potential conflicts or collisions following the conservative vehicle's dynamics, so there is nothing for the two vehicles to do at this moment. It is necessary to check $\delta(t')$ since $\delta(t)$ is minimum at t'.

$$\delta(t') = \delta(t_0) - \frac{1}{2}(v_F - v_L)(t' - t_0) \tag{5.7}$$

$\delta(t') \geq \Delta$ results into the following relationship.

$$\delta(t_0) \geq \frac{(v_F - v_L)^2}{2(\bar{a} - \underline{a})} + \Delta \tag{5.8}$$

In other words, if (5.8) holds, no conflict exists during the process of speed harmonization.

Similarly, let $\delta(t') > 0$, we can get the condition where there is no collision between vehicles L and F as below.

$$\delta(t_0) > \frac{(v_F - v_L)^2}{2(\bar{a} - \underline{a})} \tag{5.9}$$

In a word, if $\Delta > \delta(t_2) > 0$, there will be a potential conflict. When $\delta(t_2) \leq 0$, the two vehicles are going to collide, and it cannot be avoided. Those conditions shall be checked by the leading vehicle L once it receives the default speed profile of sent from vehicle F via V2V communications.

5.3.3 Three-Vehicle Cases

Now, we extend the two-vehicle case by adding one more vehicle into the mix. Denote the three vehicles as 1, 2, and 3 from downstream to upstream, and their speeds as v_1, v_2, and v_3 at time t_0. We will first eliminate the case where $v_1 = v_2 = v_3$ (i.e., v_T has achieved). If any two of the three vehicles have the same speed, then it reduces to the two-vehicle case discussed in section 5.3.2. In this section, we will focus on the cases where v_1, v_2, and v_3 are different from each other. Thus, with three vehicles, the target speed v_T will be the median of v_1, v_2 and v_3, which is one of them. There are six possible cases. Table 1 shows the speeds of the three vehicles at t_0, and the potential conflict(s).

Table 1 Speeds of the Three Vehicles at t_0

Cases	Potential Conflicts
a. $v_1 = v_T, v_2 > v_T, v_3 < v_T$	Between vehicle 1 and vehicle 2
b. $v_1 > v_T, v_2 < v_T, v_3 = v_T$	Between vehicle 2 and vehicle 3
c. $v_1 = v_T, v_2 < v_T, v_3 > v_T$	Between vehicle 2 and vehicle 3
d. $v_1 < v_T, v_2 > v_T, v_3 = v_T$	Between vehicle 1 and vehicle 2
e. $v_1 < v_T, v_2 = v_T, v_3 > v_T$	Between vehicle 1 and vehicle 2, and vehicle 2 and vehicle 3
f. $v_1 > v_T, v_2 = v_T, v_3 < v_T$	None

For cases a to b, only one pair of two consecutive vehicles may be involved in conflicts. In other words, a conflict may exist between a leading vehicle and a following vehicle. Note that cases c and d are the same as the two-vehicle case (i.e., $v_F > v_T > v_L$)

analyzed in the previous section. Therefore, we will follow the notations adopted in two-vehicle cases. We redefine cases a and b as follows.

1. $v_F > v_L = v_T$
2. $v_L < v_F = v_T$

The case, where $v_1 < v_2 < v_3$ and two conflicts exist, will be analyzed as well and denoted as Case 3.

Case 1

Figure 5-4 shows the default speed profiles of vehicles L and F to reach v_T. Starting from t_0, vehicle F decelerates at rate $\underline{a}$ until t_1 while vehicle L maintains its current speed (i.e., v_T). Define t_c as the time when a potential conflict starts, i.e., $\delta(t_c) = \Delta$ and $\delta(t_c + \varepsilon) < \Delta$, where ε is a very small time increment.

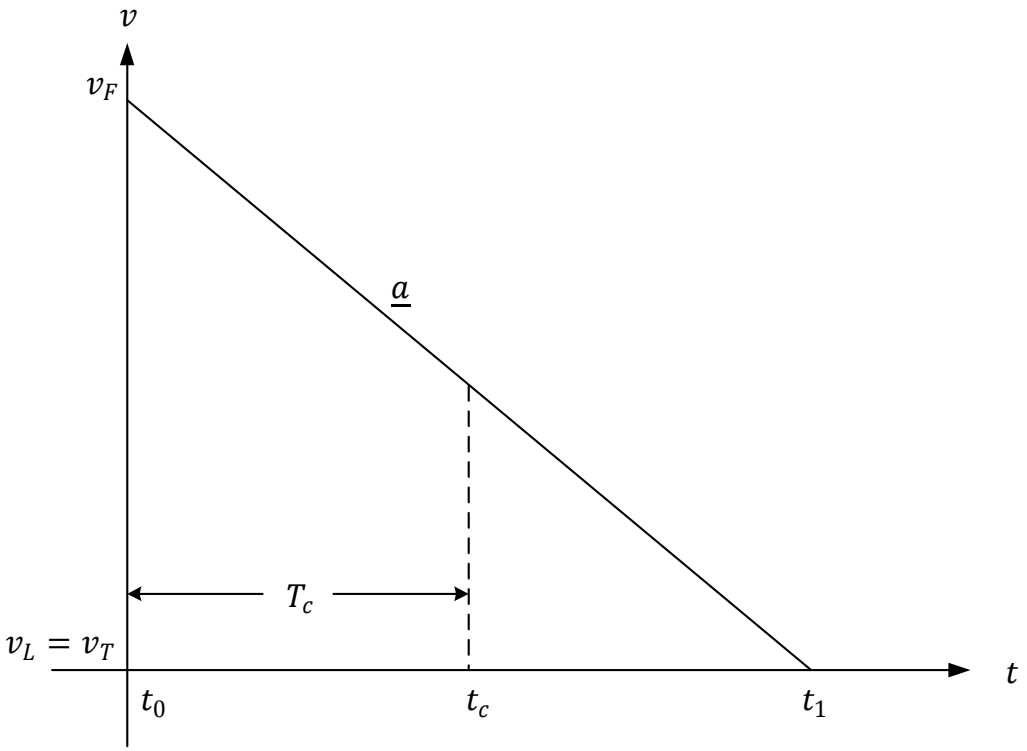

Figure 5-4 Case 1 of Three-Vehicle Case

In order to resolve the conflict, vehicle L basically needs to accelerate to a certain speed before t_c. It can accelerate from t_0 to reach the same speed as vehicle F decelerates, and then decelerate with vehicle F to v_T as illustrated in Figure 5-5 (a) in blue. If $\delta(t') > \Delta$, other speed profiles exist for vehicle L to adopt to avoid the potential conflict. For example, vehicle L can still accelerate at t_0 to some speed v' and maintain this speed until vehicle F decelerates to the same speed (see Figure 5-5 (b)).

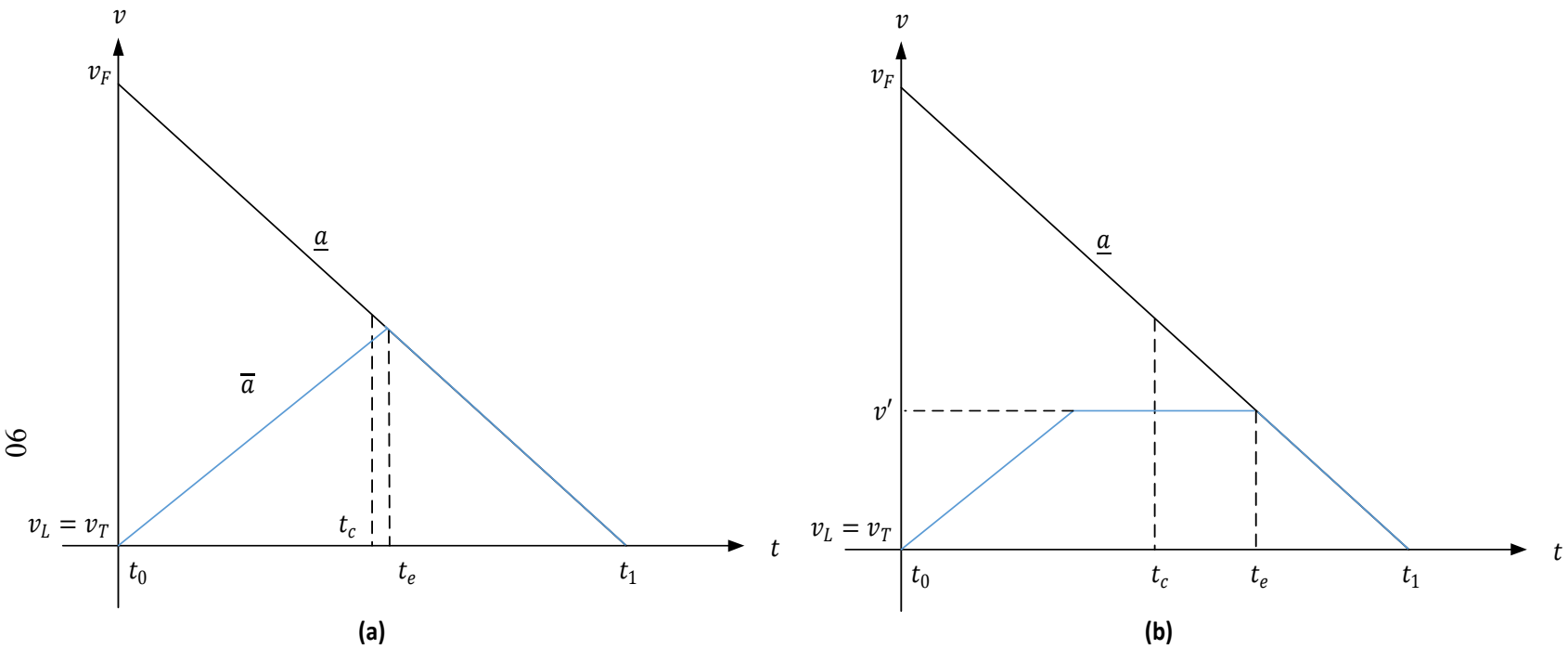

Figure 5-5 Two Possible Speed Profiles for Vehicle *L* under Case 1

Both of the two speed profiles will result into $\delta(t_e) > \Delta$ and make vehicle L deviate from its original position following the default speed profile. If there are surrounding vehicles downstream of vehicle L, the deviation may lead to new conflicts. On the other hand, it will take the same time for the two vehicles with the adjusted speed profiles to achieve v_T. However, the durations for the two vehicles to reach the same speed are different, which is $t_e - t_0$ in Figure 5-5. In the following analyses, we will denote the starting time as t_s.

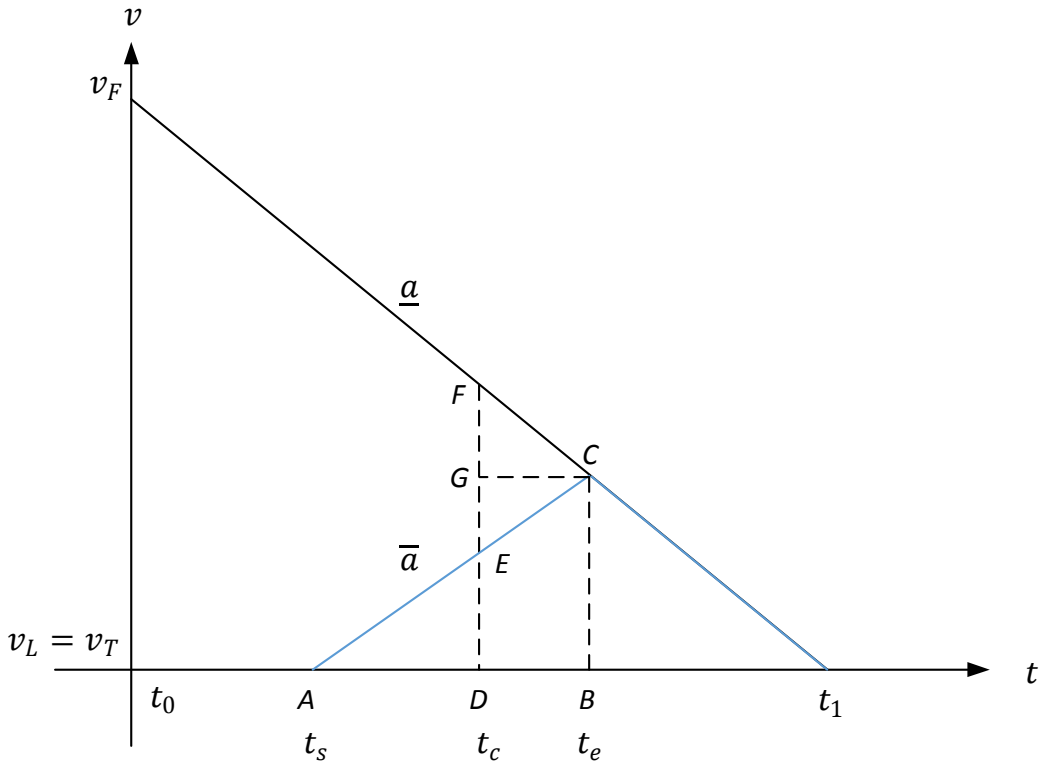

Figure 5-6 Preferred Speed Profile for Vehicle L under Case 1

Therefore, we would like to create a profile to minimize the deviation and duration. It is possible to design a speed profile such that when vehicle L reaches the same speed as

vehicle L after it accelerates before t_0, the relative distance between them is Δ. Figure 5-6 shows such a speed profile. At t_e, $\delta(t_e) = \Delta$.

Define

$\delta_D(t_c)$ as the relative distances at t_c following the default speed profile,

$\delta_D(t_e)$ as the relative distances at t_e following the default speed profile,

S_{BDFC} as the area of trapezoid $BDFC$,

S_{ABC} as the area of triangle ABC,

S_{ADE} as the area of triangle ADE,

S_{CEF} as the area of triangle CEF.

With the above definitions, it is able to obtain

$$\delta_D(t_e) = \delta_D(t_c) - S_{BDFC} \tag{5.10}$$

$$\delta(t_e) = \delta_D(t_e) + S_{ABC} \tag{5.11}$$

Since $\delta_D(t_c) = \delta(t_e) = \Delta$,

$$S_{ABC} = S_{BDFC} \tag{5.12}$$

$$S_{ADE} = S_{CEF} \tag{5.13}$$

Let $T_1 = AD$, $T_2 = CG$, $T_c = t_c - t_0$, and $C_I = v_F + \bar{a}T_c - v_T$, we can obtain the following two equations with the geometric relationships shown in Figure 5-6.

$$\begin{cases} \bar{a}T_1^2 = (\bar{a} - \underline{a})T_2^2 \\ \bar{a}T_1 + (\bar{a} - \underline{a})T_2 = C_I \end{cases} \tag{5.14}$$

It gives

$$T_1 = \frac{C_I}{\bar{a} + \sqrt{\bar{a}(\bar{a} - \underline{a})}} \tag{5.15}$$

If $t_s < t_0$, then the conflict cannot be avoided. In other words, the above speed profile will be feasible if the following condition is satisfied.

$$\frac{C_I}{\bar{a} + \sqrt{\bar{a}(\bar{a} - \underline{a})}} \leq t_c - t_0 \tag{5.16}$$

Case 2

In Case 2, $v_F = v_T$ and $v_L < v_T$. Figure 5-7 shows the default speed profiles of vehicles L and F. If a conflict exists between the two vehicles, vehicle F needs to decelerate as illustrated in the blue line.

Similar to Case 1, the following condition is required

$$S_{ADE} = S_{CEF} \tag{5.17}$$

Let $C_{II} = v_T - (v_L + \bar{a}T_c)$, $T_1 = AD$, and $T_2 = CG$, then

$$T_1 = \frac{C_{II}}{-\underline{a} + \sqrt{\underline{a}(\underline{a} - \bar{a})}} \tag{5.18}$$

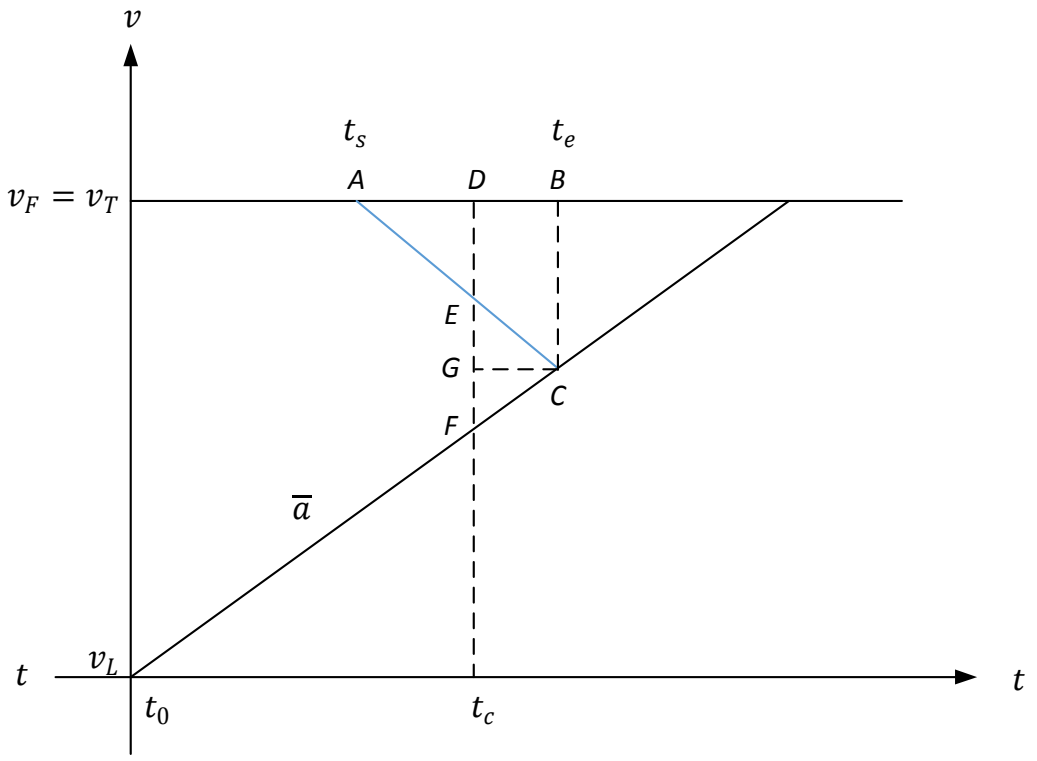

Figure 5-7 Case 2 of Three-Vehicle Case

The following relationship needs to hold so that the speed profile will be feasible.

$$\frac{C_{II}}{-\underline{a} + \sqrt{\underline{a}(\underline{a} - \bar{a})}} \geq t_0 \tag{5.19}$$

Note that the third vehicle can only be traveling at a speed less than v_T downstream to vehicle F for Case 1 or a higher speed than v_T upstream to vehicle F for Case 2. With the conservative vehicle dynamics and definition of v_T for the speed harmonization process, t_1 will be the earlies time for all the three vehicles to reach the target speed. It is possible that the third vehicle is able to reach v_T at t_e with a higher acceleration/deceleration rate than the default one. Under this condition, the speed of vehicle F at t_e could be an

alternative target speed, which will lead to less synchronization time and less maneuvers (and possible savings in fuel consumption) than the preferred speed profiles shown in Figure 5-6 and Figure 5-7.

Case 3

In the above two cases, only one possible conflict exists among the three vehicles. With Case 3, we have $v_1 < v_2 = v_T < v_3$, and two possible conflicts exist. One is between vehicles 1 and 2, and the other one is between vehicles 2 and 3. The default speed profiles for the three vehicles to harmonize their speeds will be one of the three subfigures illustrated in Figure 5-8.

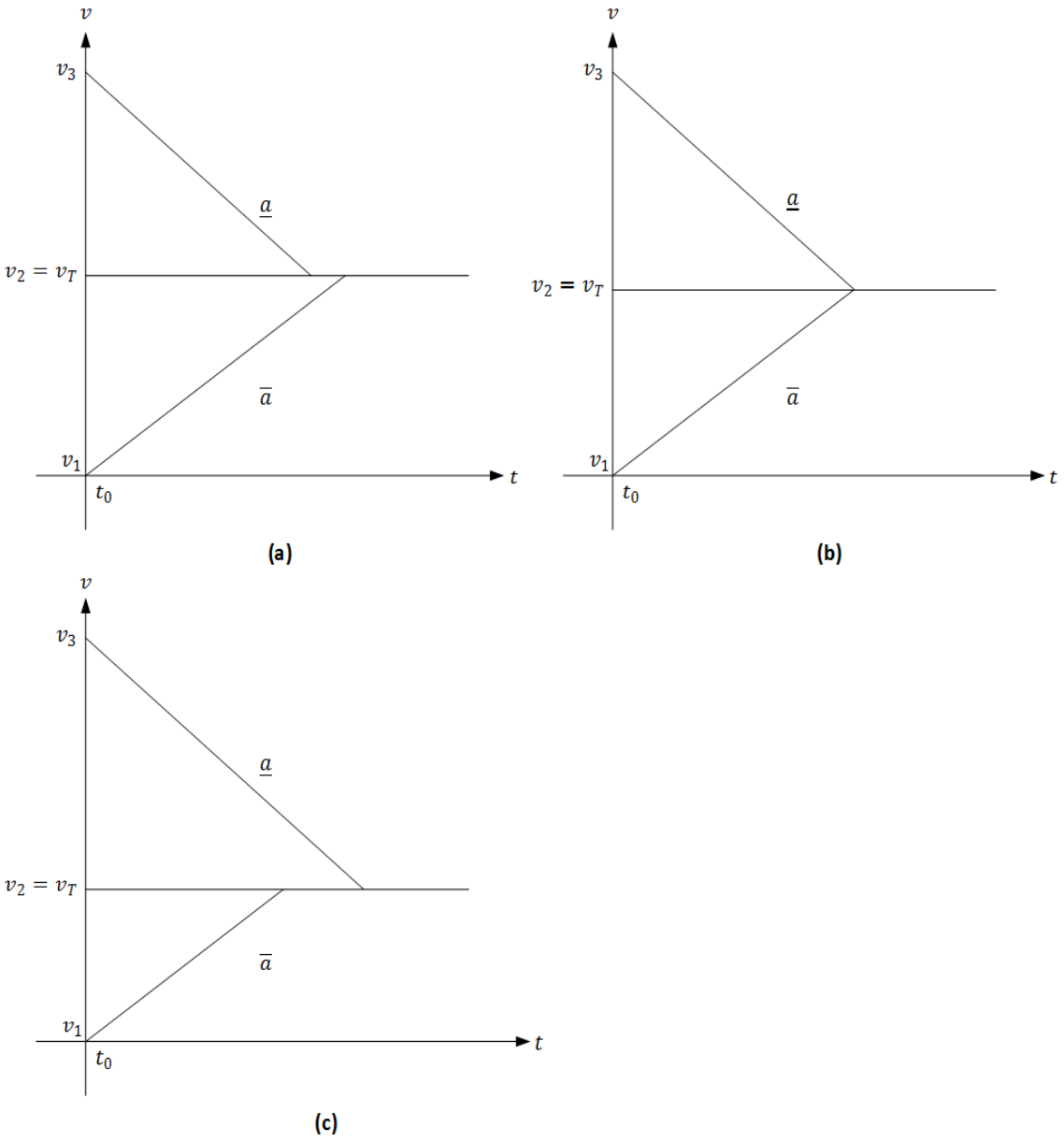

Figure 5-8 Case 3 of Three-Vehicle Case

Define

T_1: time duration for vehicles 1 and 2 to reach the same speed if vehicle 2 decelerates from t_0,

T_2: time duration for vehicles 2 and 3 to reach the same speed if vehicle 2 accelerates from t_0,

T_3: time duration for vehicles 1 and 3 to reach the same speed without consideration of v_T,

$\delta_1(t)$: relative distance between vehicles 1 and 2 at time t,

$\delta_2(t)$: relative distance between vehicles 2 and 3 at time t,

$\delta_3(t)$: relative distance between vehicles 1 and 3 at time t.

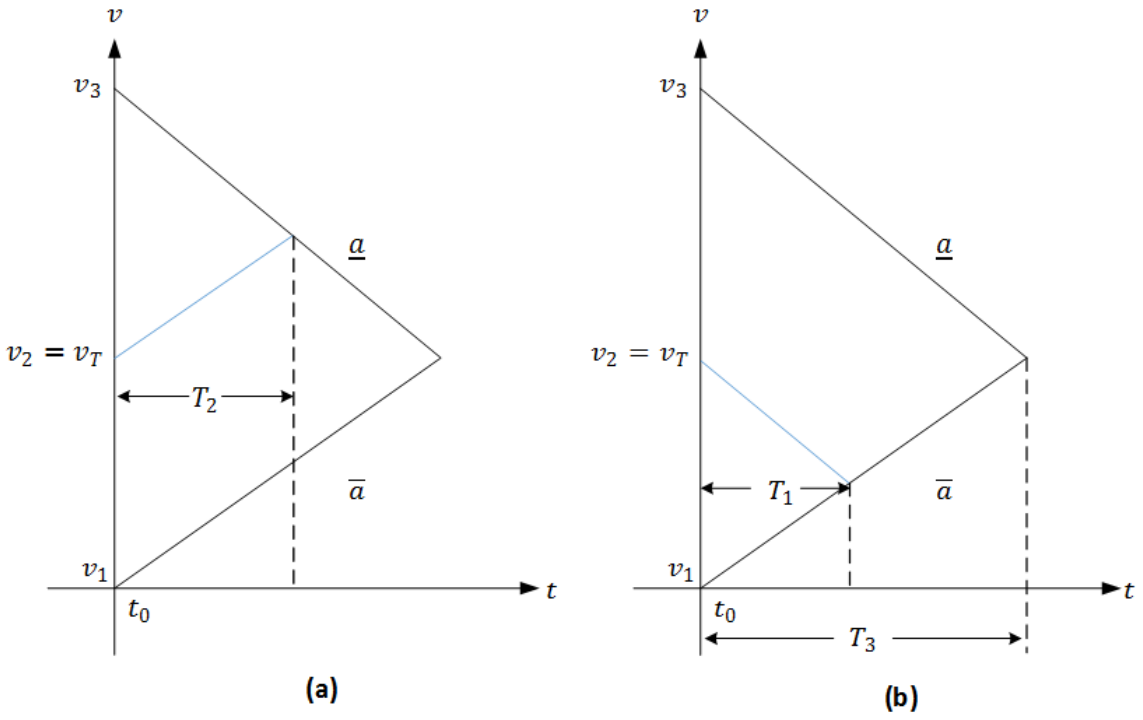

Figure 5-9 Two Possible Speed Profiles for Vehicle 2 under Case 3

Assume that vehicles are able to avoid collision when they try their best to do so. In other words,

$$\delta_1(t_0 + T_1) > 0 \tag{5.20}$$

$$\delta_2(t_0 + T_2) > 0 \tag{5.21}$$

$$\delta_2(t_0 + T_3) > 0 \tag{5.22}$$

No collision between vehicle 1 and 2 following the speed profiles shown in Figure 5-9 (b) (i.e., (5.20))

$$\delta_1(t_0) > \frac{(v_2 - v_1)^2}{2(\overline{a} - \underline{a})} \tag{5.23}$$

No collision between vehicle 2 and 3 following the speed profiles shown in Figure 5-9 (a) (i.e., (5.21)).

$$\delta_2(t_0) > \frac{(v_3 - v_2)^2}{2(\overline{a} - \underline{a})} \tag{5.24}$$

No collision between vehicle 1 and 3 (i.e., (5.22))

$$\delta_3(t_0) > \frac{(v_3 - v_1)^2}{2(\overline{a} - \underline{a})} \tag{5.25}$$

With (5.23)-(5.25), we are able to obtain the following inequality.

$$\frac{(v_3 - v_1)^2}{2(\overline{a} - \underline{a})} > \frac{(v_2 - v_1)^2}{2(\overline{a} - \underline{a})} + \frac{(v_3 - v_2)^2}{2(\overline{a} - \underline{a})} \tag{5.26}$$

This indicates that it is possible that both (5.23) and (5.24) hold if (5.25) is met. If Case 3 occurs, all the three inequalities (i.e., (5.23), (5.24), and (5.25)) should be checked

starting with (5.25). Because (5.25) is more restrictive compared to (5.23) and (5.24). If (5.25) does not hold, then collisions among the three vehicles are inevitable.

If vehicle 2 follows the speed profile shown in Figure 5-9 (b), the distance between 1 and 2 (i.e., $\delta_1(t)$) will not change after $t_0 + T_1$. Assume there is no collision between vehicle 2 and 3, we can get

$$\delta_3(t_0 + T_3) > \delta_1(t_0 + T_1) \tag{5.27}$$

Since $\delta_1(t_0) + \delta_2(t_0) = \delta_3(t_0)$,

$$\delta_2(t_0) > \frac{(v_3 - v_1)^2}{2(\overline{a} - \underline{a})} - \frac{(v_2 - v_1)^2}{2(\overline{a} - \underline{a})} \tag{5.28}$$

Similarly, if we assume no collision exists between vehicle 1 and 2 following the speed profiles illustrated in Figure 5-9 (a)

$$\delta_1(t_0) > \frac{(v_3 - v_1)^2}{2(\overline{a} - \underline{a})} - \frac{(v_3 - v_2)^2}{2(\overline{a} - \underline{a})} \tag{5.29}$$

With (5.26), if both (5.28) and (5.29) are satisfied, then (5.23) and (5.24) will both hold since (5.28) and (5.29) are more restrictive than (5.23) and (5.24) respectively. Therefore, (5.28) and (5.29) could be first checked during the process of speed synchronization. If they both hold, vehicle 2 can then maneuver within the envelope as shown in Figure 5-10. Then the case reduces to two-vehicle case with only vehicle 1 and vehicle 3 in play.

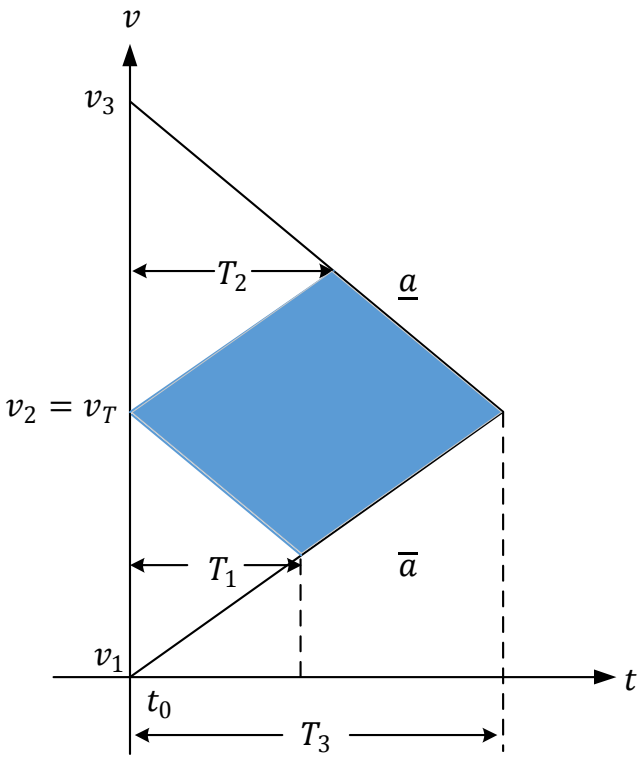

Figure 5-10 Possible Rrange for Vehicle 2 to Maneuver

The above analyses provide speed maneuver of vehicle 2 when (5.28) and (5.29) are both met. The following section will look into the opposite with the underlying assumption that (5.25) holds. Then we will have three cases as blow.

1. (5.29) holds while (5.28) not,
2. (5.28) holds while (5.29) not.
3. neither (5.28) nor (5.29) holds,

If (5.28) does not hold while (5.29) holds, we have

$$\delta_2(t_0) \le \frac{(v_3 - v_1)^2}{2(\overline{a} - \underline{a})} - \frac{(v_2 - v_1)^2}{2(\overline{a} - \underline{a})} \tag{5.30}$$

It indicates that the speed profile of vehicle 2 shown in Figure 5-9 (b) needs to be brought up to avoid possible collision with vehicle 3 (see the green line in Figure 5-11 (b)). Then it is necessary to check vehicles 1 and 2 to see if they are going to collide. If they are collision free, then

$$\frac{(v_2 - v_1)^2}{2(\overline{a} - \underline{a})} + \left[\frac{(v_3 - v_1)^2}{2(\overline{a} - \underline{a})} - \frac{(v_2 - v_1)^2}{2(\overline{a} - \underline{a})} - \delta_2(t_0)\right] < \delta_1(t_0) \tag{5.31}$$

It gives,

$$\frac{(v_2 - v_1)^2}{2(\overline{a} - \underline{a})} < \delta_1(t_0) + \delta_2(t_0) \tag{5.32}$$

This is consistent with the underlying assumption that (5.25) holds. In other words, the new speed profile of vehicle 2 can be adopted for the speed synchronization so that collisions can be avoided.

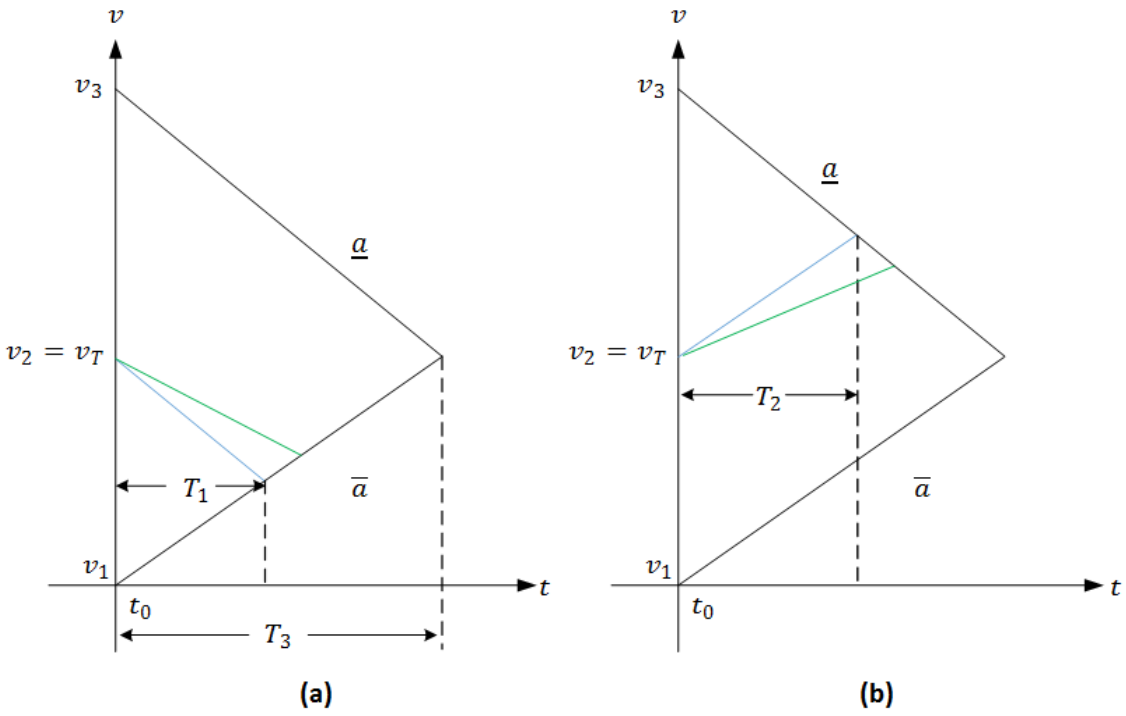

Figure 5-11 Maneuvers of Vehicle 2 if eithor (5.28) or (5.29) Holds

Similarly, if (15) is not satisfied but (14) holds, we need to bring down the speed profile of vehicle 2 (green line in Figure 5-11 (a)) and check possible collision between vehicles 2 and 3. If no collision exist, then

$$\frac{(v_3 - v_2)^2}{2(\bar{a} - \underline{a})} + \left[\frac{(v_3 - v_1)^2}{2(\bar{a} - \underline{a})} - \frac{(v_3 - v_2)^2}{2(\bar{a} - \underline{a})} - \delta_1(t_0)\right] < \delta_2(t_0) \tag{5.33}$$

We can get

$$\frac{(v_3 - v_1)^2}{2(\bar{a} - \underline{a})} < \delta_1(t_0) + \delta_2(t_0) \tag{5.34}$$

With the underlying assumption, the inequality holds and there is no collision between vehicles 2 and 3 even with the bring-down of vehicle 2's speed profile.

If neither (5.28) nor (5.29) holds, in other words,

$$\begin{cases} \delta_2(t_0) \le \dfrac{(v_3 - v_1)^2}{2(\overline{a} - \underline{a})} - \dfrac{(v_2 - v_1)^2}{2(\overline{a} - \underline{a})} \\ \delta_1(t_0) \le \dfrac{(v_3 - v_1)^2}{2(\overline{a} - \underline{a})} - \dfrac{(v_3 - v_2)^2}{2(\overline{a} - \underline{a})} \end{cases} \tag{5.35}$$

With $\delta_3(t_0) = \delta_1(t_0) + \delta_2(t_0)$, then we have

$$\delta_3(t_0) \le \frac{(v_3 - v_1)^2}{2(\overline{a} - \underline{a})} + \left[\frac{(v_3 - v_1)^2}{2(\overline{a} - \underline{a})} - \frac{(v_2 - v_1)^2}{2(\overline{a} - \underline{a})} - \frac{(v_3 - v_2)^2}{2(\overline{a} - \underline{a})}\right] \tag{5.36}$$

Since $\left[\frac{(v_3-v_1)^2}{2(\overline{a}-\underline{a})} - \frac{(v_2-v_1)^2}{2(\overline{a}-\underline{a})} - \frac{(v_3-v_2)^2}{2(\overline{a}-\underline{a})}\right] > 0$ (from (5.26)), the above inequality does not necessarily mean that (5.25) is violated. If (5.25) is valid, it is still possible for (5.23) and (5.24) to hold. In this case, the question becomes whether we can find a sub-region inside the envelope shown in Figure 5-10 such that no collisions exist among the three vehicles if the speed profile of vehicle 2 is within the sub-region (illustrated in Figure 5-12).

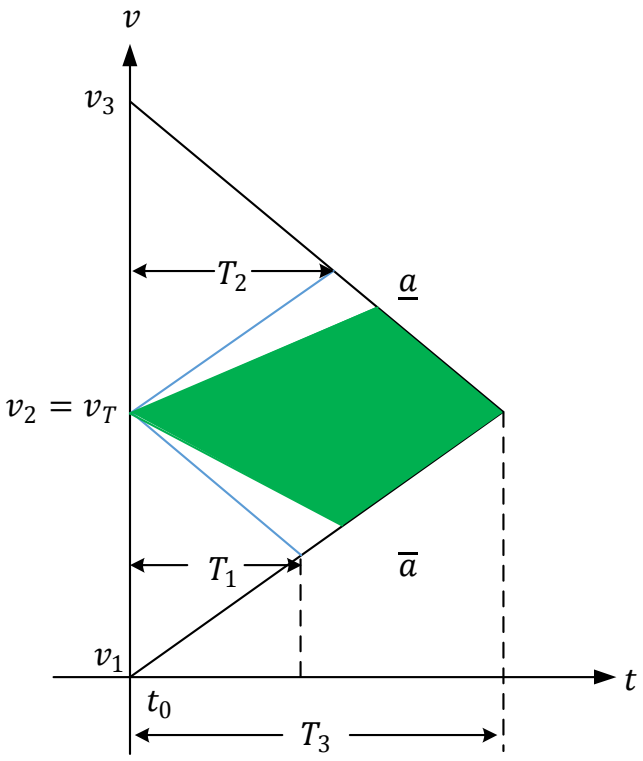

Figure 5-12 Sub-Rrange for Vehicle 2 to Maneuver if Neither (5.28) nor (5.29) Holds

According to the above analyses, the procedure of cooperative speed harmonization with two conflicts under three-vehicle cases under is summarized into the flow chart (see Figure 5-13).

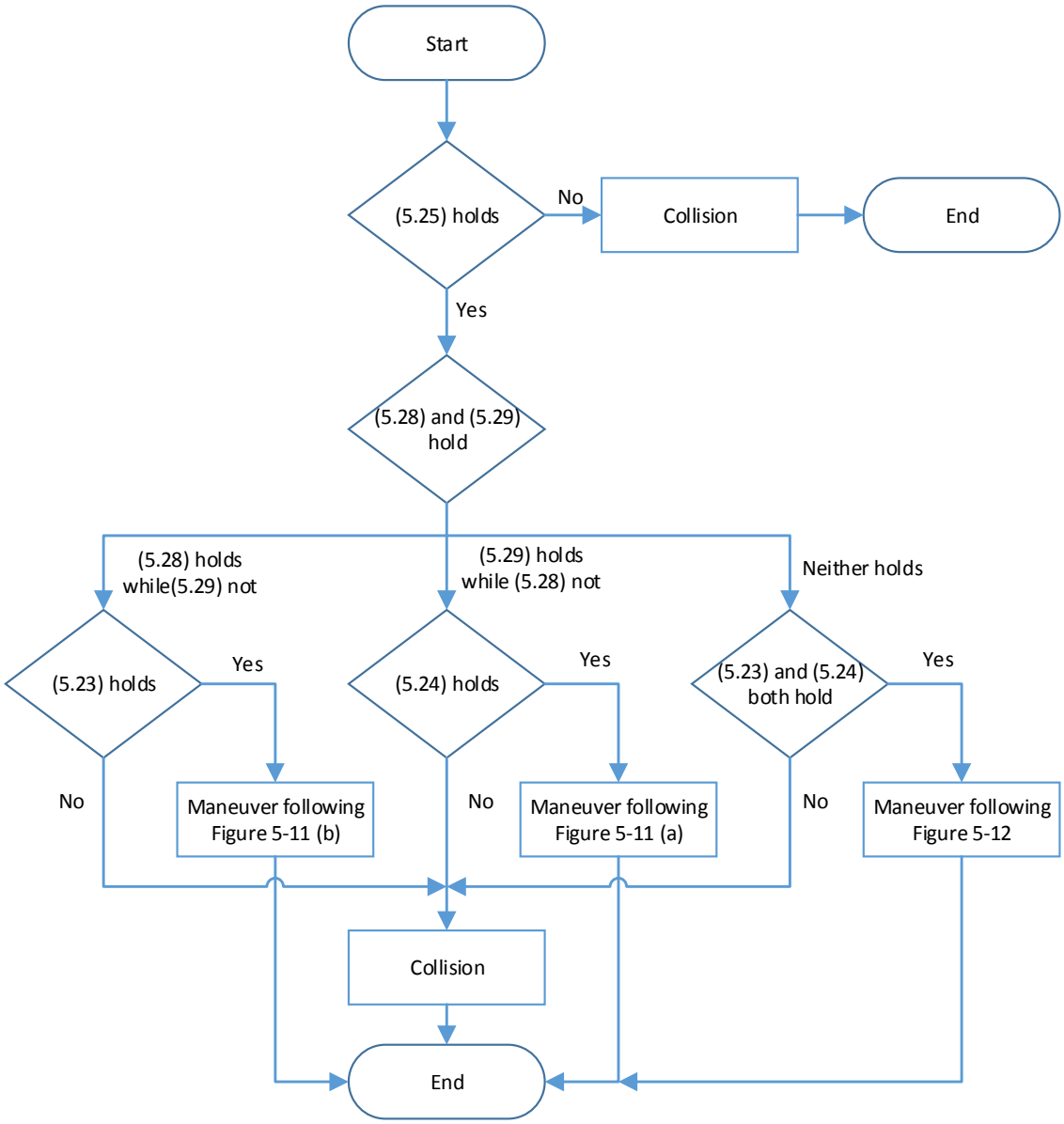

Figure 5-13 Flow Chart of Cooperative Speed Harmonization for Two Conflicts

5.3.4 Multi-Vehicle Cases

Sections 5.3.2 and 5.3.3 analyzed speed synchronization for two-vehicle cases and three-vehicle cases. Four basic cases involved cooperative speed harmonization are identified,

namely, three one-conflict cases and one two-consecutive-conflict case. The corresponding collision/conflict-free conditions are explored along with amended speed profiles for cooperative speed harmonization. Our analyses on multi-vehicle cases will start with two more one-conflict cases supplementary to the three cases followed by discussion on cases with more than one conflict.

One Conflict

With more than three cases in a platoon, if there only exists a conflict for two consecutive vehicles. The relationship of their speeds to v_T may not be the same as the three one-conflict cases. Follow the notation used for one-conflict cases, two new cases are possible.

1. $v_F > v_L > v_T$
2. $v_T > v_F > v_L$

Case 1

This case requires both vehicles L and F to decelerate to v_T following the speed profiles in Figure 5-14. Basically, vehicle F needs to accelerate at some time t_s before t_c to resolve a potential conflict. Depending on the relative location of t_c to t_1, we will have the following three different instances.

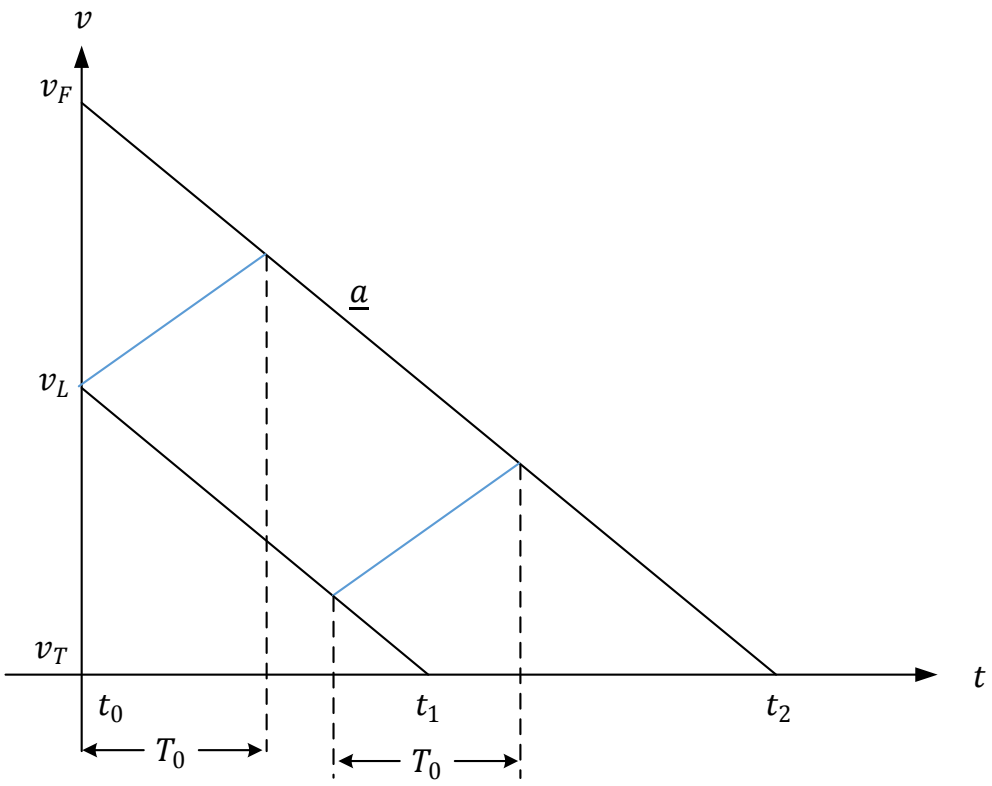

Figure 5-14 Case 1 of Multi-Vehicle Cases

Instance I

If $t_c \leq t_1$, then $t_s < t_1$ and the adjusted speed profile is illustrated in Figure 5-15. With the assumption that $\underline{a}$ is the same over all vehicles, segments $v_F t_2$ and $v_L t_1$ are parallel to each other. The time for vehicle L to accelerate to the same speed of vehicle F will be the same for any t_s between t_0 and t_1. Denote the time as T_0 (see Figure 5-14 for illustration).

$$v_L + \bar{a}T_0 = v_F + \underline{a}T_0 \tag{5.37}$$

$$DF + BG = T_0 \tag{5.38}$$

where, $T_0 = \frac{v_F - v_L}{\bar{a} - \underline{a}}$.

Similar to Case 1 under three-vehicle cases,

$$S_{ABC} = S_{CDE} \tag{5.39}$$

Since $ABC \sim CDE$

$$DF = BG \tag{5.40}$$

Then

$$T_1 = DF = \frac{v_F - v_L}{2(\bar{a} - \underline{a})} \tag{5.41}$$

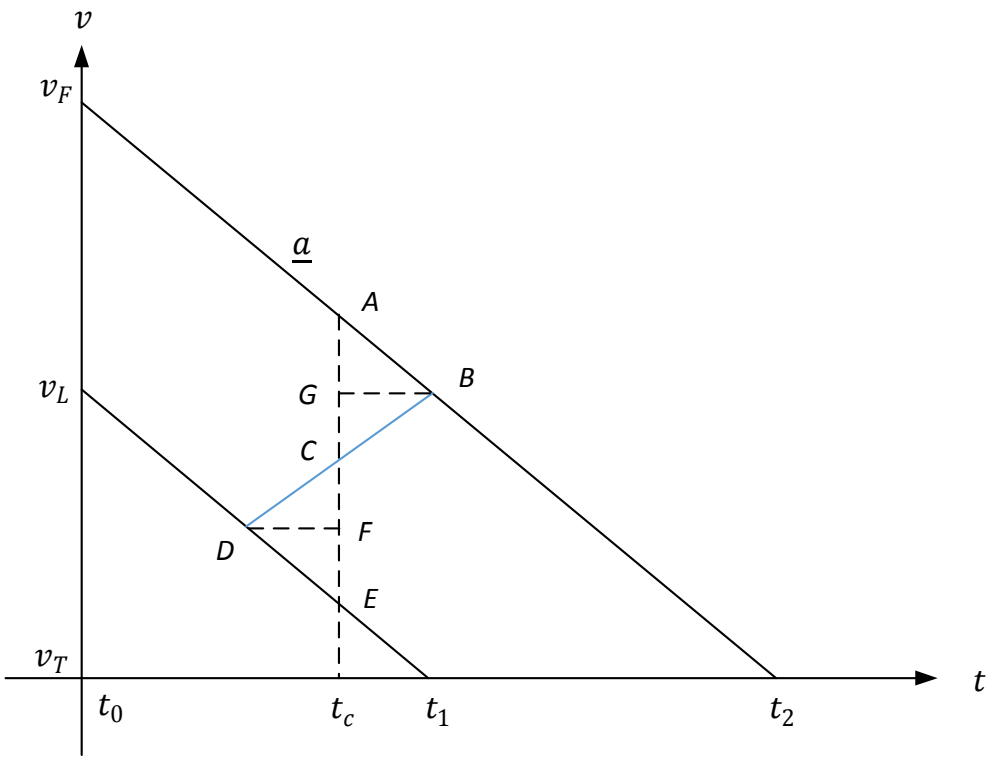

Figure 5-15 Instance I under Case 1

It is possible that we cannot find a triangle CDE with same area as triangle ABC if $t_s < t_0$. In other words, if the following relationship holds we can guarantee that the conflict can be always resolved following the speed profile in Figure 5-15.

$$T_1 \geq t_c - t_0 \tag{5.42}$$

Substitute T_1, we have

$$t_c \leq \frac{v_F - v_L}{2(\bar{a} - \underline{a})} + t_0 \tag{5.43}$$

Instance II

If $t_c > t_1$ and $t_e \geq t_1$, we will have Instance II as shown in Figure 5-16. Since the speed of vehicle L has become v_T, this instance is exactly the same as Case 1 under three-vehicle cases. So,

$$T_1 = DE = \frac{C_I}{\bar{a} + \sqrt{\bar{a}(\bar{a} - \underline{a})}} \tag{5.44}$$

where, $C_I = v_F + \bar{a}T_c - v_T$.

From Figure 5-16, we know that the following relationship should be satisfied

$$t_s \geq t_1 \tag{5.45}$$

This is equivalent to

$$t_c - T_1 \geq t_1 \tag{5.46}$$

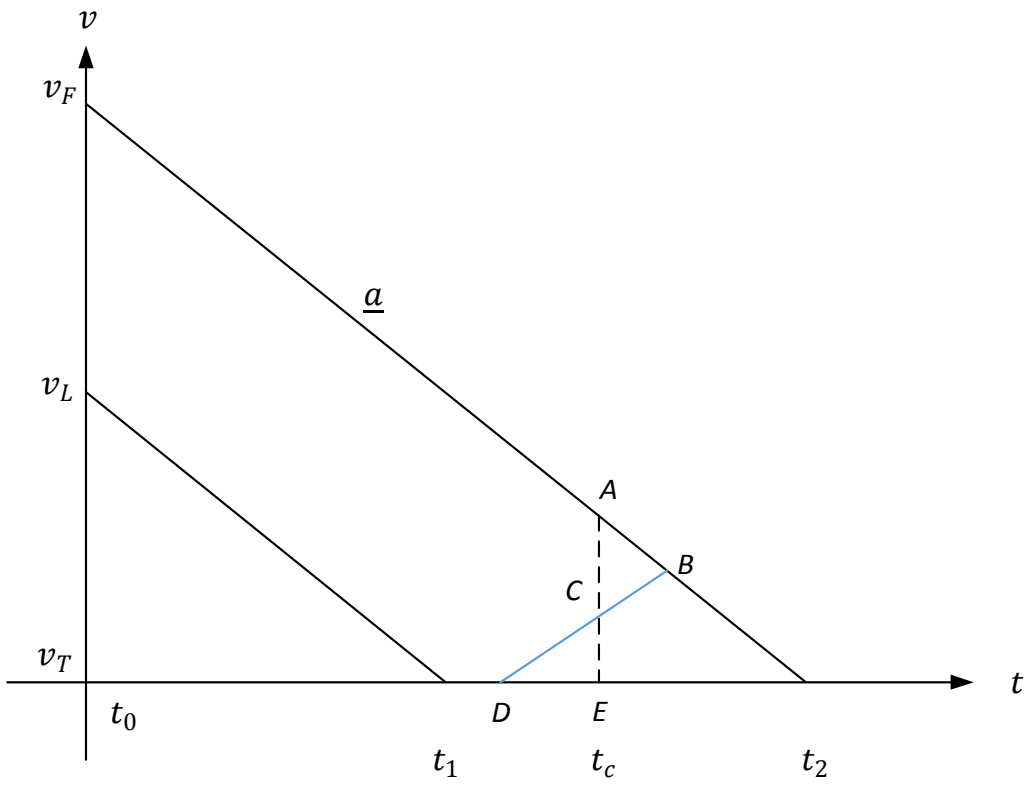

Figure 5-16 Instance II under Case 1

Substitute T_1

$$t_c \geq \frac{C_I}{\bar{a} + \sqrt{\bar{a}(\bar{a} - \underline{a})}} + t_1 \tag{5.47}$$

Since $t_c < t_2$,

$$\frac{C_I}{\bar{a} + \sqrt{\bar{a}(\bar{a} - \underline{a})}} + t_1 \leq t_c < t_2 \tag{5.48}$$

Instance III

Figure 5-17 illustrates Instance III, where $t_c > t_1$ and $t_s < t_1$.

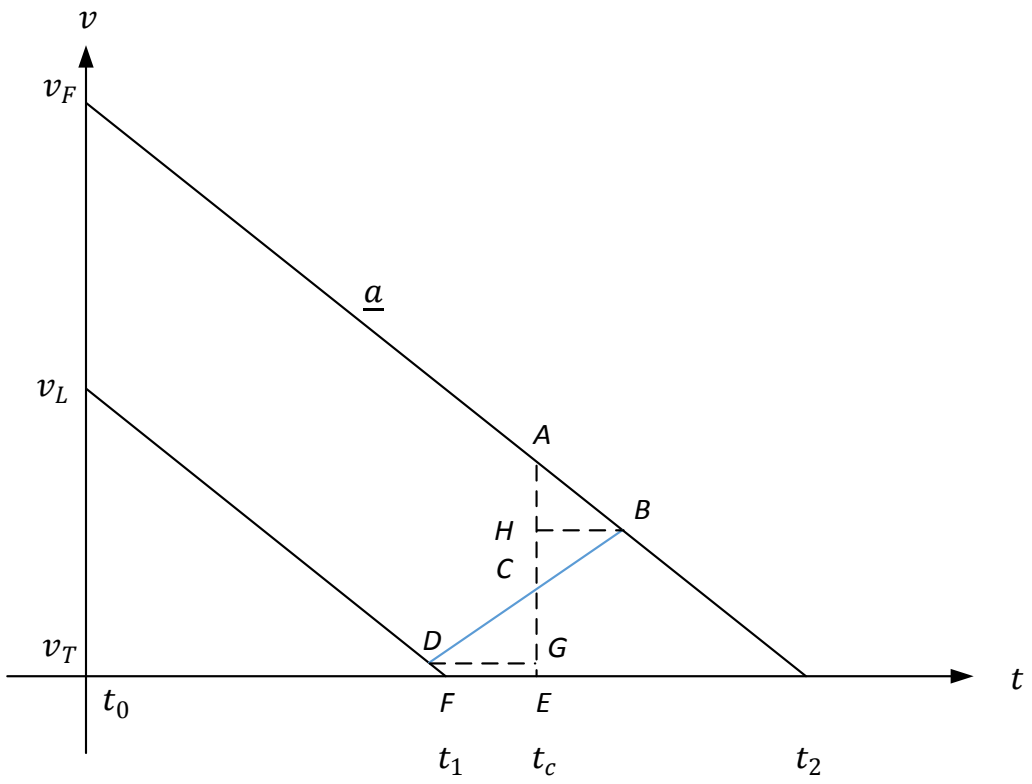

Figure 5-17 Instance III under Case 1

Adopt the conclusion from Case1 in section 5.3.3, we have

$$S_{ABC} = S_{CDFE} \tag{5.49}$$

Since $S_{CDFE} = S_{CDG} + S_{EFDG}$,

$$T_1 = DG = \frac{\left[C_{III} - \underline{a}(t_c - t_1)\right]T_0 - \underline{a}(t_c - t_1)^2}{C_{III} - \underline{a}(t_c - t_1) + (\overline{a} - \underline{a})T_0} \tag{5.50}$$

where, $C_{III} = v_F + \underline{a}T_c - v_T$.

The following inequality should hold for T_1 is valid.

$$t_c - T_1 < t_1 \tag{5.51}$$

With $t_c > t_1$, we get

$$t_1 < t_c < \frac{C_{III} T_0}{C_{III} + \overline{a} T_0} \tag{5.52}$$

where, $T_0 = \frac{v_F - v_L}{\overline{a} - \underline{a}}$.

Case 2

In Case 2 under multi-vehicle cases, both vehicles *L* and *F* need to accelerate to v_T as shown in Figure 5-18. In order to resolve the potential conflict, deceleration of vehicle *F* is necessary before t_c. Case 2 is very similar to Case 1, which also includes three different instances.

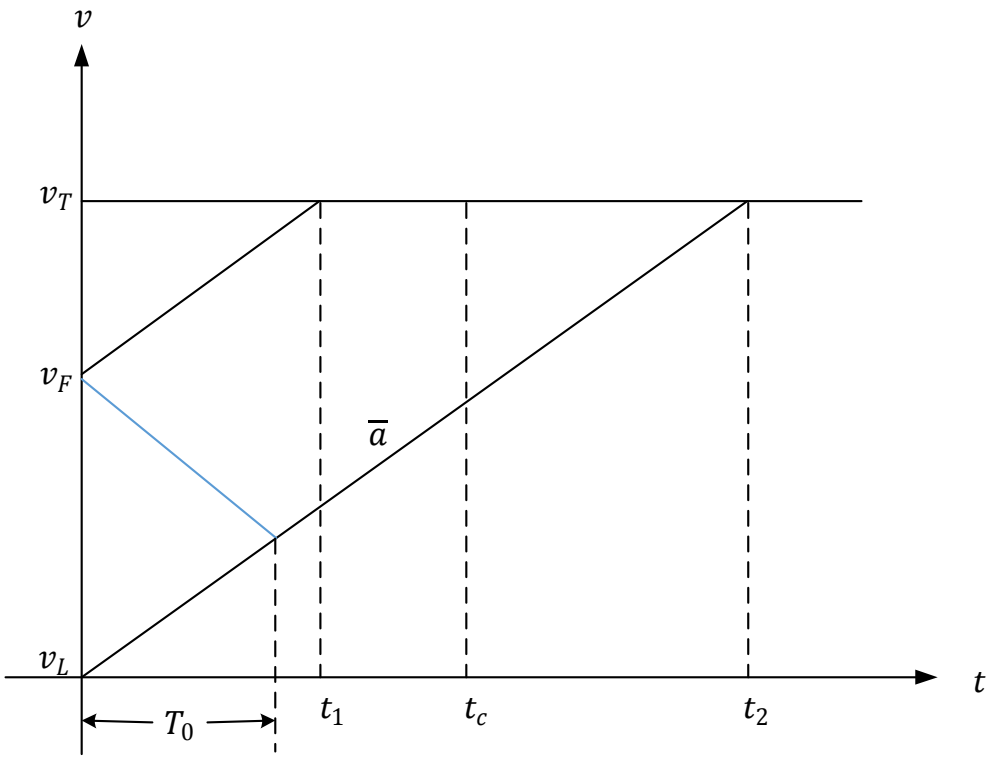

Figure 5-18 Case 2 of Multi-Vehicle Cases

Instance I

Instance I requires $t_c \leq t_1$ as illustrated in Figure 5-19. Similar to Case 2 of three-vehicle cases in 5.3.3, we have

$$\begin{cases} v_L + \bar{a}T_0 = v_F + \underline{a}T_0 \\ T_1 + T_2 = T_0 \\ T_1 = T_2 \end{cases} \tag{5.53}$$

where, $T_1 = DG$, $T_2 = BH$, and $T_0 = \frac{v_F - v_L}{\bar{a} - \underline{a}}$.

Solve for T_1,

$$T_1 = \frac{v_F - v_L}{2(\bar{a} - \underline{a})} \tag{5.54}$$

To make sure the above derivation valid, the following relationship should be satisfied.

$$T_1 \geq t_c - t_0 \tag{5.55}$$

Substitute T_1, we have

$$t_c \leq \frac{v_F - v_L}{2(\bar{a} - \underline{a})} + t_0 \tag{5.56}$$

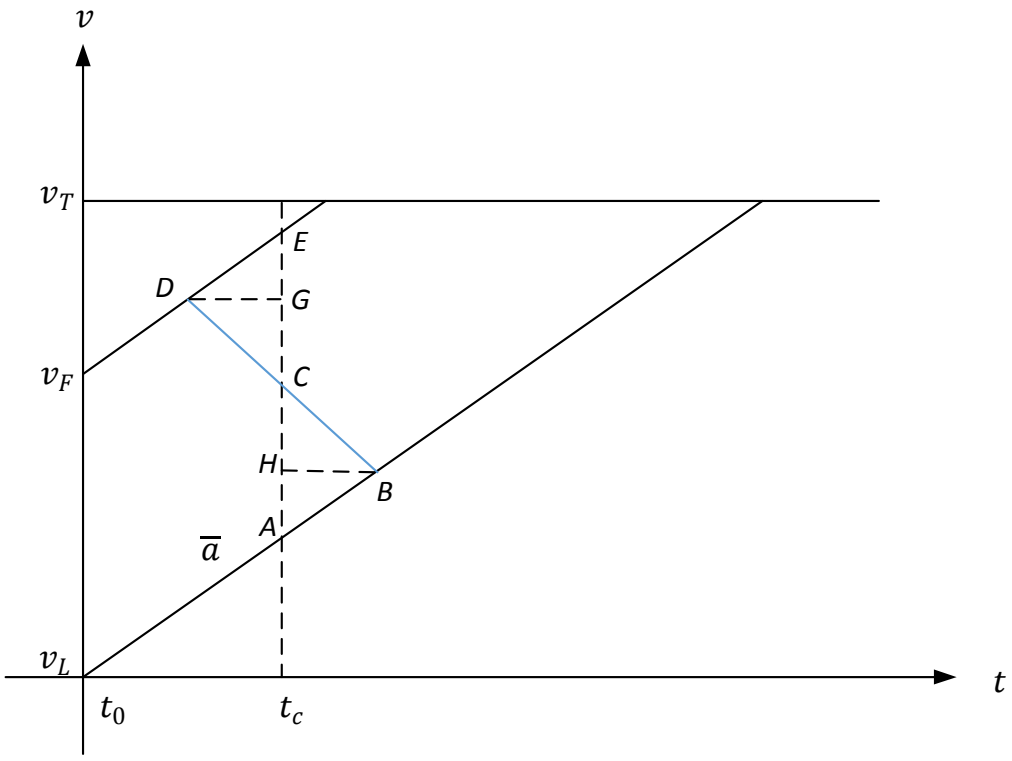

Figure 5-19 Instance I under Case 2

Instance II

Figure 5-20 shows the speed profiles in Instance II under Case 2, where $t_c > t_1$ and vehicle F needs to decelerate after its speed becomes v_T. Instance II is exactly the same with Case 2 in section 5.3.3. Thus, we get

$$T_1 = DE = \frac{C_{II}}{-\underline{a} + \sqrt{\underline{a}(\underline{a} - \bar{a})}} \tag{5.57}$$

where, $C_{II} = v_T - (v_L + \bar{a}T_c)$.

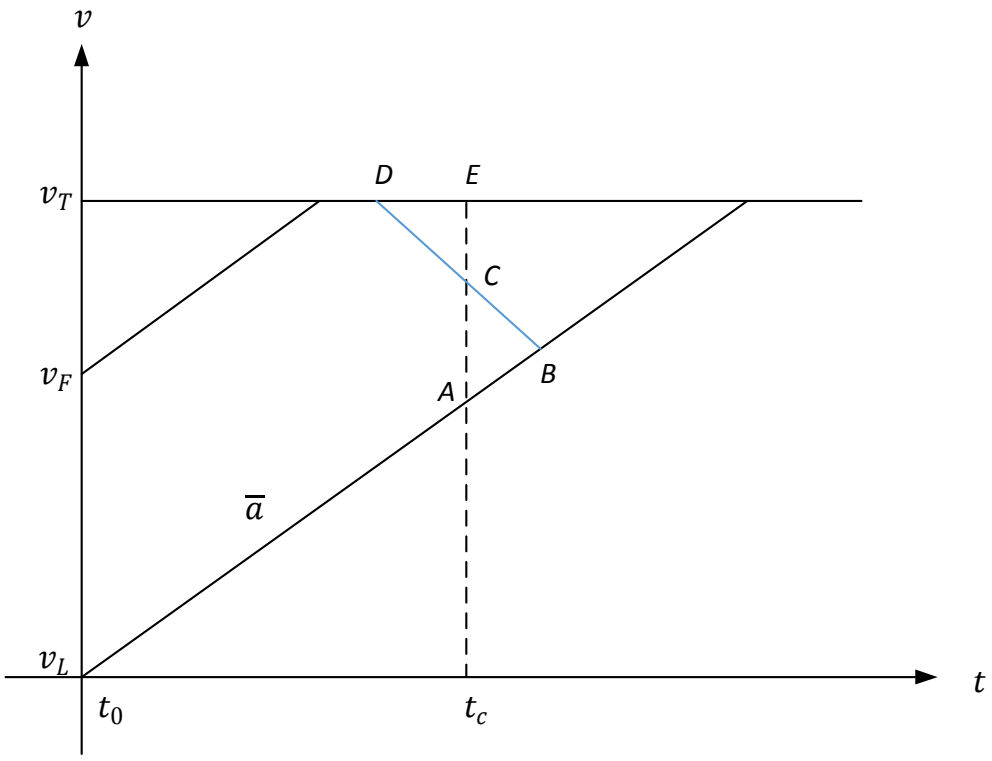

Figure 5-20 Instance II under Case 2

Similarly, we have

$$t_s \geq t_1 \tag{5.58}$$

It is equivalent to

$$t_c - T_1 \geq t_1 \tag{5.59}$$

Substitute T_1,

$$t_c \geq \frac{C_{II}}{-\underline{a} + \sqrt{\underline{a}(\underline{a} - \bar{a})}} + t_1 \tag{5.60}$$

With $t_c < t_2$,

$$\frac{C_{II}}{-\underline{a} + \sqrt{\underline{a}(\underline{a} - \bar{a})}} + t_1 \leq t_c \leq t_2 \tag{5.61}$$

It gives the feasible range of t_c for Instance II.

Instance III

The adjusted speed profile of vehicle F under Instance III is shown in blue line in Figure 5-21, where $t_c > t_1$ and $t_s < t_1$.

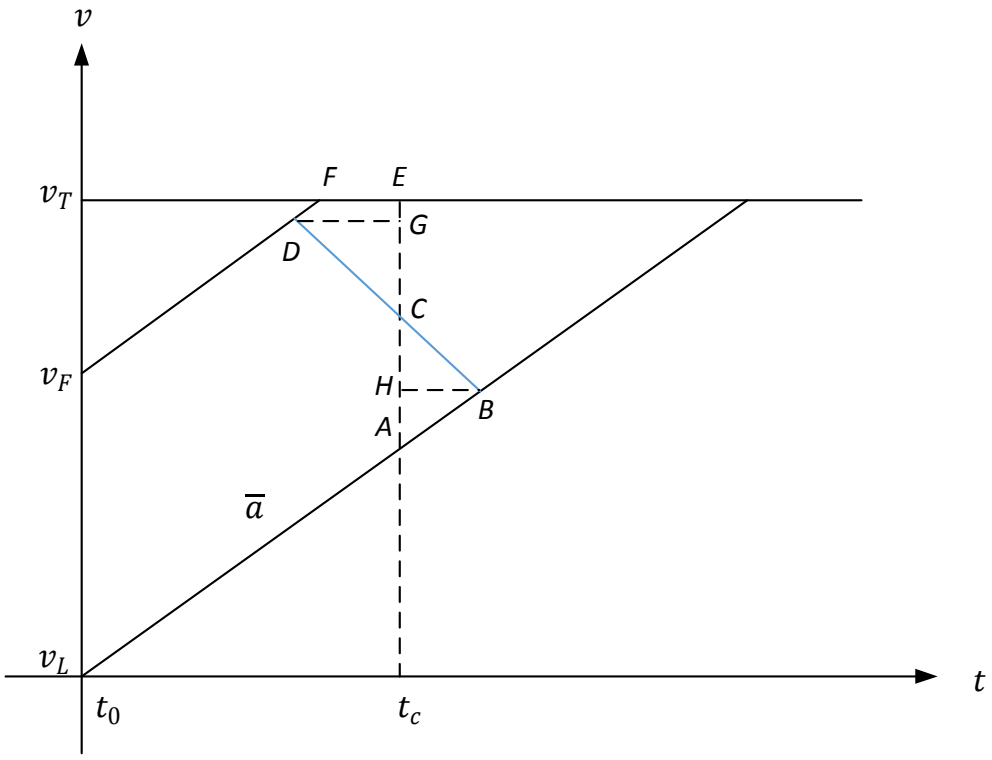

Figure 5-21 Instance III under Case 2

Under the adjusted speed profile,

$$S_{ABC} = S_{CDFE} \tag{5.62}$$

Since $S_{CDFE} = S_{CDG} + S_{EFDG}$,

$$T_1 = DG = \frac{[C_{IV} + \overline{a}(t_c - t_1)]T_0 + \overline{a}(t_c - t_1)^2}{C_{IV} + \overline{a}(t_c - t_1) + (\overline{a} - \underline{a})T_0} \tag{5.63}$$

where, $C_{IV} = v_L + \overline{a}T_c - v_T$.

To make sure T_1 is valid, the following inequality should hold

$$t_c - T_1 < t_1 \tag{5.64}$$

With $t_c > t_1$,

$$t_1 < t_c < \frac{C_{IV}T_0}{C_{IV} - \underline{a}T_0} + t_1 \tag{5.65}$$

where, $T_0 = DG = \frac{v_F - v_L}{\overline{a} - \underline{a}}$.

Discussion on More than One Conflict

Under multi-vehicle cases, more than one conflict might happen during the process of speed synchronization. We are still able to break it down into two different scenarios and have different strategies correspondingly.

The first scenario is that the conflicts are not consecutive. In other words, there are serval separate one-conflict cases which would interact with each other. Under this scenario, one-conflict cases presented before in this chapter can be directly applied. With the two

new cases, there are five one-conflict cases. They cover all the possible conflict situation where only two consecutive vehicles are involved.

The other scenario states the condition that the conflicts are adjacent one by one. As we can see from the three-vehicle cases, when it involves two consecutive conflicts, it becomes more complicated than one-conflict cases and requires cooperation among the three vehicles to resolve the potential conflicts.

The consecutive conflicts are just combinations of individual one-conflict cases. Take a platoon with four vehicles for example, vehicles 1, 2, 3, and 4 (a higher vehicle index indicates a more upstream position) are travelling at v_1, v_2, v_3 and v_4 respectively. Assume $v_1 < v_2 < v_T < v_3 < v_4$. In the worst case, conflicts will appear between any two consecutive vehicles, i.e., 1 and 2, 2 and 3, 3 and 4. Case 3 in the three-vehicle case actually provides a guideline to analyze such a combination. Under this specific case, potential conflicts / collisions may not be avoided by amending the speed profiles of the boundary vehicles 1 and 4 (since they are doing their best to avoid conflicts/collisions). Similar to Cases 3 under three-vehicle cases, vehicles 2 and 3 may have space to adjust their speed profiles to prevent potential conflicts/collisions from happening. The boundaries and feasible maneuvers for vehicles 2 and 3 can be determined by following the procedure illustrated in Figure 5-13.

A platoon with more vehicles is likely to have more consecutive conflicts than one with fewer vehicles. The more consecutive conflicts, the more complicated the cooperative speed harmonization. We could artificially limit the platoon size through the platoon identification process, assign a temporal target speed for it to achieve first, and then

synchronize speeds between the two sub-platoons. It may simplify the analyses. However, the temporal speed is left to be determined, and it may bring out the issue on interactions between two consecutive platoons. Nonetheless, cooperative speed harmonization for multiple consecutive cases need further investigation in future research.

On the other hand, for the two-vehicle and three-vehicle cases, the analyses are conducted for conditions that the minimum safety headway will be violated and cooperative speed harmonization is needed to help better resolve the conflict. The probability that a conflict occurs really depends on the traffic fluctuation within a platoon in terms of speed difference and space headway, which are both considered in identifying micro-discontinuity between two consecutive platoons in the traffic monitoring and platoon information aggregation framework. In other words, vehicles in a platoon identified through the framework should have similar traffic sates in terms of speed and space headway. It is very likely that multiple conflicts especially more than two consecutive ones are in a low probability to be occurring within a platoon. Moreover, two consecutive platoons actually reflect two groups of vehicles with different traffic states. A conflict may exist between them and has a higher occurrence probability than that within platoon. However, further investigation through simulation data and field data are still needed to determine the probability distribution.

5.4 Stage II: Platoon-Based Speed Profile Planning

Our goal at Stage II is to develop a platoon-based trajectory planning algorithm which can serve as the foundation of automated intersection control for connected and

autonomous vehicles. A vehicle trajectory is equivalent to a set of linear speed segments (i.e., speed profile) over time. Compared to trajectory representation, speed profiles are all linear and with less parameters, which will lead to a more intuitive representation and a more efficient computation.

Along with the two stages, we envision two control zones prior to the intersection for each approach. Control Zones I and II are associated with Stages I and II respectively. Once all the vehicles in a platoon have harmonized into the same speed v_T in Zone I, we are able to treat a platoon of vehicles as a single vehicle at Stage II in Zone II. Assume that once a platoon enters Zone II, its speed profile until it passes the intersection will be determined immediately. In other words, the speed profile of each platoon already in Zone II is always known. It enables us to plan the speed profile for newly entered platoons.

With conflicting traffic, the goal of speed profile planning is to generate a speed profile for a platoon to pass through an intersection at a high average speed, while avoiding potential conflicts with either platoons from conflicting approaches or downstream platoons on the same approach. As a first step, we will start with a simple network, which is a one-direction highway segment with a single lane. The problem we explore in this subsection is described as below:

Given the speed profile of the leading platoon $\boldsymbol{\Theta}^L$, plan/construct the speed profile of the following platoon $\boldsymbol{\Theta}^F$, such that either a target headway, or the maximal speed v_{max} is achieved as soon as possible and maintained from that point on. This chapter will focus

on space headway. Analyses and discussions on speed profile planning using time headway can be found in APPENDIX A.

In Stage II, we assume platoons have the same maximal deceleration rate $\underline{a}$ and will apply this rate during the process. However, they can have different acceleration rates. Notations used in this subsection are defined as below and illustrated in Figure 5-22.

Δ: critical space headway,

s^n: initial distance between platoons n and $n-1$,

$\delta(t)$: relative distance between two consecutive platoons at time t,

t_0^n: time when platoon n enters Zone II,

$i^n(t)$: the index of the segment that contains time t for platoon n,

$v^n(t)$: speed of platoon n at time t,

v_{max}: maximal speed,

$\bar{a}^n$: acceleration rate for platoon n,

$\underline{a}$: maximal deceleration rate for all platoons,

$\boldsymbol{\theta_k^n} = [p_k^n, v_k^n, a_k^n, t_k^{n,s}, t_k^{n,e}]$: a linear segment k of the speed profile for a given platoon n,

$\boldsymbol{\Theta^n} = \{\boldsymbol{\theta_1^n}, \boldsymbol{\theta_2^n}, \dots, \boldsymbol{\theta_K^n}\}$: the whole trajectory (speed profile) of a given platoon n,

Where,

p_k^n: starting position of a linear segment k for platoon n,

v_k^n: starting speed of a linear segment k for platoon n,

a_k^n: acceleration of a linear segment k for platoon n,

$t_k^{n,s}$: starting time of a linear segment k for platoon n,

$t_k^{n,e}$: ending time of a linear segment k for platoon n.

$k \in \mathrm{Z}$ and $k \geq 1$.

t_1: time for platoon n to decelerate from its original speed with $\underline{a}^n$ until it reaches the same speed as platoon $n-1$ (only exists when $v_0^n > v_0^{n-1}$) or zero,

t_2: time for platoon n to accelerate from its original speed with $\overline{a}^n$ until it reaches the same speed as vehicle $n-1$ (only exists when $v_0^n < v_0^{n-1}$ or $v_0^n > v_0^{n-1}\ and\ \overline{a}^n < \overline{a}^{n-1}$),

t_3: time for platoon n to accelerate from its original speed to v_{max} with $\overline{a}^n$

t_4: time for platoon n to accelerate from its original speed to v_{max} with $\overline{a}^n$ and then decelerate to the same speed as vehicle $n-1$ with $\underline{a}$.

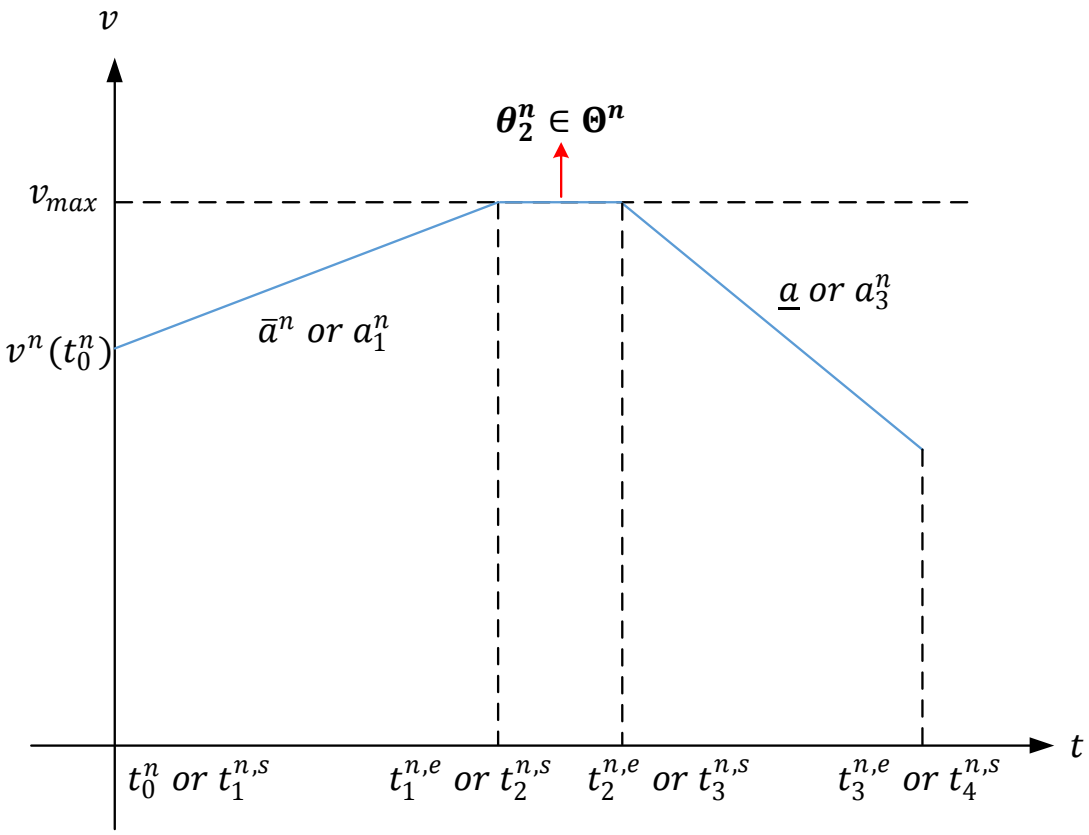

Figure 5-22 Speed Profile $\boldsymbol{\Theta^n}$ of Platoon n

5.4.1 Patterns of Speed Profile

When platoon n enters Zone II at time t_0^n, the ideal case is that platoon n has the same speed as platoon $n-1$ and their space headway is Δ (referred as the control goal). Then vehicle n will follow the speed profile of platoon $n-1$ starting from t_0^n.

In most cases, the control goal is not met at t_0^n. Our mission here is to design a speed profile starting from t_0^n such that a platoon is able to catch up its predecessor and achieve the control goal as soon as possible. Since the speed profile of each platoon varies with each other, it is not easy to develop a general algorithm for speed profile planning.

With the mission, there exists four basic patterns of speed profile for a newly entered platoon n before it reaches the control goal given the speed profile of its predecessor $n-1$.

I. Deceleration

II. Acceleration

III. Acceleration and then deceleration

IV. Acceleration, maintaining v_{max}, and then deceleration

Denote the them as Patterns I, II, III, and IV respectively. They are illustrated in Figure 5-23 and Figure 5-24.

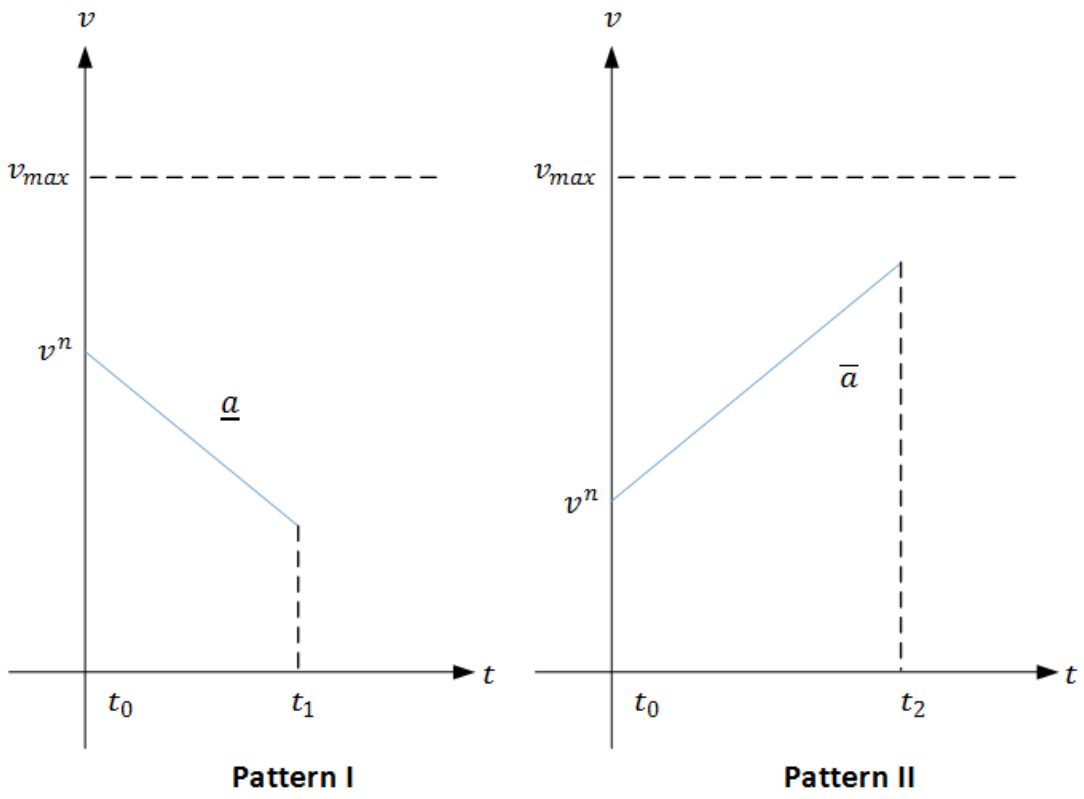

Figure 5-23 Basic Patterns I and II of Speed Profile

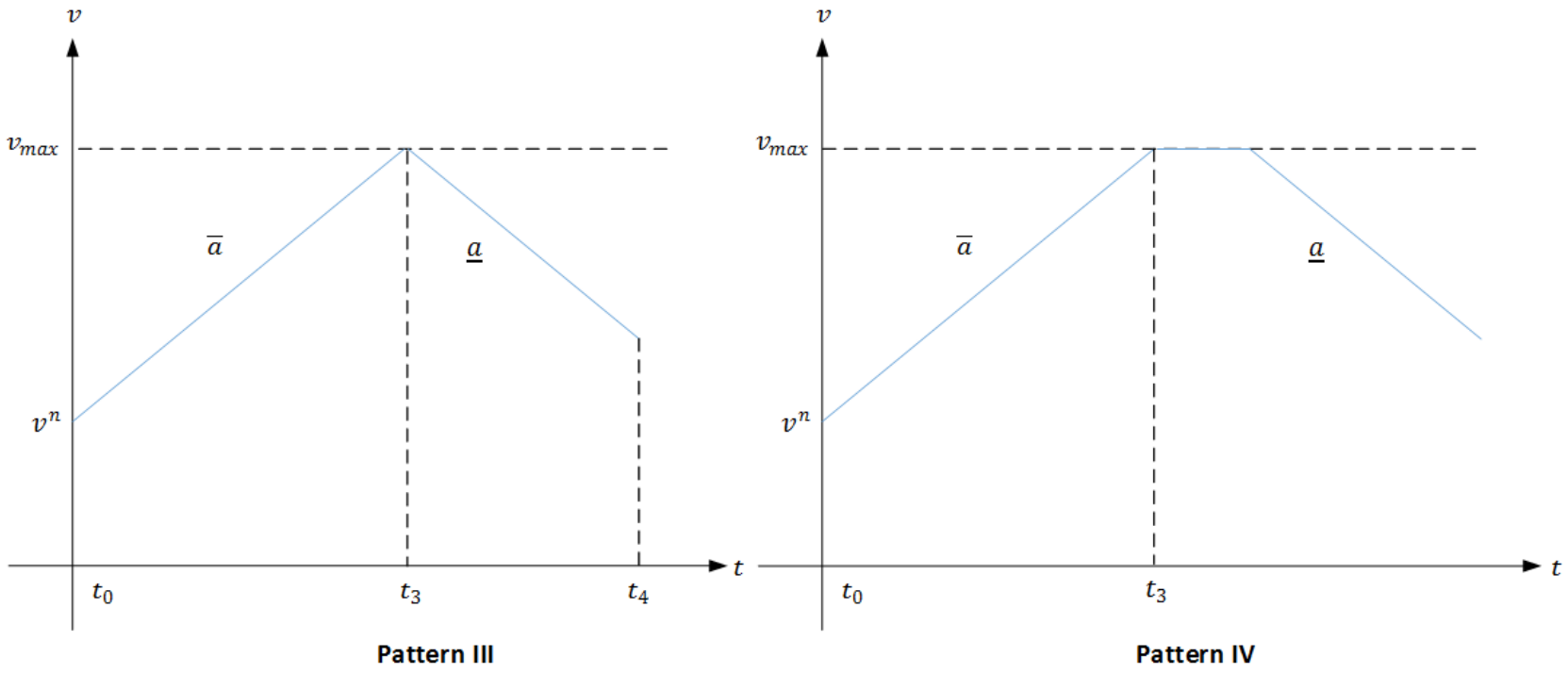

Figure 5-24 Basic Patterns III and IV of Speed Profile

Along with the four basic patterns, there are two initial actions for platoon n at t_0^n, which are deceleration and acceleration. It is possible that the initial speed is already v_{max} and it needs to maintain v_{max} for some time. Consider $v^n(t_0^n) = v_{max}$ as an action of acceleration taking no time.

The initial actions play a very important role in determining the basic patterns of the speed profile and depend on the states of two consecutive platoons at time t_0^n in terms of their speeds and relative distance.

Deceleration

The extreme case is that the minimum headway has violated just when platoon n enters Zone II, i.e., $s^n < \Delta$. Immediate deceleration is needed to resolve a potential collision. Including this case, there are three cases where immediate deceleration is necessary.

$s^n < \Delta$

If the minimum headway is violated at the very beginning, then there are two different cases in terms of the relationship between $v^n(t_0^n)$ and $v^{n-1}(t_0^n)$.

If $v^n(t_0^n) \leq v^{n-1}(t_0^n)$, then a collision may not occur with the assumption that all platoons have the same maximal deceleration rate. It can be resolved by platoon n decelerating until $\delta(t) = \Delta$. It is possible that $v^n(t_0^n) = 0$ and $\delta(t) < \Delta$. In this case, platoon may stop for a while until $\delta(t) = \Delta$.

If $v^n(t_0^n) > v^{n-1}(t_0^n)$, a collision will happen for sure if $\delta(t_1) \leq 0$. If $\delta(t_1) > 0$, the following actions will be the same as those under $v^n(t_0^n) \leq v^{n-1}(t_0^n)$.

$s^n = \Delta$ and $v^n(t_0^n) > v^{n-1}(t_0^n)$

The relative distance $\delta(t)$ between the two platoons will keep decreasing until a collision happens or when $v^n(t) = v^{n-1}(t)$ (i.e., time t_1). Similar to $s^n < \Delta$ and $v^n(t_0^n) > v^{n-1}(t_0^n)$. We will first check $\delta(t)$ at time T_1. If $\delta(t_1) \leq 0$, the two platoons are going to collide with each other anyway. Otherwise, follow the actions discussed for $s^n < \Delta$ and $v^n(t_0^n) > v^{n-1}(t_0^n)$.

$s^n > \Delta$, $v^n(t_0^n) > v^{n-1}(t_0^n)$, and $\delta(t_1) \leq \Delta$

This case is very similar to the previous one except $s^n > \Delta$. The subsequent actions after t_1 depend on $\delta(t_1)$. If $\delta(t_1) < \Delta$, it is equivalent to those in the case where $s^n < \Delta$ and $v^n(t_0^n) > v^{n-1}(t_0^n)$. The ideal case is that $\delta(t_1) = \Delta$ and platoon n simply would start following the speed profile of platoon $n-1$ from t_1.

After analyzing the above three cases, we actually find the similarity between that $s^n < \Delta$ and $v^n(t_0^n) > v^{n-1}(t_0^n)$ and that $s^n > \Delta$, $v^n(t_0^n) > v^{n-1}(t_0^n)$, and $\delta(t_1) \leq \Delta$. Thus, the conditions for immediate deceleration can be generalized as $s^n < \Delta$ or $\delta(t_1) \leq \Delta$ if t_1 exists.

Acceleration

If the control goal is not obtained at t_0^n, then either deceleration or acceleration is needed. In other words, the two basic actions are supplemental to each other. In the previous sections, we summarize the conditions for deceleration as either $s^n < \Delta$ or $\delta(t_1) \leq \Delta$ if t_1 exists. Therefore, acceleration is needed to achieve the control goal under conditions other than these two. The conditions are

1. $s^n = \Delta$, $v^n(t_0^n) < v^{n-1}(t_0^n)$
2. $s^n > \Delta$, $v^n(t_0^n) \leq v^{n-1}(t_0^n)$
3. $s^n > \Delta$, $v^n(t_0^n) > v^{n-1}(t_0^n)$, $\delta(t_1) > \Delta$

For condition 1, if T_2 exists, then it is possible for the control to achieve at t_2 (i.e., $v^n(t_2) = v^{n-1}(t_2)$ and $\delta(t_2) = \Delta$). It actually defines Pattern II. If $\delta(t_2) > \Delta$ or T_2 does not exist, platoon n needs acceleration to a higher speed (e.g.v_{max}). In other words, Patterns III and IV may need to achieve the control goal.

In order to determine which pattern will apply, we need to first calculate the time for platoon n to accelerate to v_{max} and then decelerate to the same speed as platoon $n-1$ (i.e., t_4) and $\delta(t_4)$.

The ideal case is $\delta(t_4) = \Delta$ such that platoon n will start following the speed profile of platoon $n-1$ at t_4. It represents Pattern III.

If $\delta(t_4) < \Delta$, it indicates that platoon n accelerating to v_{max} is an over-compensation of its initial distance to platoon $n-1$. In this case, platoon n only needs to accelerate to a certain speed v (smaller than v_{max}) and then decelerate as shown in Figure 5-25 (a). The speed profile here belongs to Pattern III as well. Denote the two critical time points as t_c and t_m. The calculation of v, t_c, and t_m will be discussed later.

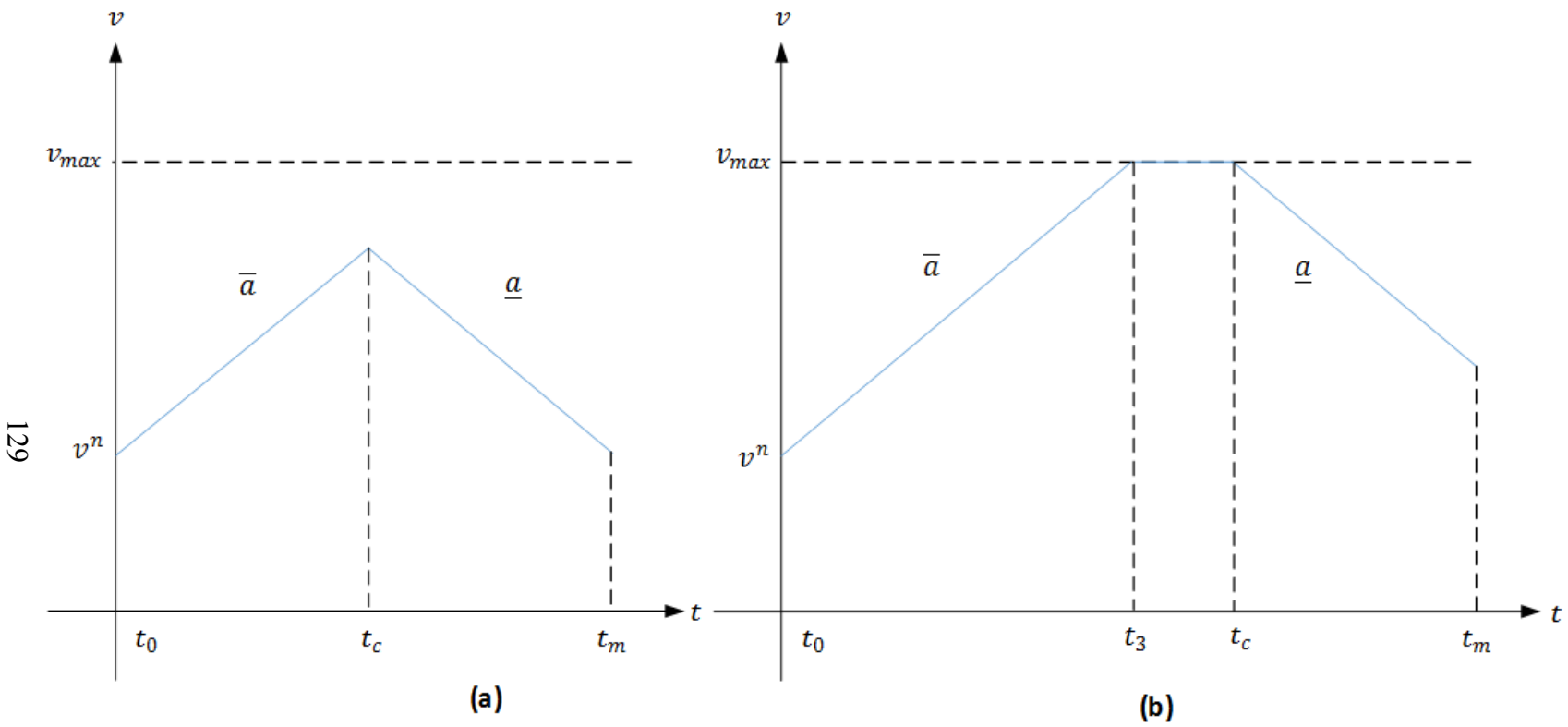

Figure 5-25 Crtical Time Points in Basic Patterns III and IV

If $\delta(t_4) > \Delta$, it is necessary for platoon n to maintain v_{max} for a while before it decelerates again. This is Pattern IV introduced at the beginning of this section. As illustrated in Figure 5-25 (b), it also contains two critical time points, t_c and t_m, which defines the time when platoon n decelerates from v_{max} and that when platoon n reaches the same speed as platoon $n-1$ while their relative distance equals to Δ.

5.4.2 Extension to Heterogeneous Acceleration Rates

Deceleration and the corresponding Pattern I would not be affected by heterogeneous acceleration rates. With homogeneous acceleration rates, segments of acceleration will be parallel to each other, and there is no intercept between them. In other words, two platoons cannot achieve the same speed if both of them accelerate from t_0^n given $v^n(t_0^n) \neq v^{n-1}(t_0^n)$. However, that would not be the case with heterogeneous acceleration rates. Take Figure 5-26 for example, $v^n(t_0^n) > v^{n-1}(t_0^n)$ and platoon $n-1$ is accelerating from t_0^n at rate $\bar{a}^{n-1}$. Assume acceleration is needed for platoon n as well and $\bar{a}^n < \bar{a}^{n-1}$, the two platoons will reach the same speed at t_2 as shown in Figure 5-26 (a). Under heterogeneous acceleration rates, T_2 may exist when $v_0^n > v_0^{n-1}$ and $\overline{a}^n < \overline{a}^{n-1}$ in addition to $v_0^n < v_0^{n-1}$ given acceleration of platoon n is necessary.

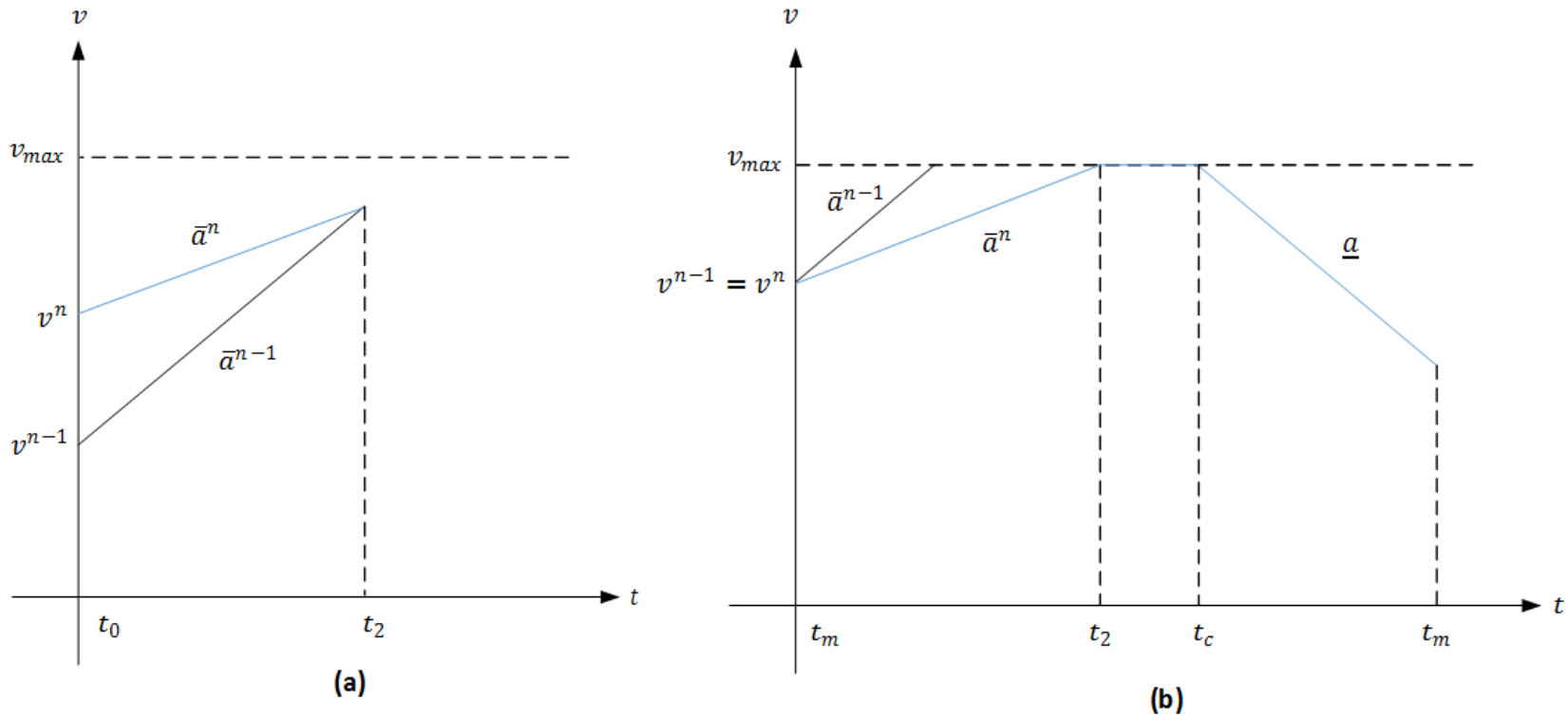

Figure 5-26 Speed Profile under Heterogenous Acceleration Rates

On the other hand, once the control goal is achieved at time t_m, it is possible that platoon n follows platoon $n-1$ to accelerate from t_m at a lower rate $\overline{a}^n$ and $\delta(t)$ keeps increasing after t_m (see Figure 5-26 (b) for details). This indicates that the control goal violates and another round of planning requires. Basically, platoon n needs accelerating to a higher speed to compensate the additional relative distance that exceeds Δ. Depending on the speed of $v^{n-1}(t_1)$, platoon n may then decelerate, or maintain v_{max} for a short while and then decelerate, which are Patterns III and IV. Therefore, if $\overline{a}^n < \overline{a}^{n-1}$, Pattern III or/and Pattern IV may be trigged more than once before platoon n leaves Zone II.

5.4.3 Construct Speed Profile

Since the speed profile of each platoon is a set of linear speed segments, which are linear functions of time t, we are able to obtain the analytical solutions to the critical time points and the corresponding speeds introduced in the previous section. They are fundamental to construct the speed profile for each newly entered platoon.

Compute Critical Time Points

For Patterns I and II, the control goal is achieved when the two platoons reach the same speed through one-time either acceleration or deceleration. t_c does not exist for those two patterns. t_m is either t_1 for deceleration or t_2 for acceleration. Assume segment 1 of platoon n will merge with segment k of platoon $n-1$ (i.e., $\boldsymbol{\theta_k^{n-1}} = [p_k^{n-1}, v_k^{n-1}, a_k^{n-1}, t_k^{n-1,s}, t_k^{n-1,e}]$) at either t_1 for Pattern I or T_2 for Pattern II. The necessary condition will be $\underline{a} < a_k^{n-1}$ and $\bar{a}^n > a_k^{n-1}$ respectively.

For Patterns I,

$$v^n(t_0^n) + \underline{a}(t_m - t_0^n) = v_k^{n-1} + a_k^{n-1}(t_m - t_k^{n-1,s}) \tag{5.66}$$

We get

$$t_m = T_1 = \frac{v_k^{n-1} - v^n(t_0^n) + \underline{a}t_0^n - a_k^{n-1}t_k^{n-1,s}}{\underline{a} - a_k^{n-1}} \tag{5.67}$$

For Pattern II,

$$v^n(t_0^n) + \bar{a}^n(t_m - t_0^n) = v_k^{n-1} + a_k^{n-1}(t_m - t_k^{n-1,s}) \tag{5.68}$$

Then

$$t_m = T_2 = \frac{v_k^{n-1} - v^n(t_0^n) + \underline{a}t_0^n - a_k^{n-1}t_k^{n-1,s}}{\bar{a}^n - a_k^{n-1}} \tag{5.69}$$

For Patterns III and IV, the very basic idea is that segment i of platoon n should merge with segment k of platoon $n-1$ at t_m and $\delta(t_m) = \Delta$. The segments are listed as below.

$$\boldsymbol{\theta_k^{n-1}} = [p_k^{n-1}, v_k^{n-1}, a_k^{n-1}, t_k^{n-1,s}, t_k^{n-1,e}]$$

$$\boldsymbol{\theta_i^n} = [p_i^n, v_i^n, a_i^n, t_i^{n,s}, t_i^{n,e}]$$

where, $t_i^{n,s} = t_c$, $t_i^{n,e} = t_m$, $i \in$ Z and $i \geq 1$.

Similar to Patterns I and II, the following relationship should satisfy in order for the segments to merge each other at t_m.

$$a_i^n > a_k^{n-1} \tag{5.70}$$

At t_m, the speeds of the two consecutive platoons are

$$v_k^{n-1} + a_k^{n-1}(t_m - t_k^{n-1,s}) \tag{5.71}$$

$$v_i^n + a_i^n(t_m - t_c) \tag{5.72}$$

Following the logic we have

$$v_k^{n-1} + a_k^{n-1}\left(t_m - t_k^{n-1,s}\right) = v_i^n + a_i^n(t_m - t_c) \tag{5.73}$$

At t_m,the positions of platoons n and $n-1$ are

$$p_k^{n-1} + v_k^{n-1}\left(t_m - t_k^{n-1,s}\right) + \frac{1}{2}a_k^{n-1}\left(t_m - t_k^{n-1,s}\right)^2 \tag{5.74}$$

$$p_i^n + v_i^n(t_m - t_c) + \frac{1}{2}a_i^n(t_m - t_c)^2 \tag{5.75}$$

With $\delta(t_m) = \Delta$, we have

$$\begin{aligned} &p_k^{n-1} + v_k^{n-1}\left(t_m - t_k^{n-1,s}\right) + \frac{1}{2}a_k^{n-1}\left(t_m - t_k^{n-1,s}\right)^2 \\ &= p_i^n + v_i^n(t_m - t_c) + \frac{1}{2}a_i^n(t_m - t_c)^2 + \Delta \end{aligned} \tag{5.76}$$

Since $t_i^{n,s} = t_{i-1}^{n,e} = t_c$ and $t_i^{n,e} = t_m$ are both left to decide, $\boldsymbol{\theta_i^n} = [p_i^n, v_i^n, a_i^n, t_c, t_m]$ is unknown. However, $\boldsymbol{\theta_i^n}$ can be stated using $\boldsymbol{\theta_{i-1}^n}$ which is known. In other words,

$$v_i^n = v_{i-1}^n + a_{i-1}^n\left(t_c - t_{i-1}^{n,s}\right) \tag{5.77}$$

$$p_i^n = p_{i-1}^n + v_{i-1}^n\left(t_c - t_{i-1}^{n,s}\right) + \frac{1}{2}a_{i-1}^n\left(t_c - t_{i-1}^{n,s}\right)^2 \tag{5.78}$$

Define

$$T_c = t_c - t_{i-1}^{n,s} \tag{5.79}$$

$$T_m = t_m - t_{i-1}^{n,s} \tag{5.80}$$

Substitute v_i^n and p_i^n, we can get

$$T_m = \frac{v_k^{n-1} - v_{i-1}^n - a_k^{n-1} t_k^{n-1,s} - (a_{i-1}^n - a_i^n) T_c}{a_i^n - a_k^{n-1}} \tag{5.81}$$

Substitute T_m,

$$\alpha (T_c)^2 + \beta T_c + \gamma = 0 \tag{5.82}$$

where, $\alpha = (a_{i-1}^n - a_i^n)(a_{i-1}^n - a_k^{n-1})$,

$$\beta = -2(a_{i-1}^n - a_i^n)(v_k^{n-1} - v_{i-1}^n - a_k^{n-1} t_k^{n-1,s}),$$

$$\gamma = \left(v_k^{n-1} - v_{i-1}^n - a_k^{n-1} t_k^{n-1,s}\right)^2 - (a_k^{n-1} - a_i^n)\left[a_k^{n-1}\left(t_k^{n-1,s}\right)^2 - 2v_k^{n-1} t_k^{n-1,s} + 2p_k^{n-1} - 2(p_{i-1}^n + \Delta)\right].$$

If $\alpha = 0$, then it becomes a linear function of t_c.

$$T_c = -\frac{\gamma}{\beta} \tag{5.83}$$

If $\alpha \neq 0$, the quadratic function has two roots which are

$$T_c = \frac{-\beta \pm \sqrt{\beta^2 - 4\alpha\gamma}}{2\alpha} \tag{5.84}$$

The two critical time points will be

$$t_c = T_c + t_{i-1}^{n,s} \tag{5.85}$$

$$t_m = T_m + t_{i-1}^{n,s} \tag{5.86}$$

Since the two segments are linear, there exists only one t_m as well as t_c.The merging point is on segment k of platoon $n-1$, we have

$$t_m \in [t_k^{n-1,s}, t_k^{n-1,e}] \tag{5.87}$$

With this condition, we are able to determine the critical time points t_c and t_m. The basic idea is very similar to Zhou et al., (2017). Instead of solving the quadratic equation for every trajectory segment of the leading vehicle, our approach will first identify the speed profile pattern and then calculate the critical time points by solving the equation only once which will lead to better computational efficiency. On the other hand, the solutions directly from the quadratic equation without identifying the corresponding speed profile may not be feasible due to the maximal speed constraint. Therefore, Zhou et al., (2017) employs a backward procedure to recalculate the critical time points and modify the constructed trajectory once a real solution exists from the equation, and it is subject to the maximal speed constraint.

Speed Profile Planning Algorithm

The index k of merging segment $\boldsymbol{\theta_k^{n-1}}$ is very important for computing the analytical solutions of critical time points for any speed profile pattern. It is very easy to determine if the graphic speed profiles of the two consecutive platoons are presented. Without knowing the graphic profiles, the merging time and speed, however, there is no analytical way to directly calculate those time points except for t_3 since v_{max} is known.

The speed profile is a set of linear speed segments. A linear segment represents a specific action, which could be acceleration, deceleration, and maintaining current speed. The

linearity of speed profile guarantees the uniqueness of each of the critical time points. This enables us to develop a backward-tracing method for determining the index.

The speed profile of platoon $n-1$ is given as $\Theta^{\mathrm{n}} = \{\theta_1^n, \theta_2^n, \dots, \theta_K^n\}$ for the planning process. Assume the two platoons' speed profile merge at segment k of $\boldsymbol{\theta_k^{n-1}}$, i.e., $t_m \in [t_k^{n-1,s}, t_k^{n-1,e})$. A right-open interval is used here since $t_k^{n-1,e} = t_{k+1}^{n-1,s}$. We are able to compute the corresponding speeds at t_0^n for Patterns I and II by constructing two virtual speed segments ending at $t_k^{n-1,s}$ and $t_k^{n-1,e}$ with slope of a, where $a = \underline{a}$ for Pattern I and $a = \bar{a}^n$ for Pattern II as illustrated in Figure 5-27.

If $t_k^{n-1,s} < t_m < t_k^{n-1,e}$, $v^n(t_0^n)$ should be within the speeds of the two virtual speed segments at t_0^n, which is $\left[v_k^{n-1} - a\left(t_k^{n-1,s} - t_0^n\right) - v^n(t_0^n)\right]\left[v_k^{n-1} + a_k^{n-1}\left(t_k^{n-1,e} - t_k^{n-1,s}\right) - a\left(t_k^{n-1,e} - t_0^n\right) - v^n(t_0^n)\right] < 0$. It is equivalent to $\left[v_k^{n-1} - a\left(t_k^{n-1,s} - t_0^n\right) - v^n(t_0^n)\right]\left[v_{k+1}^{n-1} - a\left(t_k^{n-1,e} - t_0^n\right) - v^n(t_0^n)\right] < 0$.

If $t_m = t_k^{n-1,s}$, then $v^n(t_0^n)$ should be the same as the speed of the virtual speed segment ending at $t_k^{n-1,s}$, i.e., $v_k^{n-1} - a\left(t_k^{n-1,s} - t_0^n\right) = v^n(t_0^n)$.

Denote k_0 as the index of $\boldsymbol{\theta_{k_0}^{n-1}}$, where $t_0^n \in [t_k^{n-1,s}, t_k^{n-1,e})$. Then the merging segment can be determined for Patterns I and II by checking the two following conditions for every $\boldsymbol{\theta_k^{n-1}}$ starting from k_0.

$$\left[v_k^{n-1} - a\left(t_k^{n-1,s} - t_0^n\right) - v^n(t_0^n)\right]\left[v_k^{n-1} + a_k^{n-1}\left(t_k^{n-1,e} - t_k^{n-1,s}\right) - a\left(t_k^{n-1,e} - t_0^n\right) - v^n(t_0^n)\right] < 0. \tag{5.88}$$

$$v_k^{n-1} - a\left(t_k^{n-1,s} - t_0^n\right) = v^n(t_0^n). \tag{5.89}$$

In order for segment k of platoon $n-1$ to be the merging segment, $\delta(t_m) = \Delta$ should be satisfied as well.

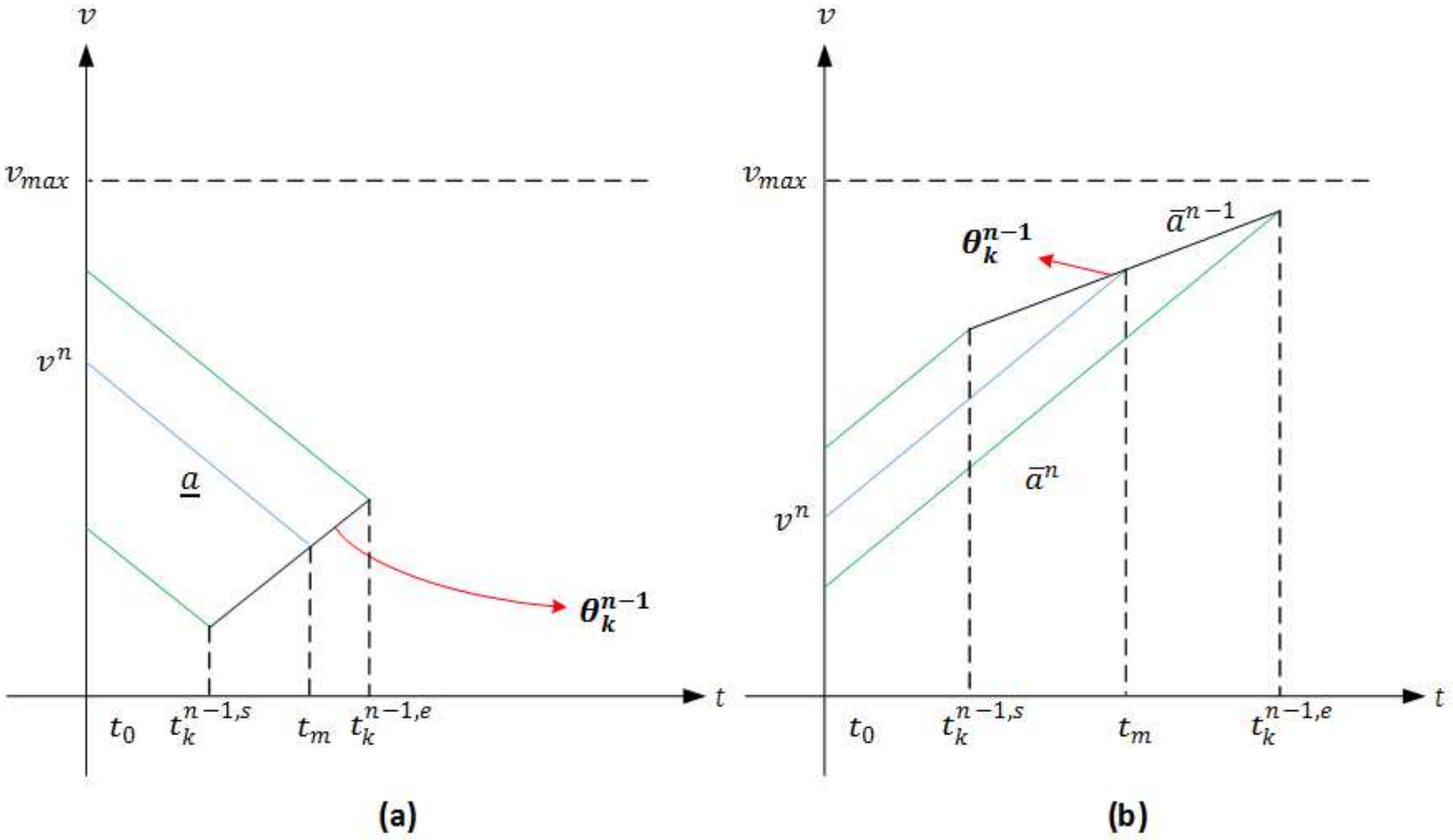

Figure 5-27 Determine Merging Segment under Patterns I and II

For Patterns III and IV, t_m and t_c are both unknown. The above method cannot be directly applied. Let us still assume that segment i of platoon n and segment k merge at t_m. We are still able to construct two virtual speed segments ending at $t_k^{n-1,s}$ and $t_k^{n-1,e}$ with slope of $\underline{a}$. They will intercept with segment $i-1$ of platoon n at t' and t'' (see Figure 5-28).

If $t_k^{n-1,s} < t_m < t_k^{n-1,e}$, then one of the relative distances between the two consecutive platoons at $t_k^{n-1,s}$ and $t_k^{n-1,e}$ should be greater than Δ while the other is not. That is

$$\left[\delta\left(t_k^{n-1,s}\right) - \Delta\right]\left[\delta\left(t_k^{n-1,e}\right) - \Delta\right] < 0 \tag{5.90}$$

If $t_m = t_k^{n-1,s}$, $\delta\left(t_k^{n-1,s}\right)$ will equal to Δ.

In a word, the merging segment is k of platoon $n-1$ if one of the two following conditions satisfies for Pattern III or IV.

$$\left[\delta\left(t_k^{n-1,s}\right) - \Delta\right]\left[\delta\left(t_k^{n-1,e}\right) - \Delta\right] < 0 \tag{5.91}$$

$$\delta\left(t_k^{n-1,s}\right) = \Delta \tag{5.92}$$

For the two sets of conditions, $a_i^n > a_k^{n-1}$ must be met to guarantee the existence of merging between segment i of platoon n and segment k of platoon $n-1$.

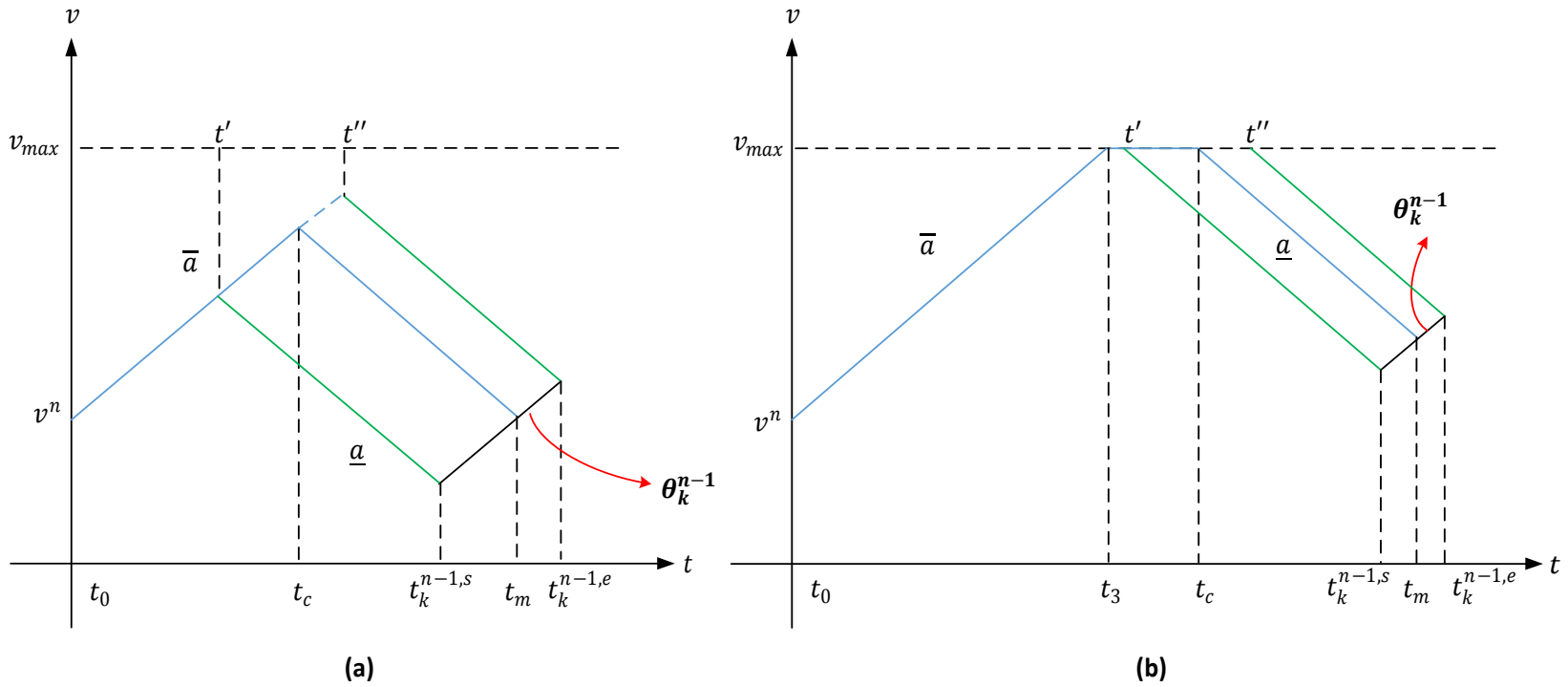

Figure 5-28 Determine Merging Segment under Patterns III and IV

The methodology presented here actually can lead to a numerical way to solve t_c and t_m for Patterns III and IV. After identifying the merging segment k of platoon $n-1$, we can still adopt bi-section method and perform the condition check until $\delta(t) - \Delta < \varepsilon$, where ε is a predefined convergence level. Then $t_m = t$ and the merging speed is $v_k^{n-1} + \bar{a}^{n-1}(t_m - t_k^{n-1,s})$. For Pattern III, t_c can be calculated by solving the following equation.

$$v^n(t_0^n) + \bar{a}^n(t_c - t_0^n) = v_k^{n-1} + \bar{a}^{n-1}\left(t_m - t_k^{n-1,s}\right) - \underline{a}(t_m - t_c) \tag{5.93}$$

It gives

$$t_c = \frac{v_k^{n-1} - v^n(t_0^n) + \bar{a}^{n-1}\left(t_m - t_k^{n-1,s}\right) - \underline{a}t_m}{\bar{a}^n - \underline{a}} \tag{5.94}$$

For Pattern IV, since the speed at t_c is known as v_{max}, computing t_c is very simple.

$$t_c = t_m + \frac{v_{max} - \left[v_k^{n-1} + \bar{a}^{n-1}(t_m - t_k^{n-1,s})\right]}{\underline{a}} \tag{5.95}$$

The pseudocodes blew describes the algorithm of speed profile planning for each newly entered platoon. Denote it as platoon n. Since it only involves communications between platoon n and its predecessor $n-1$, and simply calculations, it can be implemented in a distributed way (i.e., via platoon n itself) and performed in real-time.

Algorithm *speed profile planning*

Begin

Set Flag=False and $i = 1$;

Initialize $\boldsymbol{\Theta^n} = \{\}$ and $\boldsymbol{\theta_1^n} = [p_1^n, v^n(t_0^n), \ , t_0^n, \infty]$;

If $s^n = \Delta$,$v^n(t_0^n) = v^{n-1}(t_0^n)$ and $\bar{a}^n \geq \bar{a}^{n-1}$ **then**

Flag=True;

Follow platoon $n-1$ starting from t_0^n;

While Flag=False and $i < |\boldsymbol{\Theta^n}|$

Determine the basic action (i.e., a_k^n) using initial states;

Compute t_1, t_2, t_3 and t_4;

Determine the speed pattern by checking $\delta(t)$ at t_1, t_2 and t_4;

Determine the index i of the merging segment of its predecessor;

If speed pattern=Pattern I **then**

Set $\boldsymbol{\theta_i^n} = \left[p_i^n, v^n(t_0^n), \underline{a}, t_0^n, t_1\right]$;

If speed pattern= Pattern II **then**

Set $\boldsymbol{\theta_i^n} = [p_i^n, v^n(t_0^n), \bar{a}^n, t_0^n, t_2]$;

If speed pattern= Pattern III **then**

Calculate t_c and t_m;

Set $\boldsymbol{\theta_i^n} = [p_i^n, v^n(t_0^n), \bar{a}^n, t_0^n, t_c]$;

Set $\boldsymbol{\theta_{i+1}^n} = \left[p_{i+1}^n, v^n(t_0^n), \underline{a}, t_c, t_m\right]$;

If speed pattern= Pattern IV **then**

Calculate t_c and t_m;

Set $\boldsymbol{\theta_i^n} = [p_i^n, v^n(t_0^n), \bar{a}^n, t_0^n, t_3]$;

Set $\boldsymbol{\theta_{i+1}^n} = [p_{i+1}^n, v^n(t_0^n), 0, t_3, t_c]$;

Set $\boldsymbol{\theta_{i+2}^n} = \left[p_{i+2}^n, v^n(t_0^n), \underline{a}, t_c, t_m\right]$;

Update $\boldsymbol{\Theta^n}$;

$i = i + 1$;

$t_0^n = t_m$;

If $\bar{a}^n \geq \bar{a}^{n-1}$ **then**

Flag=True;

Follow platoon $n-1$ starting from t_m;

End While;

End;

Generally, p_{i+1}^n can be easily calculated as below.

$$p_i^n + v^n\left(t_i^{n,s}\right)\left(t_i^{n,e} - t_i^{n,s}\right) + \frac{1}{2}a_i^n\left(t_i^{n,e} - t_i^{n,s}\right)^2 \tag{5-96}$$

If a mobile controller at the intersection takes control of the planning process, the above algorithm can be implementing in a centralized manner by looping itself through newly entered platoons. In other words, once platoon n finishes speed profile planning, the controller will move to the next platoon by updating $n = n + 1$.

5.5 Summary

In this Chapter, we investigate cooperative speed harmonization for vehicles within a platoon and speed profile planning for platoons in the environment of connected and autonomous vehicles. They are the two fundamental areas for a platoon-based automated intersection control. Analytical solutions for cooperative speed harmonization of a platoon with no more than three vehicles. For a platoon with more than three vehicles, the speed synchronization among vehicles can be achieved by breaking down a platoon into

sub-platoons. Methodologies for two-vehicle and three-vehicles cases can be directly adopted. If speed harmonization is successfully accomplished and platoon enters Zone II, it can be treated as a single vehicle. Its trajectory, or equivalently, the speed profile can be planned through the time it leaves the intersection according to a specific control rule. As a first step towards this study, we investigate cases on a single-lane network where a platoon is asked to achieve the minimum space headway with its predecessor as soon as possible. An algorithm is developed for constructing the speed profile. The algorithm only involves communications between two consecutive platoons and thus can be implemented in a distributed way. The cooperative speed harmonization and speed profile planning compose an automated intersection control, which does not rely on infrastructure as well. Together with the distributed traffic monitoring and platoon information aggregation framework, this makes the proposed self-sustained traffic operation system complete.

CHAPTER 6

CONCLUSION AND FUTURE RESEARCH

6.1 Conclusion

This study investigates the two major systems underlying a self-sustained traffic operations system. They are a distributed traffic monitoring and platoon information aggregation system and a platoon-based automated intersection control for autonomous and connected vehicles.

The distributed traffic monitoring and platoon information aggregation system which serves as the fundamental part of the entire system is first explored. Its performances with respect to different MPRs is evaluated for stable traffic and queueing traffic for a freeway segment. Our simulation results show that the proposed framework lends itself better to more congested traffic conditions for any given MPR. With 50% MPR, the framework is able to provide information coverage for at least 37.76% of the simulated roadway facility under various traffic scenarios. This indicates that proposed framework could be useful with an MPR as low as 50%. Even with an MRP of 20%, the coverage ratio under relatively congested traffic can still reach around 58.82%. The framework is able to provide accurate speed estimation at high spatial resolution for the simulated roadway facility. The maximum relative error is under 10% for relatively congested traffic even with MPR as low as 20%. When there is a wider range of speed distribution (less congested traffic), the worst-case maximum relative error is still under 15% when MPR $= 20\%$. The density estimation is more sensitive to MPR, and is more accurate under

low demand and high MPR scenarios. As expected, the accuracy of both speed and density estimation increases with MPR for any given traffic scenario.

Furthermore, this study provides some insights on how traffic signal timing affects the performance of the distributed monitoring system. The performance of the monitoring framework is investigated with different g/C ratios under multiple traffic scenarios. The simulation results show that a positive correlation exists between the accuracy of speed estimation and the g/C ratio. If a traffic signal is present (g/C<1), downstream coverage ratio usually increases with the g/C ratio as well. While the upstream coverage ratio and the relative error in density do vary with g/C ratio, the variation is not significant and no distinct trends are observed. This indicates that the density estimation is more robust, and it may be desirable and possible to enhance the speed estimation method utilizing density information to achieve higher accuracy. Moreover, since accurate traffic monitoring sets the foundation for advanced traffic control strategies, we argue it is important to consider the resulting performance of traffic monitoring, together with other mobility measures when designing intersection control mechanisms.

On the other hand, the distributed traffic monitoring and platoon information aggregation system enables us to develop a platoon-based intersection control system if all vehicles are equipped. Cooperative speed harmonization among vehicles in a platoon and speed profile planning within an intersection are the two fundamental components for developing such a control system. Analytical solutions for cooperative speed harmonization are investigated for two-vehicle cases and three-vehicle cases. A platoon-based speed profile planning algorithm is developed to ensure the safety and efficiency of

intersection controls while reducing communication and computation overhead. They can serve basis for automated intersection controls with more complex traffic network and control rules.

In summary, this study provides fundamental support to an alternative / supplemental traffic operation system for transportation networks supported solely by V2V DSRC. The envisioned system is self-sustained, and thus will provide desired redundancy and is particularly suitable for facilitating mobility during the aftermath of extreme events.

6.2 Discussion and Future Research

As discussed in Chapter 3, low MPRs will lead to inferior system performance in terms of all three performance measures. While not much can be done to improve the coverage ratio within the V2V framework, simple adjustments of calculated platoon density can be made to compensate the effect of low MPR. Since platoon density is underestimated with low MPR, one simple adjustment is to divide the original calculated density by the MPR. Simulations with such adjustments were conducted. It is found that this simple adjustment is somewhat effective when MPR is extremely low (20%). For MPRs higher than 50%, the adjustment does not lead to significant performance improvement, and tends to overestimate density. Therefore, we do not recommend this simple adjustment for higher MPRs. Another possible approach is to adjust the calculated density based on macroscopic traffic flow characteristics. However, since the proposed platoon identification and traffic monitoring framework is not on a macroscopic scale, the applicability of traffic stream properties on the identified platoons is questionable. Moreover, this approach would either require pre-loaded traffic stream models into each

vehicle or some learning mechanism (which could be both communication and computation intensive) running on each vehicle. Therefore, we recommend at least 50% MPR and no adjustment to keep the proposed framework simple and light.

Although the simulation in this work only focused on a single-lane road section, the proposed framework does not restrict itself to single-lane applications. Under multi-lane scenario, each equipped vehicle will still maintain a set of its surrounding equipped vehicles (including vehicles traveling in the same direction from its own lane and other lanes). The micro-discontinuity identification process and self-correcting mechanism can be easily extended from single lane to multiple lanes, through an additional subroutine to perform a slightly more complicated calculation of relative position along the centerline of the road. After these processes are performed, a link-based platoon will have unique micro-discontinuity flags for its lead and anchor respectively, which would guarantee the proper implementation of the information aggregation process. The application of the proposed framework to multi-lane scenarios is currently being tested and will be presented in our follow-up research paper.

This study concentrates on pre-timed signal timing plans and only investigates the g/C ratio as the key factor. However, the analysis can be easily extended to advanced signal timing plans with more designated phases. The platoon identification process itself will not be affected by different signal timing plans. The same evaluation methodology can be adopted without any change as well. It will be interesting to explore the impacts of cycle length, phase sequences, and even different control modes on the system performance. Furthermore, statistical and machine learning methods (e.g. artificial neural network,

Kriging, and random decision forest, etc.) can be adopted to establish a more solid model regarding the relationship between the performance of the distributed traffic monitoring system and various signal timing parameters. Moreover, the tradeoff between the performance of the distributed traffic monitoring and mobility measures needs further investigation in the future research.

In addressing the potential conflicts between vehicles during the cooperative speed harmonization process, the study only explores platoons with no more than three vehicles. Generalized solutions to speed harmonization among multiple vehicle is very important for the control system to be complete. Future study may consider working on generalizing the multi-vehicle cases and introduce multiple platoons to mimic the real traffic conditions. Another important question with the automated intersection control is how to determine the control zones associated with the two control stages. The two zones must be sufficient in terms of length so that the cooperative speed harmonization and control goal can be achieved respectively in the two zones. Furthermore, the control strategy and corresponding speed profile planning algorithm will be explored for an intersection with conflicted traffic as well in future.

All the work in this study may be implemented in scale models as the first step towards implementations in the real world.

REFERENCES

Alonso-Ayuso, A., Escudero, L.F., Martín-Campo, F.J., 2011. Collision avoidance in air traffic management: A mixed-integer linear optimization approach. IEEE Trans. Intell. Transp. Syst. 12, 47–57. doi:10.1109/TITS.2010.2061971

Andert, E., 2017. Crossroads - A Time-Sensitive Autonomous Intersection Management Technique. Arizona State University.

Au, T.-C., Shahidi, N., Stone, P., 2011. Enforcing Liveness in Autonomous Traffic Management. AAAI'11 Proc. Twenty-Fifth AAAI Conf. Artif. Intell. 1317–1322.

Ban, X. (Jeff), Hao, P., Sun, Z., 2011. Real time queue length estimation for signalized intersections using travel times from mobile sensors. Transp. Res. Part C Emerg. Technol. 19, 1133–1156. doi:10.1016/j.trc.2011.01.002

Bauza, R., Gozalvez, J., Sanchez-Soriano, J., 2010. Road traffic congestion detection through cooperative Vehicle-to-Vehicle communications. Proc. - Conf. Local Comput. Networks, LCN 606–612. doi:10.1109/LCN.2010.5735780

Bayar, B., Sajadi-Alamdari, S.A., Viti, F., Voos, H., 2016. Impact of different spacing policies for adaptive cruise control on traffic and energy consumption of electric vehicles. 24th Mediterr. Conf. Control Autom. MED 2016 1349–1354. doi:10.1109/MED.2016.7535939

Carlino, D., Boyles, S.D., Stone, P., 2013. Auction-based autonomous intersection management. IEEE Conf. Intell. Transp. Syst. Proceedings, ITSC 529–534. doi:10.1109/ITSC.2013.6728285

Chaudhary, N., Abbas, M.M., Charara, H., Parker, R., 2003. Platoon identification and accommodation system for isolated traffic signals on arterials.

Chen, L., Englund, C., 2016. Cooperative Intersection Management: A Survey. IEEE Trans. Intell. Transp. Syst. 17, 570–586. doi:10.1109/TITS.2015.2471812

Chen, R., Jin, W., Regan, A., 2010. Multi-Hop Broadcasting in Vehicular Ad Hoc Networks with Shockwave Traffic. 2010 7th IEEE Consum. Commun. Netw. Conf. 1–5. doi:10.1109/CCNC.2010.5421584

Christofa, E., Argote, J., Skabardonis, A., 2013. Arterial Queue Spillback Detection and Signal Control Based on Connected Vehicle Technology, in: The 2013 Annual Meeting Compendium of Papers. Transportation Research Board, Washington, D.C.

Comert, G., Cetin, M., 2011. Analytical evaluation of the error in queue length estimation at traffic signals from probe vehicle data. IEEE Trans. Intell. Transp. Syst. 12, 563–573. doi:10.1109/TITS.2011.2113375

Comert, G., Cetin, M., 2009. Queue length estimation from probe vehicle location and the impacts of sample size. Eur. J. Oper. Res. 197, 196–202. doi:10.1016/j.ejor.2008.06.024

Datesh, J., Scherer, W.T., Smith, B.L., 2011. Using K-Means Clustering to Improve Traffic Signal Efficacy in an IntelliDrive Environment, in: 2011 IEEE Forum on Integrated and Sustainable Tranpsortation Systems. IEEE, Vienna, Austria, pp. 122–127. doi:10.1109/FISTS.2011.5973659

Dey, K.C., Yan, L., Wang, X., Wang, Y., Shen, H., Chowdhury, M., Yu, L., Qiu, C., Soundararaj, V., 2016. A Review of Communication, Driver Characteristics, and Controls Aspects of Cooperative Adaptive Cruise Control (CACC). IEEE Trans. Intell. Transp. Syst. 17, 491–509. doi:10.1109/TITS.2015.2483063

Dornbush, S., Joshi, A., 2007. Street Smart Traffic Discovering and Disseminating Automobile Congestion Using VANET's, in: IEEE 65th Vehicular Technology Conference, 2007. IEEE, Dublin, pp. 11–15. doi:10.1109/VETECS.2007.15

Dresner, K., Stone, P., 2008. A Multiagent Approach to Autonomous Intersection Management. J. Artif. Intell. Res. 31, 591–653.

Dresner, K., Stone, P., 2004. Multiagent traffic management: a reservation-based intersection control mechanism. Proc. Third Int. Jt. Conf. Auton. Agents Multiagent Syst. 2004. AAMAS 2004. 530–537. doi:10.1109/AAMAS.2004.242421

Du, L., Ukkusuri, S., 2007. Geometric Connectivity of Vehicular Ad Hoc Networks : Analytical Characterization Categories and Subject Descriptors, in: VANET '07 Proceedings of the Fourth ACM International Workshop on Vehicular Ad Hoc Networks. pp. 79–80. doi:10.1145/1287748.1287765

Federal Highway Administration, 2017. EDC-1: Adaptive Signal Control Technology [WWW Document]. URL https://www.fhwa.dot.gov/innovation/everydaycounts/edc-1/asct.cfm (accessed 11.13.17).

Feng, Y., Khoshmagham, S., Zamanipour, M., Head, K.L., 2015. A real-time adaptive signal phase allocation algorithm in a connected vehicle environment, in: The 2015 Annual Meeting Compendium of Papers. Transportation Research Board, Washington, D.C.

Fukumoto, J., Sirokane, N., Ishikawa, Y., Wada, T., Ohtsuki, K., Okada, H., 2007. Analytic method for real-time traffic problems by using Contents Oriented Communications in VANET. ITST 2007 - 7th Int. Conf. Intell. Transp. Syst. Telecommun. Proc. 40–45. doi:10.1109/ITST.2007.4295830

Füßler, H., Widmer, J., Käsemann, M., Mauve, M., Hartenstein, H., 2003. Contention-based forwarding for mobile ad hoc networks. Ad Hoc Networks 1, 351–369. doi:10.1016/S1570-8705(03)00038-6

Gaur, A., Mirchandani, P., 2001. Method for Real-Time Recognition of Vehicle Platoons. Transp. Res. Rec. J. Transp. Res. Board 1748, 8–17. doi:10.3141/1748-02

Goodall, N., Smith, B., Park, B., 2013. Traffic Signal Control with Connected Vehicles. Transp. Res. Rec. J. Transp. Res. Board 2381, 65–72. doi:10.3141/2381-08

Hao, P., Ban, X. (Jeff), 2013. Long Queue Estimation Using Short Vehicle Trajectories for Signalized Intersections, in: The 2013 Annual Meeting Compendium of Papers. Transportation Research Board, Washington, D.C.

Hausknecht, M., Au, T., Stone, P., 2011. Autonomous Intersection Management : Multi-Intersection Optimization.

He, Q., Head, K.L., Ding, J., 2012. PAMSCOD: Platoon-based arterial multi-modal signal control with online data. Transp. Res. Part C Emerg. Technol. 20, 164–184. doi:10.1016/j.trc.2011.05.007

Head, L., 2013. Multi-Modal Intelligent Traffic Signal System - System Design.pdf.

Huang, D., Shere, S., Ahn, S., 2010. Dynamic highway congestion detection and prediction based on shock waves. Proc. seventh ACM Int. Work. Veh. InterNETworking - VANET '10 11–20. doi:10.1145/1860058.1860061

Jiang, Y., Li, S., Shamo, D.E., 2006. A platoon-based traffic signal timing algorithm for major-minor intersection types. Transp. Res. Part B Methodol. 40, 543–562. doi:10.1016/j.trb.2005.07.003

Jin, W.-L., Recker, W.W., 2006. Instantaneous information propagation in a traffic stream through inter-vehicle communication. Transp. Res. Part B Methodol. 40, 230–250. doi:10.1016/j.trb.2005.04.001

Jin, W.-L., Wang, H.-J., 2008. Modeling Connectivity of Inter-Vehicle Communication Systems with Road-Side Stations. Open Transp. J. 2, 1–6. doi:10.2174/1874447800802010001

Jin, W.-L., Yang, H., 2013. The Lighthill-Whitham-Richards Model for a Platoon of Vehicles, in: The 2013 Annual Meeting Compendium of Papers. Transportation Research Board, Washington, D.C.

Jin, W., Recker, W.W., 2007. A monte carlo simulation model of inter-vehicle communication. Transp. Res. Rec. J. Transp. Res. Board 8–15. doi:http://dx.doi.org/10.3141/2000-02

Lakas, A., Cheqfah, M., 2009. Detection and dissipation of road traffic congestion using vehicular communication. 2009 Mediterrannean Microw. Symp. MMS 2009. doi:10.1109/MMS.2009.5409762

Lee, U., Zhou, B., Gerla, M., Magistretti, Eugenio Bellavista, P., Corradi, A., 2006. Mobeyes: smart mobs for urban monitoring with a vehicular sensor network. Wirel. Commun. IEEE 13, 52–57. doi:10.1109/WC-M.2006.250358

Li, J.-Q., Zhou, K., Shladover, S., Skabardonis, A., 2013. Estimating Queue Length Under Connected Vehicle Technology: Using Probe Vehicle, Loop Detector, and Fused Data, in: The 2013 Annual Meeting Compendium of Papers. Transportation Research Board, Washington, D.C.

Lighthill, M.J., Whitham, G.B., 1955. On Kinematic Waves. II. A Theory of Traffic Flow

on Long Crowded Roads. Proc. R. Soc. A Math. Phys. Eng. Sci. 229, 317–345. doi:10.1098/rspa.1955.0089

Lin, L., Osafune, T., 2011. Road congestion detection by distributed vehicle-to vehicle communication systems. US 7,877,196 B2.

Lou, Y., Li, P., Hong, X., 2016. A distributed framework for network-wide traffic monitoring and platoon information aggregation using V2V communications. Transp. Res. Part C Emerg. Technol. 69. doi:10.1016/j.trc.2016.06.003

Ma, J., Li, X., Shladover, S., Rakha, H.A., Lu, X.-Y., Jagannathan, R., Dailey, D.J., 2016. Freeway Speed Harmonization. IEEE Trans. Intell. Veh. 1, 78–89. doi:10.1109/TIV.2016.2551540

Miller, J., 2008. Vehicle-to-vehicle-to-infrastructure (V2V2I) intelligent transportation system architecture. IEEE Intell. Veh. Symp. Proc. 715–720. doi:10.1109/IVS.2008.4621301

Mirchandani, P., Head, L., 2001. A real-time traffic signal control system: Architecture, algorithms, and analysis. Transp. Res. Part C Emerg. Technol. 9, 415–432. doi:10.1016/S0968-090X(00)00047-4

Priemer, C., Friedrich, B., 2009. A decentralized adaptive traffic signal control using V2I communication data. 2009 12th Int. IEEE Conf. Intell. Transp. Syst. 765–770. doi:10.1109/ITSC.2009.5309870

Quinlan, M., Au, T.C., Zhu, J., Stiurca, N., Stone, P., 2010. Bringing simulation to life: A mixed reality autonomous intersection. IEEE/RSJ 2010 Int. Conf. Intell. Robot. Syst. IROS 2010 - Conf. Proc. 6083–6088. doi:10.1109/IROS.2010.5651993

Raravi, G., Shingde, V., 2007. Merge algorithms for intelligent vehicles. Next Gener. Des. … 51–65. doi:10.1007/978-1-4020-6254-4_5

Richards, P.I., 1956. Shock Waves on the Highway. Oper. Res. 4, 42–51.

Schonhof, M., Kesting, A., Treiber, M., Helbing, D., 2006. Coupled vehicle and information flows: Message transport on a dynamic vehicle network. Phys. A-Statistical Mech. Its Appl. 363, 73–81. doi:10.1016/j.physa.2006.01.057

Stephanopoulos, G., Michalopoulos, P.G., Stephanopoulos, G., 1979. Modelling and analysis of traffic queue dynamics at signalized intersections. Transp. Res. Part A Gen. 13, 295–307. doi:10.1016/0191-2607(79)90028-1

Terroso-sáenz, F., Valdés-vela, M., Sotomayor-martínez, C., Toledo-moreo, R., Gómez-skarmeta, A.F., 2012. Detection With Complex Event Processing and VANET. IEEE Trans. Intell. Transp. Syst. 13, 914–929. doi:10.1109/TITS.2012.2186127

Trop, J., 2017. Cadillac Leaps Toward Autonomous Driving With Its New Super Cruise System [WWW Document]. URL https://www.forbes.com/sites/jaclyntrop/2017/10/16/cadillac-leaps-toward-autonomous-driving-with-its-new-super-cruise-system/#4acaf7ae28ce (accessed

10.31.17).

Ubiergo, G.A., Jin, W.L., 2016. Mobility and environment improvement of signalized networks through Vehicle-to-Infrastructure (V2I) communications. Transp. Res. Part C Emerg. Technol. 68, 70–82. doi:10.1016/j.trc.2016.03.010

USDOT, 2016. History of ITS [WWW Document]. URL https://www.its.dot.gov/about/HistoryITS_Timeline.pdf (accessed 1.1.17).

USDOT, 2015. Intelligent Transportation Systems - Connected Vehicle [WWW Document]. URL https://www.its.dot.gov/cv_basics/cv_basics_20qs.htm (accessed 10.31.17).

USDOT, n.d. Intelligent Transportation Systems - CV Pilot Deployment Program [WWW Document]. URL https://www.its.dot.gov/pilots/cv_pilot_apps.htm (accessed 10.31.17a).

USDOT, n.d. Intelligent Transportation Systems - Connected Vehicle Pilot Deployment Program [WWW Document]. URL https://www.its.dot.gov/pilots/pilots_nycdot.htm (accessed 10.31.17b).

USDOT, n.d. Intelligent Transportation Systems - Dynamic Mobility Applications (DMA) [WWW Document]. URL https://www.its.dot.gov/research_archives/dma/bundle/mmitss_plan.htm (accessed 11.14.17c).

USDOT, n.d. Intelligent Transportation Systems - Connected Vehicle Pilot Deployment Program [WWW Document]. URL https://www.its.dot.gov/pilots/pilots_thea.htm (accessed 10.31.17d).

Vaqar, S. a., Basir, O., 2009. Traffic pattern detection in a partially deployed vehicular Ad Hoc network of vehicles. IEEE Wirel. Commun. 16, 40–46. doi:10.1109/MWC.2009.5361177

Wang, B.X., Yin, K., Qin, X., 2011. An approximate Bernoulli process for information propagation along two parallel roads. Transp. Res. Part C Emerg. Technol. 19, 469–484. doi:10.1016/j.trc.2010.07.006

Wang, X., 2007. Modeling the process of information relay through inter-vehicle communication. Transp. Res. Part B Methodol. 41, 684–700. doi:10.1016/j.trb.2006.11.002

Wei, Y., Liu, J., Belezamo, B., Zhou, X., 2017. Dynamic programming-based multi-vehicle longitudinal trajectory optimization with simplified car following models. Transp. Res. Part B 0, 1–28. doi:10.1016/j.trb.2017.10.012

Wischhof, L., Ebner, A., Rohling, H., 2005. Information dissemination in self-organizing intervehicle networks. IEEE Trans. Intell. Transp. Syst. 6, 90–101. doi:10.1109/TITS.2004.842407

Wu, H., Lee, J., Hunter, M., Fujimoto, R., Guensler, R.L., Ko, J., 2005. Efficiency of

Simulated V2V Message Porpagation on I75 in Atlanta. Transp. Res. Rec. J. Transp. Res. Board 82–89.

Yang, X., Recker, W., 2005. Simulation studies of information propagation in a self-organizing distributed traffic information system. Transp. Res. Part C Emerg. Technol. 13, 370–390. doi:10.1016/j.trc.2005.11.001

Yin, K., Wang, X. (Bruce), Zhang, Y., 2013. Vehicle-to-vehicle connectivity on two parallel roadways with a general headway distribution. Transp. Res. Part C Emerg. Technol. 29, 84–96. doi:10.1016/j.trc.2013.01.005

Younes, M.B., Boukerche, A., 2013. Efficient traffic congestion detection protocol for next generation VANETs. IEEE Int. Conf. Commun. 3764–3768. doi:10.1109/ICC.2013.6655141

Zhang, Y.J., Malikopoulos, A.A., Cassandras, C.G., 2015. Optimal Control and Coordination of Connected and Automated Vehicles at Urban Traffic Intersections 6227–6232. doi:10.1109/ACC.2016.7526648

Zhou, F., Li, X., Ma, J., 2017. Parsimonious shooting heuristic for trajectory design of connected automated traffic part I: Theoretical analysis with generalized time geography. Transp. Res. Part B Methodol. 95, 394–420. doi:10.1016/j.trb.2016.05.007

Zhou, J., Peng, H., 2015. Range Policy of Adaptive Cruise Control Vehicles for Improved Flow Stability and String Stability 6, 229–237.

Zhou, L., Tong, L. (Carol), Chen, J., Tang, J., Zhou, X., 2017. Joint optimization of high-speed train timetables and speed profiles: A unified modeling approach using space-time-speed grid networks. Transp. Res. Part B Methodol. 97, 157–181. doi:10.1016/j.trb.2017.01.002

Zhuang, Y., Pan, J., Cai, L., 2010. A probabilistic model for message propagation in two-dimensional vehicular ad-hoc networks. Proc. seventh ACM Int. Work. Veh. InterNETworking - VANET '10 31. doi:10.1145/1860058.1860064

Zohdy, I.H., Kamalanathsharma, R.K., Rakha, H., 2012. Intersection management for autonomous vehicles using iCACC. IEEE Conf. Intell. Transp. Syst. Proceedings, ITSC 1109–1114. doi:10.1109/ITSC.2012.6338827

APPENDIX A

SPEED PROFILE PLANNING FOR INSTANTANEOUS HEADWAY

In Chapter 5, we discuss the speed profile planning with a constant space headway. Under most of the cases, the minimum safety headway and the same speed between two consecutive platoons can be achieved simultaneously. On the other hand, time headway as another important spacing strategy and its corresponding behaviors under speed profile planning is really of interest. This section will look into instantaneous headway by exploring a very simple two-vehicle case as illustrated in Figure A-1. More specifically, we are interested to see if a minimum headway and the same speed can be achieved simultaneously. Preliminary results are provided. First, define the following variables and parameters:

$h(t)$: instantaneous time headway for the following vehicle at time t,

Δ_t: critical time headway,

s: initial distance between the vehicles,

v_L: initial speed of the leading vehicle,

$\bar{a}$: acceleration rate,

$\underline{a}$: deceleration rate,

T: time that the two vehicles reach the same speed. Note that $T = t_0 + \frac{\bar{a}t_0}{\underline{a}} = \frac{\bar{a}+\underline{a}}{\underline{a}} t_0$,

δ: time difference between t_0 and the time when the minimum time headway is achieved.

Besides, we have three basic assumptions to simplify the analysis.

1. $v_L > 0$.
2. The following vehicle F and the leading vehicle L have the same initial speed, and $s > v_L \Delta_t$.
3. The following vehicle will follow the speed profile below.

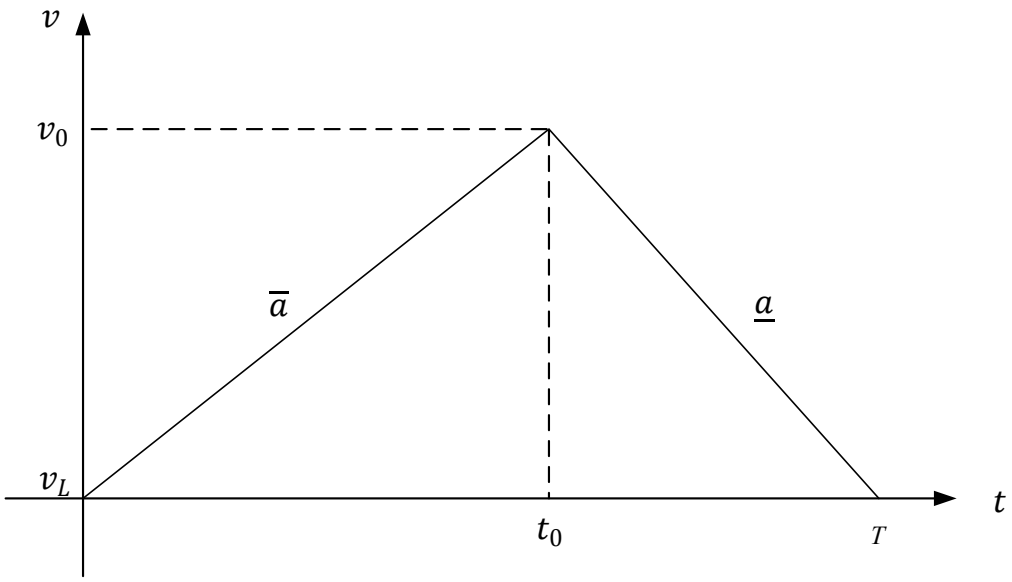

Figure A-1 Speed Profile of Vehicle L for Instantaneous Time Headway Analysis

Instantaneous Time Headway

Instantaneous Time headway, $h(t)$, is defined as the time required for the following vehicle speed to reach the current position of its immediate leading vehicle at $v_F(t)$.

$$h(t) = \begin{cases} \dfrac{s - \overline{a}t^2/2}{v_L + \overline{a}t} & t < t_0 \quad \text{(A.1)} \\ \dfrac{s - \overline{a}t_0^2/2 - \overline{a}t_0(t - t_0) + \underline{a}(t - t_0)^2/2}{v_L + \overline{a}t_0 - \underline{a}(t - t_0)} & t \geq t_0 \quad \text{(A.2)} \end{cases}$$

Derivative of $h'(t)$

When $t < t_0$,

$$h'(t) = -\frac{(\overline{a}t)^2 + 2\overline{a}(v_L t + s)}{2(v_L + \overline{a}t)^2} \quad \text{(A.3)}$$

$h'(t) < 0$ for any $t < t_0$. In other words, $h(t)$ is a monotonically decreasing function for $t < t_0$.

When $t \geq t_0$, let $s_0 = s - \frac{1}{2}\overline{a}t_0^2$ and $v_0 = v_L + \overline{a}t_0$, which represent the distance between the vehicles at time t_0 and the speed of the following vehicle at time t_0 respectively. Then

$$h(t) = \frac{s_0 - \overline{a}t_0(t - t_0) + \underline{a}(t - t_0)^2/2}{v_0 - \underline{a}(t - t_0)} \quad \text{(A.4)}$$

Its derivative is as below

$$h'(t) = \frac{-\underline{a}^2(t - t_0)^2 + 2\underline{a}v_0(t - t_0) + 2\underline{a}s_0 - 2\overline{a}v_0t_0}{2\left[v_0 - \underline{a}(t - t_0)\right]^2} \quad \text{(A.5)}$$

The denominator is always positive (speed of the following vehicle is greater than or equal to V_L). The numerator is a parabolic function symmetric around $t - t_0 = \frac{v_0}{\underline{a}}$.

To summarize, $h'(t)$ will be

$$\begin{cases} -\dfrac{(\overline{a}t)^2 + 2\overline{a}(v_L t + s)}{2(v_L + \overline{a}t)^2} & t < t_0 \quad \text{(A.6)} \\ \dfrac{-\underline{a}^2(t-t_0)^2 + 2\underline{a}v_0(t-t_0) + 2\underline{a}s_0 - 2\overline{a}v_0 t_0}{2\left[v_0 - \underline{a}(t-t_0)\right]^2} & t \geq t_0 \quad \text{(A.7)} \end{cases}$$

Special Cases

Case I: $h(T) = \Delta_t$

From (A.2) and the definition of T, we have

$$2\underline{a}s_0 - (\bar{a}t_0)^2 = 2\underline{a}\Delta_t v_L \quad \text{(A.8)}$$

Therefore, the numerator of (A.7) becomes

$$-\underline{a}^2(t-t_0)^2 + 2\underline{a}v_0(t-t_0) + 2\underline{a}s_0 - 2\overline{a}v_0 t_0 = 2\underline{a}\Delta_t v_L > 0 \quad \text{(A.9)}$$

In other words, $h'(T) > 0$ and $\exists t \in (t_0, T)$ such that $h(t) < h(T) = \Delta_t$. This violates our safety consideration. This motivates us to find a $\hat{t} \in [t_0, T)$ where $h'(\hat{t}) = 0$. One question would be whether it is possible or not for $h(\hat{t}) = \Delta_t$. A related interesting question is what $h(T)$ would be in this case.

Case II: $h'(t_0) = 0$

$$h'(t_0) = \frac{-2\overline{a}v_0 t_0 + 2\underline{a}s_0}{2v_0^2} = 0$$

It gives

$$\underline{a}s_0 = \overline{a}v_0 t_0 \tag{A.10}$$

Since

$$\begin{cases} s_0 = s - \dfrac{1}{2}\overline{a}t_0^2 & \text{(A.11)} \\ v_0 = v_L + \overline{a}t_0 & \text{(A.12)} \end{cases}$$

We have

$$\left(\overline{a}\underline{a} + 2\overline{a}^2\right)t_0^2 + 2\overline{a}v_L t_0 - 2\underline{a}s = 0 \tag{A.13}$$

The above equation has real roots. They are

$$\frac{-\overline{a}v_L \pm \sqrt{\overline{a}^2 v_L^2 + 2\underline{a}\left(\overline{a}\underline{a} + 2\overline{a}^2\right)s}}{\overline{a}\underline{a} + 2\overline{a}^2} \tag{A.14}$$

And it is obvious that

$$\frac{-\overline{a}v_L + \sqrt{\overline{a}^2 v_L^2 + 2\underline{a}\left(\overline{a}\underline{a} + 2\overline{a}^2\right)s}}{\overline{a}\underline{a} + 2\overline{a}^2} > \tag{A.15}$$

This allows a valid solution

$$\hat{t} = t_0 = \frac{-\overline{a}v_L + \sqrt{\overline{a}^2 v_L^2 + 2\underline{a}\left(\overline{a}\underline{a} + 2\overline{a}^2\right)s}}{\overline{a}\underline{a} + 2\overline{a}^2} \tag{A.16}$$

With condition $h(t_0) = \Delta_t$

From $h(t_0) = \Delta_t$, we have

$$\overline{a}t_0^2 + 2\overline{a}\Delta t_0 + 2v_L\Delta_t - 2s = 0 \tag{A.17}$$

This equation also has a real positive solution:

$$t_0 = \frac{-\overline{a}\Delta_t + \sqrt{\overline{a}^2\Delta_t^2 + 2\overline{a}(s - v_L\Delta_t)}}{\overline{a}} \tag{A.18}$$

Combining (A.16) and (A.18), we have

$$\frac{-\overline{a}v_L + \sqrt{\overline{a}^2 v_L^2 + 2\underline{a}(\overline{a}\underline{a} + 2\overline{a}^2)s}}{(\underline{a} + 2\overline{a})} = -\overline{a}\Delta + \sqrt{\overline{a}^2\Delta^2 + 2\overline{a}(s - v_L\Delta_t)} \tag{A.19}$$

(A.19) is the condition that the variables $s, v_L, \Delta_t, \underline{a}$, and $\overline{a}$ need to satisfy in order to have $h(t_0) = \Delta$ and $h'(t_0) = 0$.

When $\underline{a} = \overline{a} = a$, then (A.19) can be simplified as

$$3a\Delta_t - v_L = 3\sqrt{a^2\Delta_t^2 + 2a(s - v_L\Delta_t)} - \sqrt{v_L^2 + 6as} \tag{A.20}$$

On the other hand

$$\begin{cases} h'(t_0) = 0 \\ h(t_0) = \Delta_t \end{cases} \tag{A.21}$$

It leads to

$$\begin{cases} \left(\overline{a}\underline{a} + 2\overline{a}^2\right)t_0^2 + 2\overline{a}v_L t_0 - 2\underline{a}s = 0 & \text{(A.22)} \\ \overline{a}t_0^2 + 2\overline{a}\Delta_t t_0 + 2v_L\Delta_t - 2s = 0 & \text{(A.23)} \end{cases}$$

From (A.23),

$$t_0^2 = \frac{2s - 2v_L\Delta_t - 2\overline{a}\Delta_t t_0}{\overline{a}} \quad \text{(A.24)}$$

Substitute t_0^2 in (A.24),

$$\left(\underline{a} + 2\overline{a}\right)(2s - 2v_L\Delta_t - 2\overline{a}\Delta_t t_0) + 2\overline{a}v_L t_0 - 2\underline{a}s = 0 \quad \text{(A.25)}$$

Then

$$t_0 = \frac{(\underline{a} + 2\overline{a})v_L\Delta_t - 2\overline{a}s}{\overline{a}v_L - \overline{a}\left(\underline{a} + 2\overline{a}\right)\Delta_t} \quad \text{(A.26)}$$

Since $t_0 > 0$, the following set of inequalities can be obtained

$$\begin{cases} (\underline{a} + 2\overline{a})v_L\Delta_t - 2\overline{a}s > 0 & \text{(A.27)} \\ v_L - \left(\underline{a} + 2\overline{a}\right)\Delta_t > 0 & \text{(A.28)} \end{cases}$$

It is equivalent to

$$\begin{cases} (\underline{a} + 2\overline{a})v_L\Delta_t - 2\overline{a}s < 0 & \text{(A.29)} \\ v_L - \left(\underline{a} + 2\overline{a}\right)\Delta_t < 0 & \text{(A.30)} \end{cases}$$

Compute T

$$\delta = \frac{v_0 - v_L}{\underline{a}} = \frac{\overline{a}}{\underline{a}} t_0 \tag{A.31}$$

Combine (A.31) and (A.26),

$$\delta = \frac{1}{\underline{a}} * \frac{(\underline{a} + 2\overline{a}) v_L \Delta_t - 2\overline{a}s}{v_L - (\underline{a} + 2\overline{a})\Delta_t} \tag{A.32}$$

Since

$$T = t_0 + \delta \tag{A.33}$$

We can get

$$\delta = (\frac{1}{\overline{a}} + \frac{1}{\underline{a}}) \frac{(\underline{a} + 2\overline{a}) v_L \Delta_t - 2\overline{a}s}{v_L - (\underline{a} + 2\overline{a})\Delta_t} \tag{A.34}$$

In other words,

$$T = (\frac{1}{\overline{a}} + \frac{1}{\underline{a}})(v_0 - v_L) \tag{A.35}$$

Compute $h(T)$

With (A.7), (A.19), and (A.31), we have

$$h(T) = \frac{s}{v_L} - \frac{(v_0 - v_L)^2}{2v_L} (\frac{1}{\overline{a}} + \frac{1}{\underline{a}}) \tag{A.36}$$

With

$$v_0 - v_L = \frac{(\underline{a} + 2\overline{a})v_L\Delta_t - 2\overline{a}s}{v_L - (\underline{a} + 2\overline{a})\Delta_t} \tag{A.37}$$

We have

$$h(T) = \frac{s}{v_L} - \frac{1}{2v_L}\left(\frac{1}{\overline{a}} + \frac{1}{\underline{a}}\right)\left[\frac{(\underline{a} + 2\overline{a})v_L\Delta_t - 2\overline{a}s}{v_L - (\underline{a} + 2\overline{a})\Delta_t}\right]^2 \tag{A.38}$$

When $\underline{a} = \overline{a} = a$

$$h(T) = \frac{s}{v_L} - \frac{a}{v_L}\left[\frac{3v_L\Delta_t - 2s}{v_L - 3a\Delta_t}\right]^2 \tag{A.39}$$

There are many different possible control goals. One of them is to minimize the difference between $h(T)$ and Δ_t, which is

$$\min h(T) - \Delta_t \tag{A.40}$$

Since Δ_t is constant, it is equivalent to

$$\min h(T) \tag{A.41}$$

With (A.38), it becomes

$$\max\left(\frac{1}{\overline{a}} + \frac{1}{\underline{a}}\right)\left[\frac{(\underline{a} + 2\overline{a})v_L\Delta_t - 2\overline{a}s}{v_L - (\underline{a} + 2\overline{a})\Delta_t}\right]^2 \tag{A.42}$$

s.t.

$$0 \le \overline{a} \le \overline{a}_{Max} \tag{A.43}$$

$$0 \le \underline{a} \le \underline{a}_{Max} \tag{A.44}$$

Note that the above formulation is simplified, and may not be complete.

Theoretically, $h(T)$ should satisfy the following condition

$$h(T) - \Delta_t > 0 \tag{A.45}$$

With (A.38) and (A.37), it is equivalent to

$$\frac{s - v_L \Delta_t}{v_L} - \frac{1}{2v_L}\left(\frac{1}{\overline{a}} + \frac{1}{\underline{a}}\right)(v_0 - v_L)^2 \tag{A.46}$$

With (A.35), we have

$$\frac{s - \frac{1}{2}(v_0 - v_L)T}{v_L} > \Delta_t \tag{A.47}$$

This is consistent with our assumption that $h(t)$ is achieved its minimum value at t_0. In other words, $h(t) > \Delta_t$ at any $t \neq t_0$.

General Case

A general case is that there exists $t > t_0$ such that

$$\begin{cases} h'(t) = 0 \\ h(t) = \Delta_t \end{cases}$$

From (A.7) and (A.4),

$$\begin{cases} \dfrac{-2\overline{a}v_0t_0 + 2\underline{a}v_0(t-t_0) - \underline{a}^2(t-t_0)^2 + 2\underline{a}s_0}{2\left[v_0 - \underline{a}(t-t_0)\right]^2} = 0 \\ \dfrac{s - \frac{1}{2}\overline{a}t_0^2 - \overline{a}t_0(t-t_0) + \frac{1}{2}\underline{a}(t-t_0)^2}{v_L + \overline{a}t_0 - \underline{a}(t-t_0)} = \Delta_t \end{cases} \tag{A.48}$$

Let$\delta = t - t_0$,

$$\underline{a}^2\delta^2 - 2\underline{a}v_0\delta + 2\overline{a}v_0t_0 - 2\underline{a}s_0 = 0 \tag{A.49}$$

$$\underline{a}^2\delta^2 + 2\underline{a}\left(\underline{a}\Delta_t - \overline{a}t_0\right)\delta - \overline{a}\underline{a}t_0(t_0 + 2\Delta_t) - 2\underline{a}\Delta_t v_L + 2\underline{a}s = 0 \tag{A.50}$$

Combine (A.49) and (A.50),

$$\begin{aligned} &-2\underline{a}v_0\delta + 2\overline{a}v_0t_0 - 2\underline{a}s_0 \\ &= 2\underline{a}\left(\underline{a}\Delta_t - \overline{a}t_0\right)\delta - \overline{a}\underline{a}t_0(t_0 + 2\Delta) - 2\underline{a}\Delta_t v_L + 2\underline{a}s \end{aligned} \tag{A.51}$$

With

$$\begin{cases} s_0 = s - \dfrac{1}{2}\overline{a}t_0^2 \\ v_0 = v_L + \overline{a}t_0 \end{cases} \tag{A.52}$$

We have

$$\delta = \frac{\overline{a}\underline{a}t_0(t_0 + \Delta_t) + \underline{a}\Delta_t v_L + \overline{a}v_L t_0 + \overline{a}^2 t_0^2 - 2\underline{a}s}{\underline{a}^2\Delta_t + \underline{a}v_L} \tag{A.53}$$

With (A.50),

$$\frac{\alpha(t_0)\,\beta(t_0)}{\left(\underline{a}\Delta_t + v_L\right)^2} - \gamma(t_0) = 0 \tag{A.54}$$

Where, $\alpha(t_0) = \left[\overline{a}\underline{a}t_0(t_0 + \Delta_t) + \underline{a}\Delta_t v_L + \overline{a}v_L t_0 + \overline{a}^2 t_0^2 - 2\underline{a}s\right]$,

$$\beta(t_0) = \left[(\overline{a}\underline{a} + \overline{a}^2)t_0^2 + 2\underline{a}^2\Delta_t^2 - \left(\overline{a}\underline{a}\Delta_t + \overline{a}v_L\right)t_0 + 3\underline{a}\Delta_t v_L - 2\underline{a}t_0 v_L\right],$$

$$\gamma(t_0) = -\overline{a}\underline{a}t_0(t_0 + 2\Delta_t) - 2\underline{a}\Delta_t v_L + 2\underline{a}s.$$

It is an equation of t_0, which can be solved using numerical methods. Another constraint for the general case is that $h'(t_0) < 0$. After solving t_0 from the above equation using a numerical method (e.g. bi-section method), we are able to check whether the constraint holds or not.

Summary

Under instantaneous headway, the consecutive two vehicles cannot achieve the same speed while maintain the minimum safety distance Δ_t at the same time for this special two-vehicle case. It is possible that $h(t)$ achieves its minimum value at t_0. The general case refers to whether exist a $\hat{t} > t_0$ such that $h(t)$ has the minimum value at $\hat{t}$ and $h(\hat{t}) = \Delta_t$. It is very complicated and impossible to get an analytical solution of $\hat{t}$. However, its numerical solution is able to obtain through numerical methods. Whether $h'(\hat{t}) = 0$ and $h(\hat{t}) = \Delta_t$ is left to determine using numerical examples.

APPENDIX B

PREDICTION ON EVOLUTION OF MIRCO-DISCONTINUITY

In Chapter 3, we adopted the concept of micro-discontinuity to measure traffic state difference and thus to identify potential vehicular platoons. A vehicular platoon is uniquely determined by a lead and an anchor vehicle. Isolated vehicles are treated as a special case of micro-discontinuity. Vehicular platoons are directly related to traffic conditions and are subject to change over time especially with queueing traffic. With the distributed traffic monitoring and information aggregation system, we are able to detect the status of micro-discontinuities and track the evolution of platoons at any time. However, it is important to have both evolution and its future prediction for a short-time period, which are the key to designing an effective and efficient virtual transportation operation system.

Figure B-1 illustrates the process of platoon evolution. There is only one vehicular platoon at the beginning. With the presence of new anchors and leads from upstream, the platoon evolves into two small platoons at $t = 71s$, which represent stopped vehicles and approaching vehicles respectively. But it is not easy to model the evolution. The existing platoon dispersion models cannot track and predict the evolution at such a microscopic level. However, the evolution of platoons is equivalent to that of micro-discontinuities. Therefore, we could predict the evolution of micro-discontinuities instead of making prediction on that of platoons directly. In this section, we propose a framework for predicting evolution of micro-discontinuities near a signalized intersection with given signal timing plans. The framework will perform on the basis of the proposed distributed traffic monitoring and information aggregation system. Two different prediction methodologies will be investigated accordingly.

This section primarily investigates evolution of micro-discontinuities identified by the proposed distributed traffic monitoring system and develop a predication framework. Traffic control information at intersections (for example, signal timing) is considered given in the proposed study. Compared to free flow traffic, queueing traffic will result into more fluctuation into the evolution of micro-discontinuities which is more of interest. This section concentrates on queueing traffic under light and heavy traffic respectively at a signalized intersection.

For light traffic, vehicular platoons are separated by large space headways and the movements of the identified discontinuities are approximately the same as the platoons. As shown in Figure B-2, while the lead is always the first vehicle at the stop bar, the evolution of anchor basically follows the trajectory of the last vehicle in the first identified platoon starting from $t = 265$s. This can be considered a shockwave prorogated forward incurred by the interactions of the two adjacent platoons which are stopped vehicles and approaching vehicles respectively. With this observation, shockwave analysis from macroscopic traffic flow theories are explored to track the movement of anchors.

For heavy traffic, the evolution of micro-discontinuities are not stationary and back-and-forth movements can be observed over a successive time period. As shown in Figure B-3, the anchor of the first vehicular platoon jumped from a downstream position to further upstream at $t = 282s$ and then moved to further downstream again. The methodology used for light traffic cannot be applied. A localized cooperative mechanism with consideration of individual movements of vehicles within the platoon as inputs that runs

on individual vehicles may be needed. The mechanism will be triggered once the value of Δ is above a predefined threshold. It should predict whether the platoon will stay together or split into multiple ones in the next several time intervals.

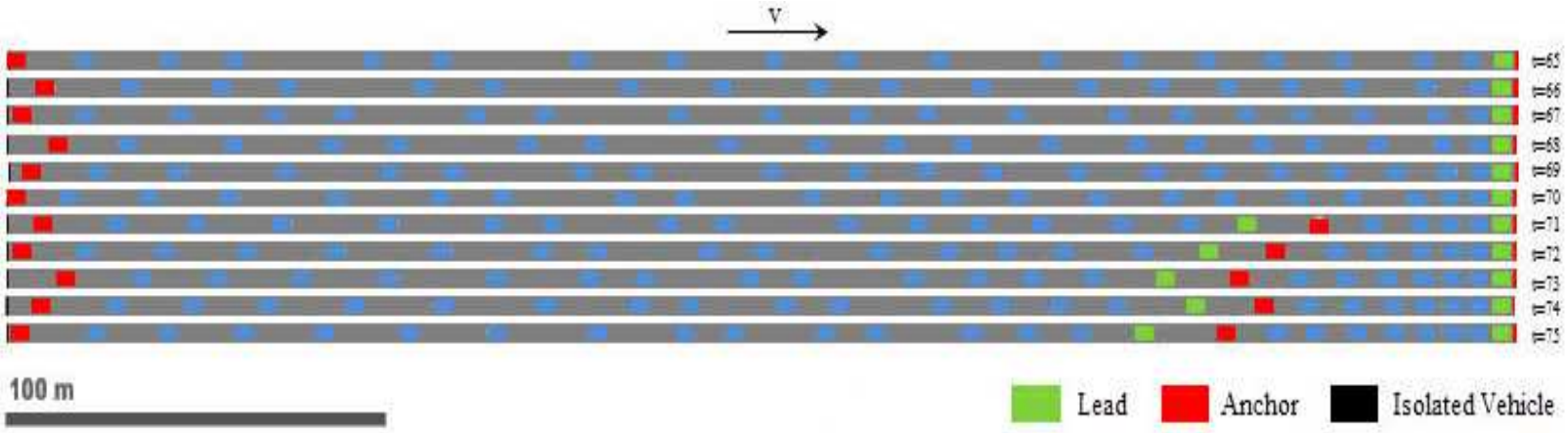

Figure B-1 Evolution of Platoons

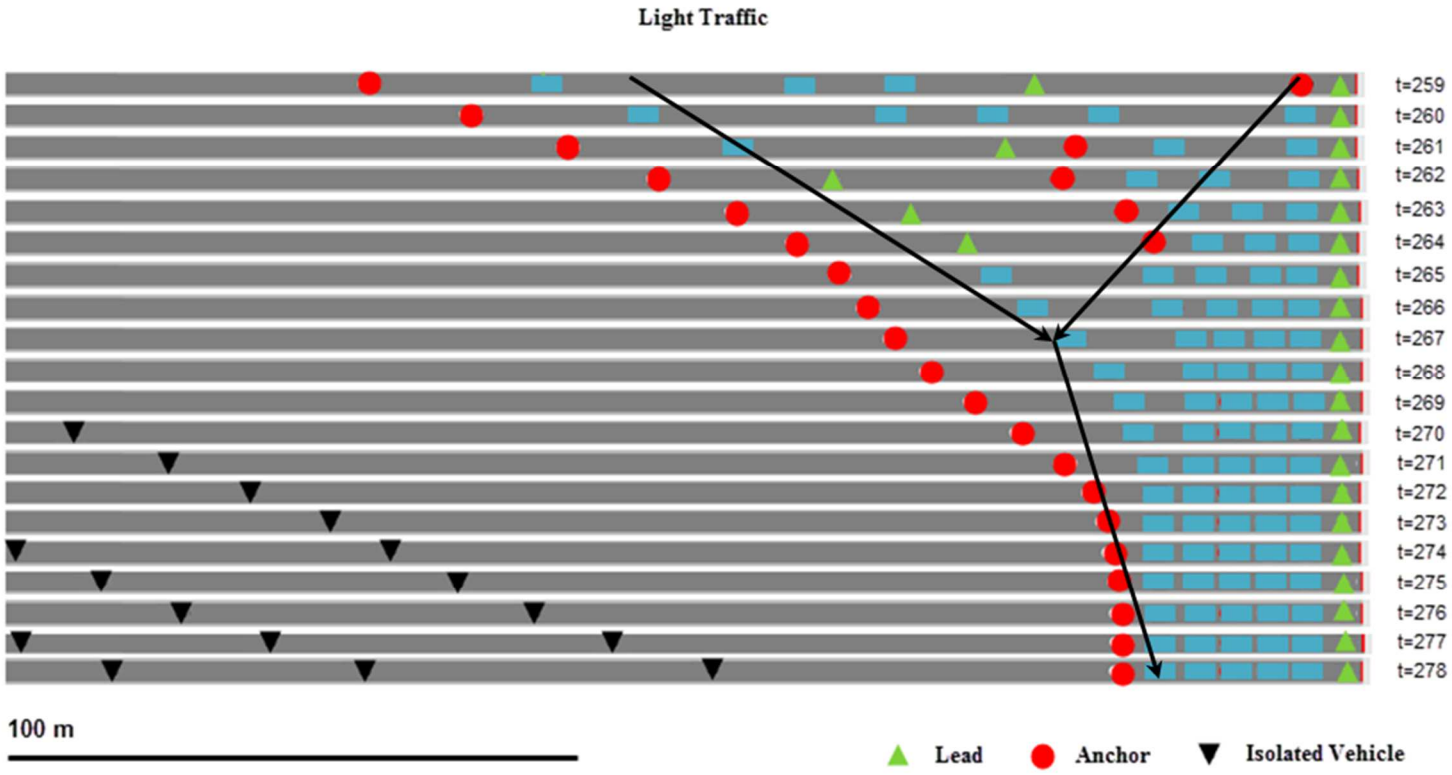

Figure B-2 Evolution of Micro-Discontinuity under Light Traffic

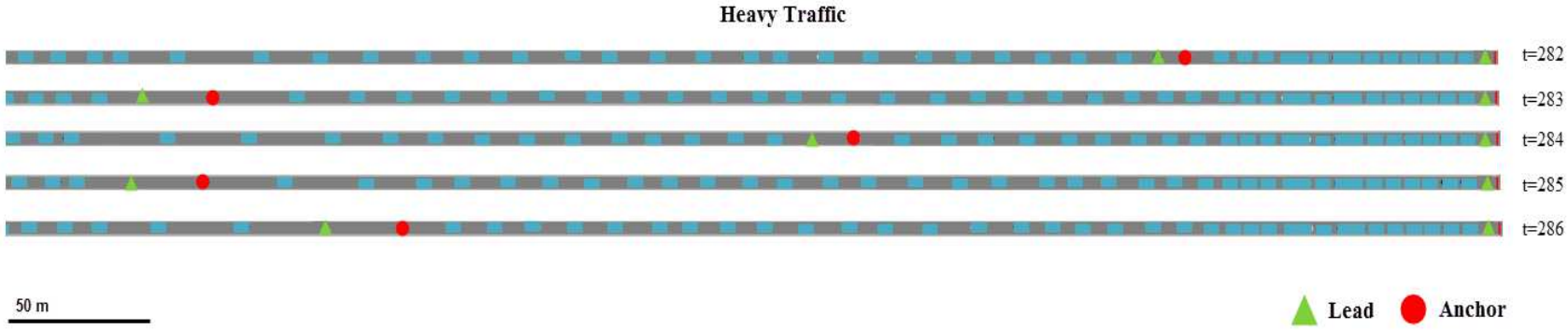

Figure B-3 Evolution of Micro-Discontinuity under Heavy Traffic

BIOGRAPHICAL SKETCH

Peiheng Li received his bachelor's degree in transportation engineering from Beijing Jiaotong University in 2009; and earned his master's degree in civil engineering from the University of Alabama in 2013.

Peiheng Li's primary research interest is mobility application of connected and autonomous vehicles. He also interests in traffic flow theory, evacuation planning/scheduling, simulation optimization, multi-objective optimization, and vehicle routing problem. He has co-authored three papers and made five presentations at national and local conferences. Peiheng Li won the second prize at the Contest of Best Student Papers at the 2015 ITS Arizona Annual Conference. He also won numerous travel grants from various sources. Due to his outstanding academic achievements, Peiheng Li was featured for National Transportation Center Student Highlights and was awarded for 2016 Roads and Streets Conference Scholarships. Furthermore, he is the member of The Honor Society of Phi Kappa Phi and that of Chi Epsilon, the National Civil Engineering Honors Society.

Peiheng Li is also active in Arizona local transportation communities. He serves in the ASU Parking and Transit Advisory Board and is a member of ITS Arizona. Besides, Peiheng Li has dedicated his time and effort to the ASU Student Chapter of Institute of Transportation Engineers (ASU-ITE). He was one of the officers for four years, as the treasurer and the president, and helped organize more than 70 transportation seminars and several other events since October 2013.